Toward adaptation in human-robot collaboration

Lorenzo Vianello

UNIVERSITÉ DE LORRAINE

École doctorale IAEM Lorraine

Toward adaptation in human-robot collaboration

THÈSE

présentée et soutenue publiquement le 12 Décembre 2022

pour l'obtention du

Doctorat de l'Université de Lorraine

(Mention Automatique, Traitement du Signal et des Images, Génie Informatique)

par

Lorenzo Vianello

Composition du jury

Rapporteurs :	Guillaume Morel, Professeur, Sorbonne Université Marie Babel, Professeur, INSA Rennes
Examinateurs :	Pedro Rodriguez-Ayerbe, Professeur, Centrale Supelec Benoît Iung, Professeur, Université de Lorraine *(président du jury)*
Invitée :	Luka Peternel, Associate Professor, TU Delft
Encadrants :	Alexis Aubry, Associate Professor, Université de Lorraine Serena Ivaldi, Chargée de Recherche, Université de Lorraine

Laboratoire CRAN — UMR 7039, LORIA — UMR 7503

Contents

List of Figures

List of Tables

List of Acronyms

CMA-ES Covariance matrix adaptation evolution strategy

DHM Digital Human Model

EMG Electromyography

GP Gaussin Process

HRC Human-Robot Collaboration

HRpI Human-Robot physical Interaction

ICC Co-Contraction Index

IK Inverse Kinematics

LEM Latent Ergonomics Map

MDP Markov Decision Process

ProMP Probabilistic Movement Primitives

QP Quadratic Programming

RULA Rapid Upper Limb Assessment

R-MSE Root Mean Square Error

VAE Variational Autoencoder

WRMSD Work-Related Musculoskeletal Disorder

Summary in French

En 1940, Asimov a publié son premier roman dédié aux robots : *Robbie*. Dans cette histoire, Asimov imagine un robot (Robbie) conçu pour jouer avec une petite fille. Le robot, nous dit Asimov, ne représente aucun danger pour la petite fille, et cette dernière établit un lien fort avec lui. À tel point que la mère s'inquiète de la sécurité et des capacités sociales de sa fille :

> "Je ne laisserai pas ma fille être confiée à une machine, et je me fiche de savoir de son intelligence. Elle n'a pas d'âme, et personne ne sait ce qu'elle peut penser. Un enfant n'est pas fait pour être gardé par une chose de métal. [...] quelque chose pourrait mal tourner. Un petit levier va se détacher et l'horrible chose va devenir folle et... et... [...] Il y a des dizaines de petits garçons et de petites filles avec lesquels elle devrait se faire des amis, mais elle ne le fera pas. Elle ne s'approchera pas d'eux à moins que je ne l'y oblige. Ce n'est pas une façon de grandir pour une petite fille. Tu veux qu'elle soit normale, n'est-ce pas ? Tu veux qu'elle soit capable de prendre sa place dans la société."

Les robots sont considérés comme des agents dangereux mais inconscients. Capables de blesser mais sans conscience et contraints à l'obéissance aux humains. Cette vision est condensée, deux ans plus tard, dans un autre roman (*Runaround*, 1942) où Asimov propose les fameuses trois lois de la robotique :

1. Un robot ne doit pas blesser un être humain ou, par son inaction, permettre qu'un être humain soit blessé.

2. Un robot doit obéir aux ordres que lui donnent les êtres humains, sauf si ces ordres entrent en conflit avec la loi 1.

3. Un robot doit protéger sa propre existence, pour autant que cette protection n'entre pas en conflit avec les lois 1 ou 2.

Ces lois portent sur la sécurité (première et troisième lois) et sur le rôle que le robot adopte pendant l'interaction (deuxième loi). Ces lois, intégrées dans la structure même du robot, sont incassables et immuables. Cela supprime toute responsabilité dans le fonctionnement du robot, car si un problème survient, on peut toujours remonter à l'humain qui commande le robot. Cela rappelle le célèbre aphorisme : "*Plus de 90% de tous les problèmes informatiques peuvent être attribués à l'interface située entre le clavier et la chaise.*".

Dans les fictions postérieures d'Asimov, les robots assument une certaine responsabilité. Pour cette raison, Asimov a également ajouté une quatrième loi, ou loi zéro, qui précède les autres :

0. Un robot ne peut pas nuire à l'humanité, ou, par son inaction, permettre à l'humanité de se nuire à elle même.

Cette dernière loi place la discussion sur la robotique sur un tout autre plan : en effet, au moment où le robot devra faire passer le bien-être de l'humanité avant celui de l'individu, il ne sera plus un être purement réactif mais devra utiliser sa capacité à prédire à court ou long terme les influences des actions actuelles sur l'humanité et choisir les meilleures actions en conséquence. Ce type d'esprit critique nécessite de peser différentes fonctions de coût, de prévoir et de s'adapter. En outre, cela place le robot dans une position de responsabilité qu'il ne possédait pas auparavant.

Dans cette thèse, nous traiterons de tous ces aspects qui préoccupent Asimov dans sa littérature mais avec un œil sur les problèmes actuels rencontrés par les robots collaboratifs : l'interaction homme-robot, l'attribution des rôles, la prédiction des actions, l'adaptation, la collaboration et la sécurité. Pour ce faire, et pour apprécier pleinement le résultat final, remontons à la naissance et au développement de la robotique et de l'automatisation.

Nous pouvons commencer ce parcours dans les années 1750. Au cours de ces années, la première révolution industrielle a converti les méthodes de production manuelles en machines actionnées par l'énergie hydraulique et la vapeur [159]. Cet événement a marqué un tournant majeur dans l'histoire: la productivité a fortement augmenté, favorisant l'augmentation de la population et du taux de croissance démographique.

Un siècle plus tard (les années 1870), ces technologies ont fait un pas en avant pendant ce qu'on appelle la deuxième révolution industrielle. Cette fois, les rôles principaux étaient les systèmes d' électrification et la division du travail de Taylor avec la production de masse et l'utilisation de convoyeurs à bande. De plus, de nombreuses industries ont commencé à rationaliser le travail afin d'augmenter leur efficacité opérationnelle. Connue également sous le nom de révolution technologique, cette phase a été marquée par des découvertes scientifiques, la normalisation, la production de masse et l'industrialisation. Ces progrès ont permis l'adoption généralisée de systèmes technologiques tels que les réseaux télégraphiques et ferroviaires, l'approvisionnement en gaz et en eau. De plus, les technologies d'automatisation se sont diffusées dans les entreprises avec l'intention de réduire l'intervention humaine dans les processus. Pour exécuter les commandes désirées, un nouveau domaine de connaissances appelé théorie du contrôle est né.

La théorie du contrôle est la base du contrôle des processus, qui est largement utilisée dans l' automatisation et pour le contrôle des navires et des avions, qui faisaient leur première apparition dans ces années-là. Maxwell a lui-même, en 1868, publié le premier traité scientifique de la théorie du contrôle.

La naissance de la robotique moderne remonte aux années 1950. Ce qu'on appelle la première génération de robots [79, 256] date des années 1950 à 1967. Les robots de cette génération étaient essentiellement des machines programmables contrôlées par des actionneurs pneumatiques. Ils n'avaient pas la capacité de contrôler réellement la modalité d'exécution de la tâche, et ils étaient utilisés pour une seule tâche, car il était très compliqué de les reprogrammer. De plus, ils n'avaient aucune communication avec l'environnement extérieur. Une caractéristique particulière de ces robots est le fort bruit qu'ils produisaient lorsque leurs bras entraient en collision avec les butées mécaniques construites pour limiter le mouvement des axes.

Le tournant de la robotique industrielle a eu lieu en 1961 avec la naissance d'Unimate par Unimation, qui est considéré comme le premier robot industriel de l'histoire. Unimate, qui était actionné hydrauliquement, a été immédiatement installé dans une entreprise automobile, plus précisément dans l'usine de General Motors (New Jersey, USA). Dans les mêmes années, plusieurs entreprises de fabrication de robots sont nées, notamment dans le secteur automobile. Des entreprises comme Ford et General Motors ont commencé à envisager l'automatisation de leurs établissements de production et avaient besoin de dispositifs tels que les nouveaux robots pour atteindre cet objectif. Il y a donc eu une augmentation soudaine des commandes de dispositifs robotiques. En 1969, le Japon a commencé à produire des robots pour le marché asiatique. Cette tendance précoce a permis au Japon de devenir l'un des

principaux pays dans le domaine de la robotique. La diffusion des robots en Europe a eu lieu plus ou moins en même temps : 1967 en Suède et 1969 en Norvège. En 1972, FIAT a installé les premiers robots de soudage en Europe dans ses établissements de Turin (Italie).

La troisième révolution industrielle, dans les années 1970, a de nouveau changé le scénario scientifique et industriel du vingtième siècle. Elle est principalement associée au passage de la technologie électronique mécanique et analogique à l'électronique numérique. Au cœur de cette révolution se trouvent la production de masse et l'utilisation généralisée de la logique numérique et de ses technologies dérivées, notamment les ordinateurs, les microprocesseurs et Internet. Ces innovations technologiques ont transformé les techniques traditionnelles de production et de commerce.

Grâce en grande partie à la diffusion de ces nouvelles technologies, une nouvelle série de robots industriels est arrivée [244]. En fait, la deuxième génération de robots industriels remonte aux années 68 à 77 [79, 256]. Le passage des actionneurs hydrauliques aux actionneurs électriques a eu lieu dans les années 1970, lorsque les composants électroniques nécessaires au contrôle d'un robot ont atteint leur pleine maturité technique, modifiant profondément la structure du robot. La situation économique et géopolitique au niveau international a également poussé la tendance vers les robots à entraînement électrique. Les entreprises ont ainsi été contraintes de trouver des moyens de production plus efficaces. Cela a donné un coup de fouet aux installations de robots industriels, qui ont augmenté de plus de 30% par an dans la seconde moitié des années 1970. Ces robots utilisaient des servocommandes, ce qui leur permettait d'effectuer aussi bien des mouvements point à point que des trajectoires continues.

Le premier prototype de robot actionné par des moteurs électriques et contrôlé par un microprocesseur PDP-6 était le Stanford Arm (Fig. 1b). Ce robot a été conçu en 1969 par Victor Scheinman, un étudiant en génie mécanique de l'université de Stanford. Les caractéristiques introduites par Scheinman dans le Stanford Arm et dans son successeur (Vicarm) ont été si appréciées qu'Unimation a racheté la société et a exploité son savoir-faire pour concevoir et fabriquer (en 1978) le célèbre robot PUMA (Programmable Universal Machine for Assembly). Entre-temps, d'autres entreprises ont développé et fabriqué d'autres types de robots industriels : Famulus de KUKA en 73 (Fig. 1c), IRB-6 de ASEA (aujourd'hui ABB) en 74, et la même année HI-T-HAND Expert de Hitachi. Ce dernier était équipé d'un système de retour de force et était capable d'atteindre une grande précision dans les opérations d'insertion.

L'évolution technique et scientifique a permis de nouvelles avancées dans le domaine de la robotique. La troisième génération de robots s'étend de 1978 à 2000. Les robots industriels de la troisième génération se caractérisaient par une plus grande interaction avec l'opérateur et l'environnement. Ils disposaient également de certaines capacités d'autoprogrammation et pouvaient se reprogrammer, bien que dans une faible mesure, afin d'exécuter différentes tâches. Ils pouvaient être programmés en temps réel ou en différé, en étant connectés à un PC, ce qui permettait d'utiliser un langage de programmation de haut niveau. La possibilité d'une programmation offline de haut niveau a élargi le potentiel opérationnel des robots : par exemple, ils pouvaient élaborer des données à partir des relevés de capteurs pour ajuster les mouvements du robot tout en tenant compte des changements dans l'environnement. En outre, une sorte d'"intelligence" était présente dans les robots de la troisième génération, avec certaines capacités d'adaptation (bien que limitées). Par exemple, en utilisant les données provenant des systèmes de vision ou de perception (par exemple, les caméras, les capteurs de force, les scanners laser), ils pouvaient localiser les objets et les pièces à manipuler. Le logiciel de commande est devenu plus "intelligent" en introduisant certaines techniques liées à l'intelligence artificielle. Ces deux aspects ont augmenté la polyvalence et la flexibilité des robots, qui ont pu être utilisés pour des tâches de plus en plus complexes.

Les robots ont proliféré au début des années 2000 : en 1995, on comptait 1,6 robot industriel installé pour mille travailleurs ; en 2007, ce nombre était de 4,2 [53]. En conséquence, et suivant les tendances lancées par les trois révolutions industrielles, une nouvelle idée de l'industrie a progressivement émergé : l'industrie 4.0. L'industrie 4.0 est un nouveau concept de fabrication et d'automatisation industrielle,

intégrant de nouvelles technologies de production afin d'améliorer les conditions de travail et d'accroître la productivité et la qualité. Le nouveau paradigme de l'industrie 4.0 permet la communication entre les humains et les machines, augmentant ainsi l'interconnectivité et l'automatisation intelligente. Dans ce contexte, la vision de la robotique (quatrième génération de robots) est également mise à jour en proposant des robots dotés de capacités "intelligentes" de haut niveau, telles que l'exécution de calculs avancés, le raisonnement logique, l'apprentissage profond, les stratégies complexes, les comportements collaboratifs.

Un résultat concret de ces approches est l'émergence de cobots. Les cobots, ou robots collaboratifs, sont des robots industriels conçus pour pouvoir interagir physiquement avec les humains lors d'activités communes et dans un espace partagé (Fig. 1e). L'objectif des cobots est d'améliorer les performances de production en permettant une répartition plus efficace et évolutive des tâches entre les humains et les machines. L'idée derrière ces technologies est de combiner les grandes capacités mentales des humains avec des robots qui peuvent prendre en charge les parties fatigantes des tâches. Cet aspect permet aux robots collaboratifs d'être génériques, tant dans la manière dont ils sont construits que dans celle dont ils sont programmés. D'une manière générale, nous pouvons définir les capacités suivantes des robots collaboratifs [70]:

1. La mobilité: La possibilité de déplacer facilement le cobot dans l'usine de production;
2. La capacité d'adaptation: La conscience des ressources, des caractéristiques du poste et de leurs implications;
3. Connectivité: La capacité de communiquer avec les opérateurs et les autres robots dans l' environnement de travail, en collectant et en fournissant des informations;
4. Actionnement: La capacité à développer des trajectoires sûres et fluides;
5. Cohérence: La capacité de travailler en continu sans problème, sauf en cas de dysfonctionnement;
6. La sécurité: La capacité de travailler en synergie avec les opérateurs, sans aucun risque pour sa santé physique et mentale;

Un aspect important à garder à l'esprit lorsqu'on discute du domaine croissant de la robotique est l'impact sur la société, qu'il s'agisse des opinions, des attitudes, de l'organisation du travail ou de l'emploi. La littérature dans ce domaine est divisée entre ceux qui disent que l'automatisation (et donc la robotique) réduit les emplois et ceux qui disent qu'elle aura un impact neutre ou positif sur l'emploi [248]. Des différences substantielles dans cette tendance ont été mesurées au niveau des groupes sectoriels [53], des pays [64, 236], et des entreprises [62]. Néanmoins, nous pensons qu'il y a un manque de distinction entre les différentes technologies en particulier, à notre connaissance, il n'existe pas d'étude sur l'impact des robots collaboratifs sur l'emploi. En effet, ce type de technologie n'est pas destiné à remplacer les employés humains mais plutôt à travailler à leurs côtés et à améliorer la qualité de leur travail. Les cobots ont également un impact en termes d'organisation du travail, car ils nécessitent une collaboration plus approfondie entre les humains et les machines.

Les capacités cognitives humaines peuvent être utilisées pour superviser les capacités physiques des robots. Cependant, les mouvements soudains et les forces importantes exercées par les robots peuvent causer des blessures graves à leurs partenaires humains. Pour cette raison, une grande attention est accordée à la sécurité pendant l'interaction. Les solutions proposées pour la sécurité sont, par exemple, une division de l'espace ou l'imposition d'une relation asymétrique laissant un faible pouvoir de décision au robot [100]. Grâce à l'amélioration des capacités de détection et de contrôle, les robots ont gagné en importance dans les collaborations récentes entre humains et robots. Les robots estiment l'état physique,

physiologique et cognitif de l'homme afin de collaborer efficacement avec leur partenaire humain. L'état humain est une donnée essentielle pour le processus de décision du robot. La perception de l'état humain repose sur des capteurs qui peuvent être placés dans l'environnement, intégrés dans le robot ou portés par l'humain. En outre, les estimations du comportement humain futur pourraient améliorer la collaboration.

L'importance de connaître l'état et la condition humaine actuelle et future liée à la nécessité de réduire les troubles musculo-squelettiques, l'un des principaux problèmes de l'industrie d'aujourd'hui et que l'industrie 4.0 espère remédier avec de nouvelles technologies et des robots collaboratifs. En effet, les mouvements répétitifs peuvent entraîner des activités professionnelles nocives à long terme. Le stress physique est souvent corrélé au développement de troubles musculo-squelettiques liés au travail. Ces derniers figurent parmi les premières causes de maladies professionnelles dans le monde, représentant un enjeu sanitaire majeur, avec des coûts pour les entreprises et la société [201]. Selon l'Organisation internationale du travail, le troubles musculo-squelettiques constituent la principale cause de pertes économiques liées aux maladies [165, 221].

Non seulement les robots partagent le même espace de travail que les opérateurs humains, mais ils jouent également un rôle plus important dans la collaboration. De nouvelles définitions de la relation entre l'homme et le cobot ont été nécessaires (par exemple, Coopération et Collaboration [99]). Ces relations peuvent être spécifiées par des rôles spécifiques (leader, suiveur) ou par des formes relationnelles d'interaction (réciproque, en miroir). A leur tour, ces comportements se traduisent directement en lois de contrôle pour le robot.

Ce manuscrit présente plusieurs contributions dans le domaine de la collaboration homme-robot qui sont pertinentes pour les cobots et l'industrie 4.0. Plus en détail, cette thèse a été réalisée dans le cadre de C-Shift. C-Shift est un projet exploratoire multidisciplinaire de l'Université de Lorraine qui s'attaque à certains des challenges représentés par l'utilisation de ces nouveaux équipements robotisés dans l'industrie. C-Shift se veut pluridisciplinaire en mobilisant les nombreuses compétences et ressources fournies par les différents laboratoires de l'université impliqués allant de la psychologie, la sociologie à l'informatique, la robotique et l'automatique (CRAN, LORIA, DevAH, PErSEUS, UP&S DITEX, CEREFIGE, AIP-PRIMECA - Pôle S.mart Lorraine, Ergosim). D'autres acteurs extérieurs à l'université soutiennent la recherche, comme l'INRS, le SDIS 54, et des entreprises comme Eclatec et Thyssen Krupp. Structuré autour de trois axes (Adaptation, Organisation, et Santé), le projet vise à faire progresser les connaissances dans l'étude de l'effet des cobots au travail.

L'axe adaptation vise à fournir des outils de modélisation et d'évaluation de l'adaptation des gestes aux trajectoires, de l'adaptabilité des trajectoires et de la réappropriation des tâches par les humains. L'axe organisation vise à étudier l'évolution des routines de production, l'évolution des motivations, et les transitions en termes de compétences en présence de systèmes collaboratifs. Enfin, l'axe santé s'intéresse plus particulièrement à la modélisation de l'activité humaine en relation avec le cobot sur la base de paramètres physiologiques et psychologiques afin de pouvoir calculer des indicateurs clés de performance pour évaluer les risques potentiels (ex : TMS, charges cognitives).

Ces trois axes ont été conçus de manière interdépendante et ont donné lieu à des réflexions interdisciplinaires, soit par l'étude de cas industriels communs, soit par l'expérimentation des résultats sur des plateformes en se rapprochant le plus possible d'un environnement industriel. Par exemple, l'utilisation du modèle numérique et la simulation de l'activité permet à des scientifiques de différents domaines tels que l'organisation de l'entreprise, le contrôle des robots, et la biomécanique de travailler ensemble dans le but de développer une méthode d'intégration d'un cobot sur une unité de production. Cette méthode est en partie basée sur la simulation ergonomique permettant de prédire les comportements gestuels et posturaux et donc les contraintes biomécaniques des opérateurs.

Ce manuscrit illustre le travail effectué dans l'axe "Adaptation" : spécifiquement, nous avons abordé une situation où un humain et un cobot interagissent physiquement. Nos questions de recherche allaient de l'estimation et de la prédiction de la posture et de l'ergonomie de l'humain à la modélisation de

l'adaptation pendant la collaboration. Nous pensons que la combinaison de ces cadres peut apporter une grande contribution à la collaboration. En effet, un robot capable de déterminer le comportement de l'humain avec lequel il collabore est en mesure de concevoir des stratégies qui maximisent la qualité de la collaboration.

L'objectif principal de cette thèse est de fournir des outils pour améliorer la collaboration homme-robot.

Notre approche est résumée comme suit:

1. Utilisation d'une simulation de modèle humain numérique pour évaluer les indicateurs d'ergonomie d'un mouvement du corps entier pour l'exécution d'une tâche.

2. Prédire les mouvements humains en présence de restrictions cinématiques imposées par la collaboration avec le robot.

3. Évaluer différentes lois de commande du robot afin d'émuler le comportement moteur humain pour une meilleure collaboration dans la réalisation des tâches.

4. Étudier l'adaptabilité de l'homme aux changements de la stratégie du robot.

Ces approches comprennent à la fois l'évaluation de l'ergonomie de la posture du corps entier et l'analyse de l'interaction dyadique, à partir de laquelle une application homme-robot peut tirer parti d'une meilleure interaction physique. Compte tenu de la nature pluridisciplinaire des sujets abordés, pour la clarté de la présentation, chaque chapitre présente une analyse de l'état de l'art sur les sujets qui le concernent.

Le chapitre 1 présente une revue de la littérature principale sur l'interaction homme-robot. Nous faisons le point sur les compétences de coopération dont le robot a besoin pour aider les humains à atteindre leurs objectifs, et sur la manière dont ces compétences de haut niveau se traduisent dans les commandes de contrôle de bas niveau du robot. Nous présentons et analysons les réalisations actuelles d'un point de vue centré sur l'homme, en considérant que les robots interagissant avec les humains devraient les aider à améliorer leur santé ou leurs conditions de travail. Enfin, nous présentons les applications de l'interaction physique homme-robot.

Le chapitre 2 passe en revue l'état des technologies de pointe pour l'évaluation ergonomique d'une situation de collaboration humain-robot et nous présentons un nouvel ensemble d'outils pour l'évaluation ergonomique. Nos outils permettent d'évaluer et de visualiser en temps réel les efforts et les postures d'un travailleur, même lorsqu'il interagit physiquement avec un robot. Un modèle humain numérique est utilisé pour estimer la cinématique et la dynamique humaines et visualiser les positions non ergonomiques des articulations, sur la base des données en direct acquises à partir d'un dispositif portable de suivi des mouvements.

Le chapitre 3 passe en revue l'état de l'art des méthodes de prédiction de l'état humain, en particulier lors de la collaboration avec des robots. De plus, nous proposons une méthode pour prédire, en termes probabilistes, les postures d'un opérateur humain pour une trajectoire robot donnée exécutée dans un scénario de collaboration. Nous formalisons le problème comme étant la prédiction de la vitesse des articulations humaines compte tenu de la posture actuelle et de la vitesse de l'effecteur du robot. Nous montrons sur un cas simulé et simplifié et sur des données réelles d'interaction homme-robot que notre méthode est capable d'améliorer la prédiction de la posture humain.

Dans le chapitre 4, nous nous concentrons sur une tâche de co-manipulation homme-robot où un objet doit être extrait avec précaution d'un tube et inséré dans un autre, sans faire de contacts. Cette tâche exige de la précision, et nous attendons à ce que la rigidité de chaque agent soit critique pour rejeter les perturbations qui peuvent mener à l'échec de la tâche. Dans ce contexte, nous posons les questions suivantes : est-il plus efficace et plus performant pour la dyade de coopérer ou de collaborer ? En cas de collaboration, le robot doit-il présenter un comportement d'impédance similaire à celui d'un collaborateur humain ? Parmi les stratégies de collaboration possibles, le robot doit-il imiter le comportement de rigidité de l'humain ou lui rendre la pareille ? Pour répondre à ces questions, nous avons étudié les performances et la rigidité du bras de l'humain interagissant avec un robot Franka.

Dans le chapitre 5, nous proposons une étude humaine dans laquelle 18 participants ont exécuté une tâche de sciage en collaboration entre un robot, où le cobot changeait entre trois stratégies de contrôle différentes. Cette étude vise à donner un aperçu concret de la façon dont les humains perçoivent et réagissent aux changements de comportement du cobot. Plus précisément, comment les humains s'adaptent aux changements de rôles et de stratégies de contrôle du robot collaborateur. En fait, les robots collaboratifs (cobots) ont le potentiel d'augmenter la productivité et la qualité de vie des opérateurs humains dans le contexte de l'industrie 4.0 en leur fournissant une assistance physique. Pour cette raison, il est nécessaire de définir la relation entre l'humain et le cobot et d'étudier comment les deux agents s'adaptent l'un à l'autre. Les expériences ont été réalisées sur une installation impliquant le bras robotique Kuka LBR iiwa.

Introduction

1 A great journey: from steam power to Human-Robot Collaboration

In 1940 Asimov published his first robot novel: *Robbie*. In the story, Asimov imagines a robot (Robbie) designed to play with a little girl. The robot, Asimov tells us, poses no danger to the little girl, and the latter establishes a close bond with him. So much so that the mother worries about her daughter's safety and social skills:

> "I won't have my daughter entrusted to a machine, and I don't care how clever it is. It has no soul, and no one knows what it may be thinking. A child just isn't made to be guarded by a thing of metal. [...] something might go wrong. Some little jigger will come loose and the awful thing will go berserk and... and... [...] There are dozens of little boys and girls that she should make friends with, but she won't. She won't go near them unless I make her. That's no way for a little girl to grow up. You want her to be normal, don't you? You want her to be able to take her part in society."

Robots are seen as harmful but unconscious agents. Capable of injury but without conscience and forced into obedience to humans. This vision is condensed, two years later, in another novel (*Runaround*, 1942) where Asimov proposes the famous three laws of robotics:

1. A robot may not injure a human being or, through inaction, allow a human being to come to harm.
2. A robot must obey the orders given it by human beings except where such orders would conflict with 1.
3. A robot must protect its own existence as long as such protection does not conflict with 1 or 2.

These laws focus on safety (first and third laws) and on the role that the robot adopts during the interaction (second law). These laws, built into the very structure of the robot, are unbreakable and immutable. This removes any responsibility in the robot's operation because if any problem arises it is always traceable to the human who is commanding over the robot. This reminds of the famous aphorism: "*Over 90% of all computer problems can be traced back to the interface located between the keyboard and the chair*".

In later Asimov fiction, robots take some responsibility. For this reason, Asimov also added a fourth, or zeroth law, to precede the others:

0. A robot may not harm humanity, or, by inaction, allow humanity to come to harm.

This last law puts the discussion of robotics on a whole other plane: in fact, at the moment when the robot must put the welfare of humanity before that of the individual, it will no longer be a purely

reactive being but will have to use its ability to predict in the short or long term the influences of current actions on humanity and choose the best actions accordingly. This kind of critical thinking requires weighing different cost functions, predicting and adapting. Moreover, this places the robot in a position of responsibility that it did not possess before.

In this thesis, we will adress all these aspects that worry Asimov in his literature but with an eye on the current problems faced by collaborative robots: human-robot interaction, role assignment, action prediction, adaptation, collaboration, and safety. To do so, and to fully appreciate the ultimate result, let us look back at where robotics and automation were born and developed.

We can begin this narrative in the 1750s. In these years, the First Industrial Revolution converted manual production methods to machines actuated by water and steam power [159]. This event marked a major turning point in history: productivity greatly increased, favoring the rise in population and the rate of population growth.

A century later (the 1870s), these technologies took a step forward during the so-called Second Industrial Revolution. This time the leading roles was the electrification systems and Taylor's work division with mass production and the use of band conveyors. Moreover, many industries started to use Rationalization of work in order to increase its operating efficiency. Known also as Technological Revolution, it was a phase of rapid scientific discovery, standardization, mass production, and industrialization. These advancements enabled the widespread adoption of technological systems such as telegraph and railroad networks, gas and water supply, and sewage systems. In this scenario, automation technologies spread in factories with the intent of reducing human intervention in processes. To execute the desired commands, a new field of knowledge called control theory was born.

Control theory is the basis for process control, which is widely used in automation and for controlling ships and airplanes, which were making their first appearance in those years. Maxwell himself published the first scientific treatise of control theory.

The 1950s are traced back to the birth of modern robotics. The so-called first generation of robots [79, 256] is dated between the 1950s and 1967. The robots of this generation were basically programmable machines controlled by pneumatic actuators. They did not have the ability to really control the modality of task execution, and they were used for a single task, because it was very complicated to reprogram them. Moreover, they had no communication with the external environment. A peculiar feature of these robots is the strong noise they produced when their arms collided with the mechanical stops built to limit the movement of the axes.

The turning point for industrial robotics was, in 1961, with the birth of Unimate by Unimation, which is considered the first industrial robot in history (Fig. 1a). Unimate, which was hydraulically actuated, was immediately installed in an automotive company, preciselly in the General Motors factory (New Jersey, USA). In the same years, several robot manufacturing companies were born, especially in the automotive sector. Companies like Ford and General Motors started to consider the automatization of their production plants and needed devices such as the new robots to achieve this goal. Thus, there was a sudden increase in the orders of robotic devices. In 1969, Japan started to produce robots for the Asian market. This early trend allowed Japan to become one of the leading countries in the robotics field. The diffusion of robots in Europe took place more or less at the same time: 1967 in Sweden and 1969 in Norway. In 1972, FIAT installed the first welding robots in Europe at their plants in Turin (Italy).

The Third Industrial Revolution, in the 1970s, changed again the scientific and industrial scenario of the twentieth century. It is mostly associated with the introduction of digital work and the shifting from mechanical and analogic electronic technology to digital electronics. Central to this revolution is the mass production and widespread use of digital logic and its derived technologies, including computers, microprocessors, and Internet. These technological innovations have transformed traditional production and business techniques. Thanks in large part to the spread of these new technologies, a new wave of

(a) Unimate by Unimation is considered the first industrial robot in history. This robot, hydraulically actuated, was installed in the General Motors factory.

(b) Standford Arm: the first prototype of a robot actuated by electric motors and controlled by a microprocessor.

(c) KUKA Famulus (1973)

(d) PUMA (Programmable Universal Machine for Assembly) robot by Unimation (1978)

(e) The LBR iiwa released in 2014 by KUKA. LBR stands for “Leichtbauroboter” (German for lightweight robot), iiwa for “intelligent industrial work assistant”.

(f) Panda Arm developed by Franka Emika in 2016

Figure 1: Some examples of industrial robots from 1950 until today.

industrial robots arrived [244].

In fact, the second generation of industrial robots is traced back to the years between 68 and 77 [79, 256]. The shift from hydraulic to electric actuators took place in the 1970s, when the electronic components needed to control a robot reached full technical maturity, deeply changing the robot structure. The economic and geopolitical situation at the international level also pushed the trend toward electrically driven robots.The companies were thus forced to find more efficient ways of production. This gave a boost to the installations of industrial robots, which increased by more than 30% per year in the second half of the 1970s. These robots used servo-controllers, which enabled them to perform both point-to-point motion and continuous paths as well.

The first prototype of a robot actuated by electric motors and controlled by a PDP-6 microprocessor was the Stanford Arm (Fig. 1b). The robot was designed in 1969 by Victor Scheinman, a mechanical engineering student at Stanford University. The features introduced by Scheinman in the Stanford Arm and in its successor (Vicarm) were so appreciated that Unimation bought the company and exploited its know-how to design and manufacture (in 1978) the famous PUMA (Programmable Universal Machine for Assembly) robot. In the meanwhile, other companies developed and manufactured other types of industrial robots: Famulus by KUKA in 73 (Fig. 1c), IRB-6 by ASEA (now ABB) in 74, and in the same year HI-T-HAND Expert by Hitachi. This latter was provided with a force feedback system and was able to reach high precision in insertion operations (clearance of about 10 micrometers).

Technical and scientific evolution brought further advances in robotics. The third generation of robots is dated from 1978 to 2000. The industrial robots of the third generation were characterized by a larger extent of interaction with both the operator and the environment. They also had some self-programming capabilities and could reprogram themselves, although by a little amount, in order to execute different tasks. They could be programmed either online or offline, being connected to a PC, which allowed to use high-level language programming. The possibility of high-level offline programming enlarged the operational potential of the robots: for instance, they could elaborate data from sensor readings to adjust the robot movements while taking into account changes in the environment. In addition, some sort of "intelligence" was present in the robots of the third generation, with some (although limited) adaptive capabilities. For instance, by using the data coming from vision or perception systems (e.g. cameras, force sensors, laser scanners), they could locate the objects and the work-pieces. The control software became more "intelligent" by introducing some techniques related to Artificial Intelligence. Both these aspects increased the versatility and flexibility of the robots, which could be employed in more and more complex tasks.

Robots proliferated in early 2000s: in 1995, there were 1.6 industrial robots installed per thousand workers; in 2007, the number was 4.2 [53]. As a result, and following the trends launched by the three industrial revolutions, a new idea of industry gradually emerged: the so-called Industry 4.0. Industry 4.0 is a new concept of manufacturing and industrial automation, integrating new production technologies in order to improve work conditions and to increase productivity and quality. The new paradigm of Industry 4.0 allows communication between humans and machines increasing interconnectivity and smart automation [159]. In this context, the vision of robotics (fourth generation of robots) is also updated by proposing robots with high-level "intelligent" capabilities, such as performing advanced computations, logical reasoning, deep learning, complex strategies, collaborative behaviors.

A concrete result of these approaches is the implementation of cobots [175] . Cobots, or collaborative robots, are industrial robots designed to be able to interact physically with humans during common activities and in shared space (Fig. 1e). The objective of cobots is to improve production performance by allowing a more efficient and scalable distribution of tasks between humans and machines. The idea behind these technologies is to combine the great mental capacities of humans with robots that can take on the fatiguing parts of jobs. This aspect allows collaborative robots to be generic in both how they are built and how they are programmed. In general we can define the following **Collaborative robots**

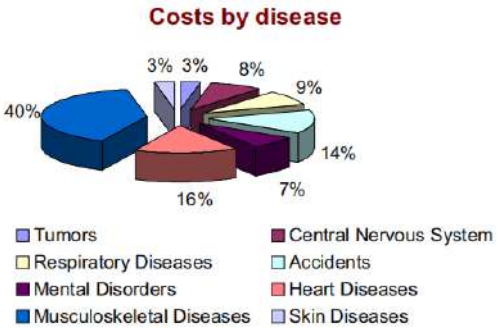

Figure 2: Distribution of costs due to work-related injuries and diseases (Image taken from an International Labor Organization report [221]).

capabilities [70]:

1. Mobility: The ability to easily move the cobot in the production plant;
2. Adaptability: The awareness of the resources, the job characteristics and their implications;
3. Connectivity The ability to communicate with operators and other robot in the work environment, collecting and providing information;
4. Actuation: The ability to develop safe and smooth trajectories;
5. Consistency: The ability to work in continuous without problems, unless malfunctions;
6. Safety: The ability to work in synergy with the operators, without any risk for his physical and mental health;

An important aspect to keep in mind when discussing the growing field of robotics is the impact on society, be that opinions, attitudes, organisation at work or employment. The literature in this field is divided between those who say that automation (and thus robotics) reduces jobs and those who say that it will have a neutral or positive impact in employment [248]. Substantial differences in this trend have been measured as sectoral groups [53], countries [64, 236], and firms [62]. Nevertheless, we think there is a lack of distinction between the different technologies in particular, to the best of our knowledge, a study of how collaborative robots affect employment is lacking. In fact, this type of technology is not intended to replace human employees but rather to work alongside them and improve the quality of their work. Cobots have an impact in terms of work organization too, as they require a deeper collaboration between humans and machines.

Human cognitive abilities can be used to supervise robotic physical capabilities. However, sudden movements and large forces exerted by robots may cause severe injuries to their human partners. For this reason, much attention is devoted to safety during the interaction. Solutions proposed for safety are, for example, a division of the space or imposing strict asymmetric relationship leaving low decision power to the robot [100]. Thanks to improved sensing and control abilities, robots gained major awareness in more recent Human-Robot Collaborations [203]. Cobots estimate the human physical, physiological and cognitive state in order to collaborate with their human partner effectively. The human state is a critical input for the robot decision process. The perception of the human state relies on sensors that can be placed in the environment, embedded in the robot, or worn by the human. Also, estimations of future human behavior could improve collaboration.

The importance of knowing the current and future human state and condition related to the need of reducing Muskular-Skeleton Disorders, one of the major problems in industry nowadays and that the Industry 4.0 hopes to address with novel technologies and collaborative robots. In fact, repetitive movements may incur in job activities that are harmful in the long term [201,213,228]. Physical stress is often correlated to the development of Work-related Musculoskeletal Disorders (WMSDs). WMSDs are among the first causes of occupational diseases worldwide, representing a major health issue, with costs for companies and society [201]. The International Labor Organization reported that the biggest single reason for economic losses regarding diseases are WMSDs [165,221] as showed in Fig.2.

Cobots not only share the same workspace with human operators but also gain a more relevant role in the collaboration. New definitions for the relationship between human and cobot were necessary (e.g.Cooperation and Collaboration [99]). These relationships can be specified through specific roles (leader, follower) or through relational forms of interaction (reciprocal, mirrored). In turn, these behaviors translate directly into control laws for the robot.

This manuscript presents several contributions in the area of human-robot collaboration that are relevant for cobots and Industry 4.0. More in detail, this thesis originated in the context of C-Shift. C-Shift is an exploratory multidisciplinary project of University of Lorraine which adresses some of challenges represented by the use of these new robotized equipments in industry. C-Shift is intended to be multidisciplinary by mobilizing the many skills and resources provided by the various laboratories of the university involved ranging from psychology, sociology to informatics, robotics and automation(CRAN, LORIA, DevAH, PErSEUS, UP&S DITEX, CEREFIGE, AIP-PRIMECA - S.mart Lorraine cluster, Ergosim). Other actors outside the university endorse the research, such as INRS, SDIS 54, and companies such as Eclatec and Thyssen Krupp. Structured around three axes (Adaptation, Organization, and Health), the project aims to advance knowledge in the study of the effect of cobots at work.

The adaptation axis aims to provide modeling and evaluation tools for the adaptation of gestures to trajectories, adaptability of trajectories, and re-appropriation of tasks by humans. The organization axis aims at studying the evolution of production routines, the evolution of motivations, and transitions in terms of skills in the presence of collaborative systems. Finally, the health axis is more specifically interested in modeling human activity in relation to the cobot on the basis of physiological and psychological parameters in order to be able to calculate key performance indicators for assessing potential risks (e.g. MSD, cognitive loads).

These three axes were conceived in an interdependent way and led to interdisciplinary reflections, either through the study of common industrial cases or the experimentation of the results on platforms by getting as close as possible to an industrial environment. For example, the use of the digital model and the simulation of the activity allows scientists from different fields such as company organization, control of robots, and biomechanics to work together with the objective of developing a method of integration of a cobot on a production unit. This method is partly based on ergonomic simulation allowing the prediction of gestural and postural behaviors and thus the biomechanical constraints of the operators.

This manuscript illustrates the work conducted in the "Adaptation" axis: specifically, we adressed a situation where a human and a cobot are physically interacting. Our reserch questions ranged from estimating and predicting the human's posture and ergonomics to modeling adaptation during collaboration. We believe that the combination of these frameworks can make a great contribution to collaboration. Indeed, a robot that is able to determine the behavior of the human with whom it collaborates is able to design strategies that maximize the quality of collaboration.

2 Contributions and Thesis Organization

The main objective of this thesis is, to provide tools to improve human robot collaboration.. Our approach is summarized as follows (Fig. 3):

1. Using a Digital Human Model simulation to evaluate ergonomics indicators of a whole-body motion for a task execution

2. Predict human movements in the presence of kinematic constraints imposed by the collaboration with the robot

3. Evaluate different robot control laws to emulate the human motor behavior for a better task collaboration

4. Study the human adaptability to changes in the robot policy

These approaches include both whole-body posture ergonomics evaluation, and dyadic interaction analysis, from which a human-robot application can leverage a better physical interaction. In Fig.3 is described the structure of the thesis dividing the various aspects covered in the HRC field into blocks. Given the multidisciplinary nature of the topics, for clarity of presentation, each chapter presents a state-

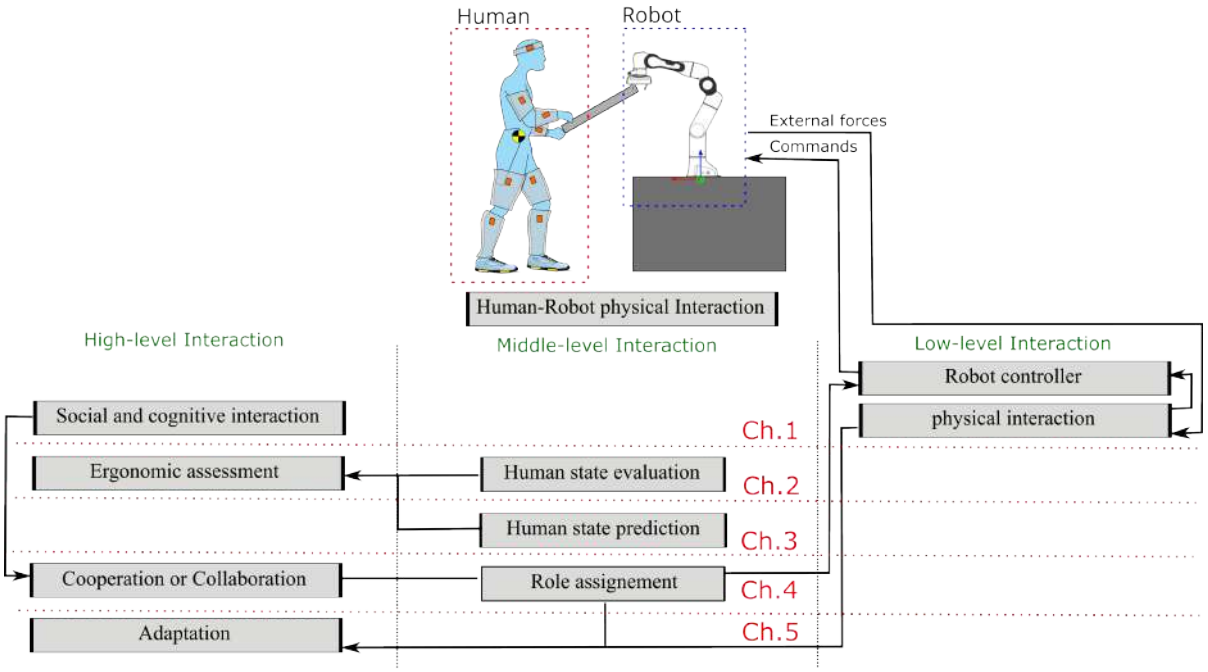

Figure 3: Overview of the thesis divided by sections

of-the-art review of its relevant topics.

Chapter 1 reviews the main literature of human-robot interaction. We report on the cooperation skills that the robot needs to help humans achieve their goals, and how these high-level skills translate into the robot's low-level control commands. We present and analyze the current achievements from a human-centered point of view, considering that robots interacting with humans should help them to improve their health or working conditions. Finally, we report applications of human-robot physical interaction.

Chapter 2 reviews state of the art technologies for ergonomic assessment and we present a novel set of tools for ergonomics assessment. Our tools provide an online evaluation and visualization of strenuous efforts and postures of a worker, also when physically interacting with a robot. A digital human model is used to estimate human kinematics and dynamics and visualize non-ergonomic joint angles, based on the on-line data acquired from a wearable motion tracking device.

Chapter 3 reviews state of the art methods for human state prediction, in particular during collaboration with robots. Moreover, we propose a method to predict, in probabilistic terms, the human postures of a human operator for a given robot trajectory executed in a collaborative scenario. We formalize the problem as the prediction of the human joints velocity given the current posture and robot end-effector velocity. We show in a simulated toy problem and on real human-robot interaction data that our method is able to improve model-based inverse kinematics prediction, sample-based prediction, and regression methods that do not consider geometric constraints.

Chapter 4 we focus on a human-robot co-manipulation task where an object has to be carefully extracted from a tube and inserted into another one, without making contacts. This task requires precision, and we expect the stiffness of each agent to be critical to reject disturbances that may lead to task failure. In this context, we ask the following questions: is it more efficient and task-performing for the dyad to cooperate or to collaborate? When collaborating, should the robot exhibit an impedance behavior similar to the one of a human collaborator? Among the possible collaboration strategies, should the robot imitate or reciprocate the human's stiffness behavior? To answer these questions, we investigated the performance and arm stiffness of the human interacting with a Franka robot.

Chapter 5 we propose a human study in which 18 participants executed a collaborative human-robot sawing task where the cobot altered between three different control strategies. This study want to give a concrete insight of how humans perceive and react to changes in the cobot behaviour. Specifically, how humans adapt to changing roles and control strategies of collaborating robot. In fact, collaborative robots (cobots) have the potential to augment productivity and the life quality of human operators in the context of Industry 4.0 by providing them physical assistance. For this reason, it is necessary to define the relationship between human and the cobot and to study how the two agents adapt to each other. The experiments were performed on a setup involving Kuka LBR iiwa robotic arm.

3 Publications

This thesis has produced several contributions in the form of academic articles, software, and video demonstrations, described below. Software that can be found on the GitLab and GitHub accounts. Datasets collected throughout the thesis can be found in Zenodo.

Accepted / Published Articles

– **Survey on Human-Humanoid interaction:** it reviews different aspects of human-humanoid interaction, such as social factors, robot interaction control, human perception and human behavior modelling. Additionally it also reviews relevant applications on the field.

  Contribution: Our contribution was related to the state-of-the-art on controlling an humanoid robot while it is interacting with humans.

Lorenzo Vianello, Luigi Penco, Waldez Gomes, Yang You, Salvatore Anzalone, Pauline Maurice, Vincent Thomas, and Serena Ivaldi. Human-humanoid interaction and cooperation: a review. *Current Robotics Reports*, 2021

– **Human Posture Prediction during Physical Human-Robot Interaction**

Contribution: We proposed a tool for predicting human movements in a probabilistic way and considering kinematic constraints imposed by the collaboration with the robot.

Lorenzo Vianello, Jean-Baptiste Mouret, Eloïse Dalin, Alexis Aubry, and Serena Ivaldi. Human posture prediction during physical human-robot interaction. *IEEE Robotics and Automation Letters*, 6(3):6046–6053, 2021

Video is available at: video posture prediction.

– **Latent Ergonomics Maps:** Real-time visualization of estimated ergonomics of human movements during human-robot co-manipulation task.

Contribution: We participated to the development of the Digital Human Model, and to the data collection for the experiments, the design of the Latent Ergonomic Map, and the control of the Franka Robot. We proposed Latent Ergonomics Maps, an important tool for ergonomics visualization.

Lorenzo Vianello, Waldez Gomes, Freek Stulp, Alexis Aubry, Pauline Maurice, and Serena Ivaldi. Latent ergonomics maps: Real-time visualization of estimated ergonomics of human movements. *Sensors*, 22(11):3981, 2022

Video is available at: video Latent Ergonomics Map.

In Preparation

– **Cooperation or collaboration?** comparison of human-inspired impedance strategy in a human-robot co-manipulation task. The dyad was analyzed according to their motion, muscle activation signals and efficiency executing the task.

Contribution: We found important differences on the motor behavior of a human-robot dyad between different forms of coordination.

Lorenzo Vianello, Waldez Gomes, Pauline Maurice, Alexis Aubry, and Serena Ivaldi. Cooperation or collaboration? on a human-inspired impedance strategy in a human-robot co-manipulation task. 2022

Video is available at: video Human-Franka co-manipulation.

– **Role transition and adaptation** we propose a human study in which participants executed a collaborative human-robot sawing task where the cobot altered between different control strategies.

Contribution: We found that, in this kind of task, not only the type the current role of the cobot, but also the past ones influence the behavior of the human operator.

Lorenzo Vianello, Serena Ivaldi, Alexis Aubry and Luka Peternel. The effects of role transitions and adaptation in human-cobot collaboration. 2022

Video is available at: video Human-Kuka adaptation.

1

Physical Human-Robot Interaction

Robots have the potential to assist humans in several domains, from agriculture to healthcare, from entertainment to manufactory. To find their place into our daily life, where complex interactions and collaborations with humans are expected, their physical interaction skills need to be further improved. Physical interaction with humans requires appropriate modeling and real-time estimation of the human state and intention. This can help prevent unintentional collisions and limit movements that can cause musculoskeletal disorders in humans. This information is required both at a high-level (e.g. human role and interaction behaviour) by the cooperative decision-making policy and at a low-level (e.g. forces and torques) by the interaction controller that implements the physical interaction. Real-time constraints induce simplified models that limit the decision capabilities of the robot during cooperation.

In this chapter, we review the current achievements in the context of human-robot interaction. We report on the cooperation skills that the robot needs to help humans achieve their goals, and how these high-level skills translate into the robot's low-level control commands. We present and analyze the current achievements from a human-centered point of view, considering that robots interacting with humans should help them to improve their health or working conditions. Finally, we report applications of human-robots physical interaction. This chapter introduces some of the terminology used in the following chapters and presents today's scenario of human-robot physical Interaction.

This chapter is based on the article hal-03413650v1, which was presenting the state of the art in human-humanoid interaction. While human-humanoid interaction is also a form of HRI, and many elements are common to humanoids and robotic manipulators, this chapter is focused on human-manipulator (or robot) interaction. For this reason, we significantly extended the discussion on some aspects of the physical interaction such as the type of interaction and compliant control laws. In particular, we presented in detail the impedance control we used in the course of this thesis. In addition, we extended the applications in which human and manipulator physically interact by presenting examples in different domains.

Human-Humanoid Interaction and Cooperation: a Review

Lorenzo Vianello[1,2†], Luigi Penco[1†], Waldez Gomes[1], Yang You[1], Salvatore Maria Anzalone[3], Pauline Maurice[1], Vincent Thomas[1] and Serena Ivaldi[1*]

[1*]Inria, Loria, Université de Lorraine, CNRS, Nancy, F-54000, France.
[2]CRAN, Nancy, F-54000, France.
[3]Laboratoire CHArt, Université Paris 8 , Paris, F-93200, France.

*Corresponding author(s). E-mail(s): serena.ivaldi@inria.fr;
Contributing authors: lorenzo.vianello@univ-lorraine.fr; luigi.penco@inria.fr; waldez.azevedo-gomes-junior@inria.fr; yang.you@inria.fr; sanzalone@univ-paris8.fr; pauline.maurice@loria.fr; vincent.thomas@loria.fr;
†These authors contributed equally to this work.

Abstract

Purpose of review: Humanoid robots are versatile platforms with the potential to assist humans in several domains, from education to healthcare, from entertainment to the factory of the future. To find their place into our daily life, where complex interactions and collaborations with humans are expected, their social and physical interaction skills need to be further improved. **Recent findings:** The hallmark of humanoids is their anthropomorphic shape, which facilitates the interaction but at the same time increases the expectations of the human in terms of advanced cooperation capabilities. Cooperation with humans requires an appropriate modeling and real-time estimation of the human state and intention. This information is required both at a high-level by the cooperative decision-making policy and at a low-level by the interaction controller that implements the physical interaction. Real-time constraints induce simplified models that limit the decision capabilities of the robot during cooperation.

Figure 1.2 shows the interconnection between the key building blocks that enable a robot to make complex decisions and take actions to cooperate with a human: it is designed to guide the reader through

the different topics and sections. In Section 1.1 we discuss the principal issues in building cognitive and social skills. In Section 1.2 we formalize the concept of physical human-robot cooperation, while in Section 1.3 we overview the main interaction control approaches that enable low-level physical interaction between the robot and the human. The knowledge of the human "state" is required by both the high and the low level control to build human-aware control plans: hence we present the main methods used to model and perceive the humans in Section 1.4. Finally, in Section 1.5, we report on the current main application of robots interacting and cooperating with humans: personal assistants, co-workers and avatars.

1.1 High-level interaction: Social and cognitive interaction

Endowing robots with cognitive skills is a pivotal step to safely blend them in our society. Such skills go beyond the abilities of reasoning, exploration, learning, and are rather oriented towards a mutual interplay between the robotic "brain", its physical embodiment and its environment. In this sense, cognitive skills emerge from a proper and coherent exploitation of internal models of the knowledge the robot has of itself and of its surrounding. These models mediate past knowledge with new perceptions and are continuously and incrementally updated according to feedback from new experiences [127]. The models are not only able to represent temporal information [250], but also spatial concepts [197].

Consistent social interaction is achieved when the robot is perceived by the human partners as "believable" [172] through its appearance and through the consistency of its actions and its social behaviors [245]. Any physical or behavioral inconsistency can be quickly spotted, perceived as "strange", making the robot become unacceptable for the human partners.

In this sense, the behavior consistency requested to robots is not limited to a coherent sequence of actions, but it is extended to the challenge of being "readable","legible"and "predictable" by human partners [222]: in cobots, these requirements led to the development of algorithms to plan legible motions, which should help humans in understanding how to better cooperate with the robot. This kind of behaviour allows to increase the trust of the human in the robot, an important aspect in these kind of relationships [9]. Achieving coherent robot behaviors in response to the human reactions strictly relies on the production of metrics, models, techniques and algorithms aimed at capturing and describing the dynamics of the social interplay [242]. The "social skills" required by cobots in industrial environment may not be advanced as these required by social robots for rehabilitation or entertainment. However, explicitly taking into account the human presence in their perception-cognition-action loop [32] is a fundamental skill for robots that have a higher degree of physical interaction with humans (e.g. cobots and exoskeletons).

To evaluate how people perceive robots, several questionnaires have been proposed, such as Godspeed [17], and Negative Attitudes Toward Robots Scale (NARS) [218]. Results from such questionnaires, together with human's behavioral metrics, are extremely useful tools to evaluate the effectiveness of the social interplay with robots in real-world scenarios [11].

To summarize, the high-level aspects that need to be considered in implementing control strategies for cobot and human-robot collaboration stations [125] are:

1. Comunication channels between human and robot (e.g. natural language, motion caption, facial expressions)

2. Readable robot intentions, this can be achieved with strategies which improves the robot transparency (e.g. robot animation to show robot behaviour, predictable motions, familiarization)

3. Interactive/active learning, robot improves its ability is performing the task

(a) Human-Robot comanipulation in Industry [210].

(b) Robotic co-worker for industrial abrasive blasting [44].

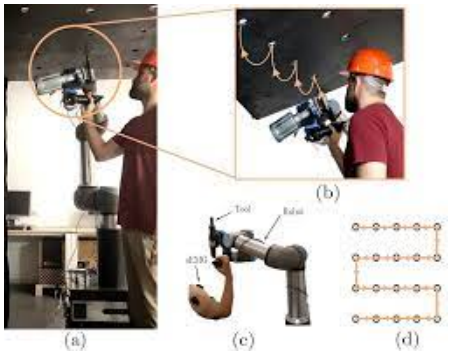

(c) Assistive collaborative robot [83]

(d) Assistive collaborative robot [178]

(e) Collaborative screwing using MOCA-MAN [111]

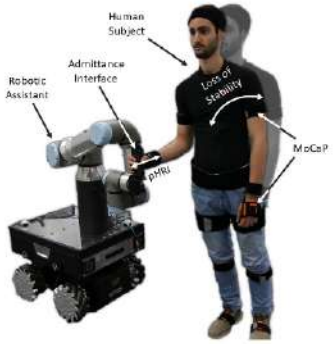

(f) Kairos platform helping Improving Standing Balance for human [193]

(g) Baxter helps olders stay active at home [74]

(h) Teleoperated Viper with shared control [81]

Figure 1.1: Examples of human-robot physical Interaction: the first three figures present examples of industrial applications while the other show scenarios still being investigated.

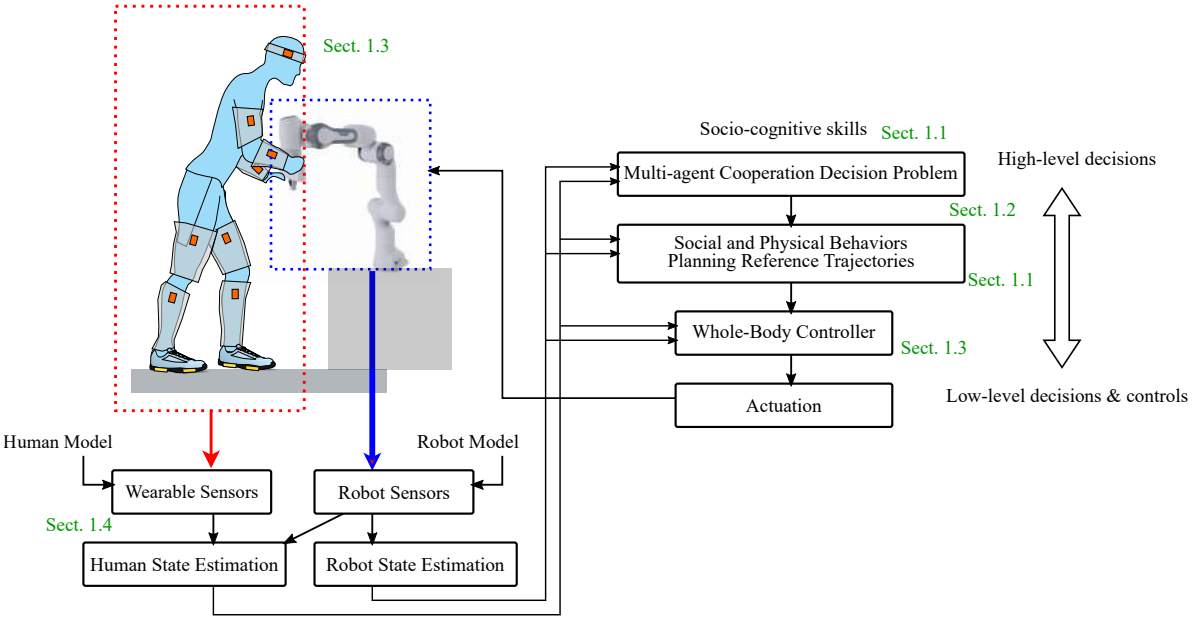

Figure 1.2: Schematic drawing of the components involved in Human-Robot Interaction and cooperation.

4. Higher robot cognitive ability to learn how to solve complex task by decompose them and find solutions.

1.2 Middle-level interaction: Cooperation, decision problem and role assignement

Social and cognitive skills are critical to make the robot believable and to ensure it can perform in day-to-day interactions to significant endeavors. These skills are the building blocks that enable a robot to pro-actively cooperate with humans and help them achieve their goals. Developing these skills requires a human-centered design of the robot's intelligence, that at many decision levels should integrate the goals and costs of the human's actions to plan suitable high-level assistance actions and translate those decisions into the robot low-level control commands. Figure 1.2 shows the interconnection between these skills: to cooperate, the robots need to formulate the problem of finding the best sequence of actions that assist the human in achieving their goals and minimizing their costs, considering the constraints and limits of the robots and the human as individuals first, then as interacting agents. This also requires cognitive reasoning, in particular taking the human perspective [199]. Solving this problem requires high-level decision making capabilities, which are then translated at a lower level into the modules producing social and physical interaction behaviors, also translated into lower-level motor commands for the robot.

Several approaches are possible to design this robot high-level decision making system. Among those approaches, the robot's policy can be designed based on expert knowledge or directly learnt through interactions with a human, however, in both cases, this would require to encompass all the possible encountered situations and the variety of human reactions (needing a complete knowledge of all the possible situations in the first case or an important amount of data in the second one).

Whereas a planning approach requires a representation of the interaction situation, a detailed knowledge of its dynamics, and an adaptation of the high-level strategy to low-level controls, it still seems a promising direction: (1) it can leverage generic models and algorithms to automatically compute a

robot's strategy from the definition of the collaborative task, (2) planning approaches are able to deal with several sources of uncertainties like sensor noises or uncertainties regarding the human behavior or mental state, (3) planning approaches are generic and various questions of paramount importance for collaborative robotics have been represented and can merge in that same framework like intention estimation [185], role attribution and/or inference of user profile [162], and, (4) planning allows to compute strategies considering the long-term consequences of the robot's behaviour which could have a huge impact in the decision process (*e.g.*, when optimizing the user's fatigue).

More precisely, in a planning context, a collaboration problem can be modeled as a Multi-Agent sequential decision problem where two agents, the human and the robot, select actions according to their respective policies in a coordinated way to achieve a common task, where typically cumulative shared rewards represent the common goal. This problem can typically be addressed in game theory framework, defining the agents' strategies and the rewards.

Due to the difficulty in modeling the complex and often unpredictable human behavior, the most common formulations of human-robot interaction and cooperation resort to single-agent problems: they only consider the robot's point of view, while the human is assumed as part of the environment and modelled as purely reactive agent with a known policy [219]. Solving a single-agent problem consists in building the long-term robot's policy and potentially influencing the human reactions in order to complete the collaborative task in the most efficient way [26]. A different approach has been proposed by Nikoladis *et al.* [164]: Human-Robot Cross-Training. Human-Robot Cross-Training is a strategy validated for human team training. Cross-training is an interactive planning method in which human and robot iteratively switch roles to learn a shared plan for a collaborative task. They encode a teaming model that captures knowledge about the role of the robot and the role of the human team member.

These kind of models are often formalized by a Partially Observable Markov Decision Process (POMDP), a general framework well suited to model different collaboration situations faced by the robot: it assumes that the robot is acting in an uncertain environment, described by a Markov Decision Process (MDP) but the robot cannot directly observe its underlying state. The uncertainty of the human reaction can be represented by considering a stochastic evolution of the system. A POMDP is usually defined by the tuple [103]:

$$< \boldsymbol{S}, \boldsymbol{A}, \boldsymbol{T}, \boldsymbol{\Omega}, \boldsymbol{O}, \boldsymbol{r}, \boldsymbol{b}_0 > \tag{1.1}$$

At each time step, the agent is in a state $s \in S$ performs an action $a \in A$ influencing the evolution of the state of the system according to a probability distribution $T(s, a, s') = P(s' \mid s, a)$ and receives an observation $o \in \Omega$ depending on the new state that has been reached and the observation function $O(o, s) = P(o \mid s)$. The agent has no direct access to the state of the system but only to those observations. Using past observations, the agent infers a belief-state, a distribution of probability over the true state of the system, and makes their decision based on this estimate.

Several algorithms can be used to build the optimal robot policy (e.g. [209]), which may also include actions to gather information about the human state and simultaneously estimate the hidden variable conditioning their actions (e.g., their profile or objective) [163]. As such, POMDPs are ideal to develop collaborative robot strategies in absence of structured rewards or structured cooperation instructions.

One of the main difficulties in using this approach lies in the modeling of the human behavior: the critical questions are how to consider the expectation of the human toward the robot and how they will adapt their policy depending on the robot's actions. Often, the interaction between human and robot is structured along "roles", .e.g, leader/follower, which may determine not only high-level decisions but also low-level actions (e.g., stiffness in impedance control). For example, in a strictly asymmetric leader-follower case, the humans' cognitive abilities can be used to supervise or to lead the robots' superior physical capabilities; whereas in an egalitarian roles distribution, where the leadership is not specified, the robot may need to continuously adjust its own role, and consequently its behavior, according to the

human's intention and estimated role [132]. Jarrasse *et al.* [100] summarise findings on the growing field of role assignment policies for human-robot motor interaction. Several human-robot relationships could be identified in the literature: leader-follower, supervisor-subordinate, partner-partner, teacher-learner and fully autonomous robot.

These relationships vary among the considered task, for instance, for lifting and carrying heavy or bulky objects, a common approach is the human-leader and robot-follower. For this reason, various platforms, such as mobile robots with a robotic arm, have been developed [117] [116]. These robots are equipped with controllers to detect the intentions of the human operator [217], in this way, the robot could follow the human-leader motions. For example, in [217], the robot follows the human guidance during a cooperative table lifting task by tracking the movement of his hands holding the table.

Equalitarian roles distribution beyond the leader-follower scheme have been investigated such as supervisor-subordinate, cooperators, or teacher-learner [97], [171]. For example, Lawitzky *et al.* [123] compared three different effort sharing policies during the transportation of a bulky object by a human and a robot. Results suggest an improvement (minimization of applied force level and tracking error) through a more proactive robot behavior. Evrad *et al.* [69] introduced a flexible role distribution enabling each partner to tune between the two distinct extreme behaviors of leader and follower using an homotopy (a weighting function that allows a continuous change between two behaviors), giving rise to an implicit bilateral coupling.

On the same path, Kheddar *et al.* [106] implemented homotopy as a speculative model for Human-Robot interaction as a time-variant, continuous interpolation function between the two extremes (leader $\mathcal{L}$ of follower $\mathcal{F}$) behaviors for each individual involved in the interaction, the following homotopy function can be defined:

$$\boldsymbol{u} = \boldsymbol{\alpha}\mathcal{L} + (1 - \boldsymbol{\alpha})\mathcal{F}$$

where u are the control actions, $\mathcal{L}$ corresponds to a leader behavior while $\mathcal{F}$ corresponds to a follower behavior. Each agent defines his/her role through the parameter $\boldsymbol{\alpha}$ (continuous and time variant). This formalization was tested in a table lifting task [68]. Mortl *et al.* [156] showed that, in a human-robot load transport task, continuous dynamic role assignment policy leads to better performance than a constant role assignment one. However, it seems that humans preferred the constant role, where robot behavior is more predictable and thus easier to consider in their motor action. We use two terms to distinguish these types of interaction [99]: cooperation and collaboration.

Cooperation occurs when different roles are ascribed to the agents prior to the beginning of a task and this distribution is not questioned until its completion. In contrast, in **collaboration**, there is no priori roles distribution but a spontaneous roles distribution depending on the interaction history. Any physical interaction with negotiations and discussions to accommodate others while considering their perspective belong to this category. While in collaboration the agents work on an even basis, cooperation has an uneven distribution of subtasks or roles during the task.

Another difficulty is defining the right rewards, so that the robot policy can truly help the human to achieve their goal. This is not an easy task since, usually, the utility we would like to optimize is not reduced to a single dimension and must consider all possible criteria. It might involve the efficiency of the task achievement but also the human ergonomics and physiological comfort, the cognitive load, as well as unknown objectives [185]. This is a problem of paramount importance due to *reward hacking problems* [10]: the produced policy will optimize the given reward but might have unexpected side effects that could be counter-productive or dangerous. Building policies able to simultaneously estimate the hidden variables determining the human reactions and consider long-term consequences of the robot actions are a key component to build adaptive robots that collaborate with humans in a proficient way. Jarrasse *et al.* [99], using neuroscience studies, formalize the humans interaction models as lead by the desire of minimizing error on task execution ($\boldsymbol{e}$) and effort ($\boldsymbol{u}$). This can be modelled as the minimization

Exchange	Interaction	Subtype	Agent 1	Agent 2
Asymmetric	**Cooperation**	assistance	$V_1 = \gamma_1 \hat{e}_2^2 + \delta_1 \hat{u}_2^2$ Follower	$V_2 = \alpha_2 e_2^2 + \beta_2 u_2^2$ Leader
Asymmetric	**Cooperation**	education	$V_1 = \gamma_1 \hat{e}_2^2 + \beta_1 u_1^2$ Teacher	$V_2 = \alpha_2 e_2^2 + \beta_2 u_2^2$ Student
Symmetric	**Collaboration**	partners	$V_1 = \alpha_1 e_1^2 + \beta_1 u_1^2 + \gamma_1 \hat{e}_2^2 + \delta_1 \hat{u}_2^2$	$V_2 = \alpha_2 e_2^2 + \beta_2 u_2^2 + \gamma_2 \hat{e}_1^2 + \delta_2 \hat{u}_1^2$
Symmetric	**Collaboration**	competitors	$V_1 = \alpha_2 e_2^2 + \beta_2 u_2^2 - \gamma_1 \hat{e}_2^2 - \delta_1 \hat{u}_2^2$	$V_2 = \alpha_2 e_2^2 + \beta_2 u_2^2 - \gamma_1 \hat{e}_2^2 - \delta_1 \hat{u}_2^2$

Table 1.1: Definition of main kinds of behaviors (in interactive tasks) as defined in [99]. With respect to the original formulation, we replaced the terminology master/slave with leader/follower.

of the cost function

$$\boldsymbol{V}(t) = \beta_e \boldsymbol{e}^2(t) + \beta_u \boldsymbol{u}^2(t) \quad \text{with} \quad \beta_e, \beta_u > 0$$

In a similar way, multi-agent interactions could be modeled as a problem of minimizing cost functions composed by an error on task execution ($\boldsymbol{e}$) and effort ($\boldsymbol{u}$) of both the agents. In Tab. 1.1 could be find the cost functions associated to different interactions behaviors as presented in [99]. For instance, a good teacher (education relationship) will try to maximize the student's independence by minimizing his own effort in order to challenge the student, let him perform according to his capabilities and eventually increase them. Following the previous paper, Li *et al.* [130] presented an interactive robot controller able to understand human's control strategy and react optimally to its movement. The cost function to be minimized is designed dependent by an error on position and by joint torques.

In the next chapters, particularly in Chapters, 4, 5 we will go into more detail about some aspects of mid-level interaction. In addition, in these chapters we present studies conducted with the intention of observing how a human subject interacts with a robot as the robot's role changes. We will present different roles associated with the robot (Robot leader, follower, reciprocal, and mirrored) and analyze which of these the human prefers. We also focused on studying how subjects adapt to different profiles of the robot. All the factors presented in the previous sections (cooperation/collaboration, human state estimation, and role assignement) directlty translate in low level robot controlling. In the next section we present how the robot has to be controlled adequately to enable physical interactions (considering external force and stability of the system).

1.3 Low-level interaction: Motion control for physical interaction

The previous section discussed how the robot can plan for cooperative actions at a high level, taking into account the human's goals and states. High-level decisions must be translated into low level commands, typically by means of desired behaviors, implemented as desired trajectories, which need to be translated into motor commands, as represented in Figure 1.2. The critical aspect that distinguishes a robot motion controller for cooperation with humans from a generic one for the robot alone in the environment is to consider the human in the design of the motion control, i.e., to design a "human-aware" controller [191]. This means to consider the human state, their dynamics [167], their intended movement [56], and use the predictions of their future states to plan suitable robot motions and physical interactions. These interactions often result in complex behaviors, where the robot needs to simultaneously control various aspects of its internal and external motion like posture, manipulation and contact stability. All these aspects are usually considered as different objectives in a multitask optimization problem. This is classically

formulated as a Quadratic Program (QP):

$$\begin{aligned} \arg\min_{\boldsymbol{u}} & \sum_k w_k(\|\boldsymbol{A}_k\boldsymbol{u}-\boldsymbol{b}_k\|^2)+\epsilon\|\boldsymbol{u}\|^2, \\ s.t. \quad & \boldsymbol{d}_{min}\leq \boldsymbol{D}\boldsymbol{u}\leq \boldsymbol{d}_{max}, \\ & \boldsymbol{u}_{min}\leq \boldsymbol{u}\leq \boldsymbol{u}_{max}, \end{aligned} \tag{1.2}$$

where the index k identifies a given task; $\boldsymbol{u}$ is the control input vector (torques, joint positions or velocities); $\boldsymbol{A}_k$ is the equivalent Jacobian matrix of the task k; $\boldsymbol{b}_k$ is the reference value for the task, ϵ is a regularization factor used to handle singularities. $\boldsymbol{u}_{min}$ and $\boldsymbol{u}_{max}$ are the control input limits, and $\boldsymbol{d}_{min}\leq \boldsymbol{D}\boldsymbol{u}\leq \boldsymbol{d}_{max}$ are other equality and inequality constraints, such as collision avoidance or contact related constraints. High priority tasks can be regarded as equality constraints while, lower priority tasks can be considered in the cost function with relative weight w_k.

The QP formulation provides extreme flexibility in the choice of the type of control, allowing one to solve inverse kinematics [173], inverse dynamics [226] problems for both position-controlled and torque-controlled robots.

In dynamic environments and in the presence of humans, torque-controlled robots are generally the preferred choice. These approaches can ensure safety and contact stability under unexpected physical interactions [80], so they are appropriate to handle possible collisions between the robot and the humans during the robot's trajectory execution. In other situations, the robot has to adapt its motion to that of the human, considering some variability in the execution of the various task references and considering perceived external forces. In this case, to achieve a stable robot behavior while maintaining contact with the human, compliant control approaches such as impedance control [34], and admittance control [187] have been applied.

In fact, whenever the robot interacts with an environment, this latter introduces disturbances in the task execution. For this reason, it is important to modulate disturbance response in order to permit control of dynamic interactions (the so-called feedback control) [94]. The general structure of an impedance control system is composed of a high-level supervisory system in an open loop and a lower level controller which controls the manipulator in real time. Let the robot equation of motion be:

$$\boldsymbol{M}(\boldsymbol{q})\ddot{\boldsymbol{q}}+\boldsymbol{C}(\boldsymbol{q},\dot{\boldsymbol{q}})\dot{\boldsymbol{q}}+\boldsymbol{g}(\boldsymbol{q})=\boldsymbol{\tau}-\boldsymbol{J}^{\top}\boldsymbol{F}_{ext} \tag{1.3}$$

with $\boldsymbol{M}\in\mathbb{R}^{n\times n}$ the inertia matrix, $\boldsymbol{C}\in\mathbb{R}^{n\times n}$ the matrix of Coriolis and centrifugal effects, $\boldsymbol{g}(\boldsymbol{q})\in\mathbb{R}^n$ the vector of gravity forces, $\boldsymbol{J}\in\mathbb{R}^{6\times n}$ the end-effector Jacobian, $\boldsymbol{\tau}\in\mathbb{R}^n$ the joint torque vector, and $\boldsymbol{F}_{ext}\in\mathbb{R}^6$ the interaction wrench at the end-effector. The impedance control law controls directly the pose (or the robot posture) and indirectly the external forces. To do that the general formulation control the interaction forces with the enviromnent as a mass-spring-damper system:

$$\boldsymbol{M}(\boldsymbol{q})(\ddot{\boldsymbol{x}}-\ddot{\hat{\boldsymbol{x}}})+\boldsymbol{D}(\dot{\boldsymbol{x}}-\dot{\hat{\boldsymbol{x}}})+\boldsymbol{K}(\boldsymbol{x}-\hat{\boldsymbol{x}})=\boldsymbol{F}_{ext} \tag{1.4}$$

where $\boldsymbol{K}\in\mathbb{R}^{6\times6}$, $\boldsymbol{D}\in\mathbb{R}^{6\times6}$ and $\boldsymbol{M}\in\mathbb{R}^{6\times6}$ are the respectively stiffness, damping and inertia matrices in Cartesian space, and $\boldsymbol{x}$ and $\boldsymbol{x}_d$ are respectively the actual and desired end-effector poses. In our works to mantain a simpler formulation we decided to consider a simplified version (spring-damper). In spring-damper cartesian impedance control the inertia component is removed. The resulting control command is calculated as:

$$\boldsymbol{\tau}=\boldsymbol{J}^T(\boldsymbol{q})[-\boldsymbol{K}(\boldsymbol{x}-\hat{\boldsymbol{x}})-\boldsymbol{D}(\dot{\boldsymbol{x}}-\dot{\hat{\boldsymbol{x}}})]+g(\boldsymbol{q}) \tag{1.5}$$

This kind of formulation is well suited for slow movements and with low accelleration ($\ddot{\boldsymbol{x}}\simeq 0$). The behavior of the controller is entirely described by the choice of control parameters (stiffness $\boldsymbol{K}$ and

damping $\boldsymbol{D}$ matrices) and the desired trajectory. Stiffness matrix defines how much the controller wants to follow the reference, similarly damping instructs how much the controller is forced to execute a reference at speed. High stiffness and damping result in a controller that is very stiff in executing its trajectory conversely low values define a more compliant controller.

Impedance control is well suited to unfamiliar environments, such as human-robot physical interaction. For these situations the coefficient of the of control law ($\boldsymbol{K}, \boldsymbol{D}$) could be learned [35, 105, 109], in other situations could be better to learn $\boldsymbol{x}_d$ expressed as reference trajectory [37] or attractor points [77]. For instance, Li *et al.* [130] presented a cartesian impedance control able to adapt to the control strategy of the human user during several interaction scenarios (namely cooperation, co-activity, competition) and able to react optimally. The controller combines and observer for the end-effector state and differential game theory to successfully perform the task with the minimum effort. In general, it is good practice to make either the reference or the controller parameters variable so as not to run into unstable situations.

Indeed, one aspect that all these solutions must satisfy is system stability. In impedance control, stability is a constraint is often associated with the passivity of the system, that is, its property of never ejecting energy. One way to verify this property is through Lyapunov-based tools. Unfortunatelly these tools become hard to use when the dynamics of the environment are unknown or when the robot is interacting with the human [2]. For this reason several solutions have been proposed: energy tank [72], fractal attractor [15], stiffness bounds [153]. These approaches limit the energy the system can exert by changing the robot's behavior if the system's energy reaches a limit. In the chapters 4, ch:chapter5 we present our implementations of impedance control. These latter follow the works cited above that allow us to consider the role the robot must perform during the interaction. Our contribution in this field is not to try to implement new impedance solutions but rather to observe how these solutions are perceived by a human collaborator.

During the interaction, one key-point for the robot is the computation of the reference task: it usually defines the robot motions, but it may also be used to influence the human motion through physical contact. An optimized choice of the interaction trajectory (for instance, at the end-effector) could be used to reduce the human effort [41] and make the cooperation more comfortable and safe [139]. This computation is highly dependent on the estimated human intention. Following the terminology of [41], we could divide the robot strategies into reactive and proactive.

In reactive strategies, the belief of the human reference task is computed online and the robot reacts accordingly. These kinds of approaches are highly dependent by the sensors integrated in the robot, which will be discussed in Sec.1.4. One good example of reactive strategy is the so-called tele-impedance control [5]. In tele-impedance, the human mechanical impedance is calculated by combination of antagonist muscle groups based on early works [93]. More recent works used tele-impedance to tune online the parameters of the robot control law [20, 88], a more thorough discussion of tele-impedance is presented in Chapter 4. In proactive strategies, the robot predicts a long-term belief of human reference task and plans solutions accordingly [131]. The state of the human can be predicted using neural networks [195] or Gaussian processes [240]. To the best of our knowledge, no type of proactive tele-impedance has yet been presented.

Once the robot has access to the human current (reactive) or long-term (proactive) intention, it can use the information to compute its own reference task. The final task computation depends on the human intention and the estimated role as cooperative agent [100].

A limitation of most existing controllers for physical human-robot interaction is the representation of the human state, which is vastly simplified as an external force or end-effector's pose; this limits the quality of the solutions proposed by the robot and the extent to which the robot can reason about the human. Recent work [191] proposed to extend the classical quadratic program formulation in the case of human-robot physical interaction and to include the human model in the system model. This allows to reason about the whole-body dynamics of the human, considering their dynamics (e.g., joint

Measure	Sensor	Pros	Cons	Applications
Whole-body kinematics	Opto-electronic motion capture	accuracy (gold standard)	hardly portable, long equipment time, occlusion, camera field of view	Bi-Manual human-robot handover [233]
	Inertial motion capture	wearable, no occlusion, no field of view issue	drift, requires model calibration	Teleoperation [173]
	RGB Video camera	cheap, less invasive solution	image processing (low accuracy), field of view, occlusions	Human Pose Estimation with Deep Learning [260]
Forces	Force plates	accuracy (gold standard)	hardly portable, expensive	Estimate Human Dynamics [122]
	Sensorized insoles	wearable	low accuracy, often only pressure component	Estimate Human CoP [137, 212]
	Force/Torque sensors	Directly measure contact forces, accuracy	expensive, not portable	Estimate human motion intention [3]
Muscle Activity	Surface EMG (sEMG)	Non-invasive	Requires calibration at each session	Estimate Arm Stiffness Modulation [179]
	High Density sEMG	Non-invasive, precise movement classifications	Relatively new in the literature, complex processing	Generate robot input from arm muscle synergy [98]
Brain Activity	Electroencephalography (EEG)	Non-invasive	Not portable, calibration	Command high-level tasks [22, 129] Predict attitude towards robots [30]
Cardio Respiratory Activity	Electrocardiography (ECG) monitor	Heart Rate	Sensors have a trade-off between portability and accuracy	Estimate cognitive workload during robot assisted surgery [261]
	Photoplethysmography (PPG)	Cheap alternative to the ECG monitor, Heart Rate	may interfere in manipulation tasks	Investigation of Mental Workload [96]
Gaze	Eye Tracker	Gaze direction, and Eyeblink Rate	Generally not portable, it may generate excessive physical loads	Estimate engagement and proactivity levels during social human robot interactions [12, 16]
	RGB-D Video Camera	Gaze, Facial expression		Visual Interest Classification [189]
Speech	Microphone	Cheap, Portable	Natural language processing is complex	Enables verbal communication [43]

Table 1.2: Sensors commonly used in human-robot studies to measure the human's movement and behavior.

torques), their posture, and even ergonomics-related quantities that may be instrumental to ensure a safe and ergonomically optimized collaborative motion. One key issue is how to model the human kinematic and dynamic properties. Depending on the extent and objectives of the cooperation, humans could be represented by a simple linear inverted pendulum [36] or a more complex Digital Human Model (DHM) [191]. Choosing the correct level of abstraction and simplification in the human model can make a difference in real-time performance. In the next section, we will discuss how to model human and how to estimate their state based on multi-modal sensor measurements.

1.4 Human perception and modeling

Cooperative robots need to estimate the human physical, physiological and cognitive state in order to collaborate with their human partner effectively: as discussed in the previous sections and shown in Figure 1.2, the human state is a critical input for the high-level decision planning and lower level motion planning and control. The perception of the human state relies on sensors that can be placed in the environment, embedded in the robot, or worn by the human. A list of sensors commonly used to perceive humans is presented in Table 1.2. State-of-the-art motion capture techniques remain widely used to provide high-fidelity and high-frequency measurements of human kinematics. However, their use is mostly limited to laboratory experiments while their use in the field is often not possible (e.g. industrial

environment). If the access to human ergonomics is not possible, the robot needs to estimate the human posture, an example of that is presented in Chapter 2. While human kinematics can serve to inform about human's intent, the on-line estimation of human dynamics is receiving a lot of attention since it enables the robot to consider aspects such as balancing or human's internal force distribution [122]. Dynamics estimation requires a measure of external forces, either via generic force/torque (F/T) sensors that can be embedded in the robot or via specific sensors such as force plates for human/ground reaction force. Wearable force sensors such as sensorized insoles are also of interest due to their portability [212].

Measurements of physiological quantities are also common in human-robot cooperation. Physiological quantities can be used as such, for instance, electromyography (EMG) signals have been used to estimate human muscle fatigue [179]. But physiological quantities can also serve to estimate the human cognitive state: electrocardiography (ECG) and galvanic skin response (GSR) signals have been linked to stress and anxiety levels [55], while eye gazing was correlated with engagement and proactivity levels during social human-robot interactions without physical contact [16].

In more recent work, there are indications that individual factors such as personality, can affect the human posture and motion while interacting with a robot [234] (motor contagion), or even the level of trust towards the robot [96]. These emotional, and perception factors should also be monitored by the robot in order to provide mental safety during interactions, when appropriate [104].

Finally, the above-mentioned measurements are often used in combination with a model of the human body, in order to retrieve further information. Many levels of detail exist to represent the human body [200], but the most widely used in human-robot cooperation are the rigid body and musculoskeletal models. In rigid body models, the human body is represented as a kinematic chain of rigid segments linked together by ideal joints. This is typically done to estimate joint torques via inverse dynamics [122]. Such robotics-based models are also used to simulate human motion at a low computational cost [146]. Musculoskeletal models [176] include muscles and possibly tendons, providing a better degree of realism, obviously at a higher computational cost. In the frameworks presented in the chapters 2, 3, we used a rigid body model with 66 degrees of freedom to represent the human. The joint configuration applied to the model is extracted from a motion tracking suite that with respect to camera sensors gives us an estimate of the posture even in the presence of obstacles in the scene as may occur during interaction with the robot itself or with other objects common to the industrial environment (tables, panels, objects of carry).

1.5 Applications of robots interacting and cooperating with humans

Robots are versatile platforms that can interact with and help humans in different contexts, relying on the cooperative and human-aware decision and control skills discussed in the previous sections. Table 1.3 reports the type of robot and its control strategy used for each application. We divided the applications into: 1) co-worker robot in the case where it directly interacts with the human in tasks that are common in the industrial environment (polishing, welding and blasting); 2) companion robot if the robot is used to assist the human in recreational or home environments; 3) avatar robot for those situations where human and robot do not interact directly but the robot is teleoperated by the human. The table also presents the roles the robot assumes during the interaction. We can see a predominance of follower robots in the applications.

Collaborative robots have received a lot of attention lately due to their potential to act as co-workers that can possibly improve working conditions. While initially focused on fixed-base robotic arms, research in this domain is now moving towards robotic manipulators mounted on wheeled mobile bases [111]. The ultimate goal is to make them proactively work side by side with humans without the need for

Tasks/Applications	Robot role	Control Strategy (Robot)	[Ref.]
Dancing in couple (companion robot)	Follower	Coupled Linear Inverted Pendulum-based compliant controller (Dance Robot)	[246]
		QP controller with skin-like sensors (REEM-C)	[113]
	Leader	Coupled Linear Inverted Pendulum-based compliant controller (Dance Robot)	[89]
Assistance in standing up (companion robot)	Mutual Adaptation	Child-Robot	[97]
	Non-specified	QP controller in combination with finite state machine (HRP-4)	[136]
		Momentum based whole-body controller (iCub)	[191]
Health-Care physical assistance (companion robot)	Non-specified	QP controller in combination with finite state machine (Pepper)	[28]
		QP controller in combination with finite state machine (HRP-4)	[136]
		QP controller in combination with finite state machine (RIBA)	[157]
		shared control algorithm for smart wheelchairs	[58] [155]
Lifting and carrying objects, guided walking (co-worker robot)	Follower	Upper body impedance controller (Cosero)	[217]
		Hybrid force-position controller (COMAN)	[120]
		Hybrid force-position controller (ARMAR-6)	[14]
		Whole-body controller: Model Predictive Control at velocity level (iCub)	[29]
		Stack of Tasks (HRP-2)	[214]
	Variable Role	Compliant controller and state space learning (HRP-2)	[68]
	Non-specified	Multi-robot QP controller at velocity level (HRP-4)	[167]
		Jerk control (iCub)	[80] [3] [257]
Kinestetic teaching of new tasks (co-worker robot)	Follower	Learning by demonstration and optimal control (HOAP-2)	[42]
		Impedance upper body, zero torque control (iCub)	[12]
		Impedance control (Justin)	[124]
		Division controls: upper body active compliance with lower body Reaction Null Space method (HOAP-2)	[115]
Welding (co-worker robot)	Follower	Impedance Control (KUKA)	[67]
Polishing (co-worker robot)	Follower	Impedance Control (KUKA)	[180] [177] [176]
Sawing (co-worker robot)	Follower	Impedance Control (KUKA)	[180] [177] [176]
Drilling (co-worker robot)	Follower	Impedance Control (KUKA)	[180] [177] [176]
Blasting (co-worker robot)	Follower	Impedance Control (KUKA)	[227] [44]
IED response (avatar robot)	Follower	Momentum based whole-body QP controller (Valkyrie))	[102]
Telexistence (avatar robot)	Follower	IK based controller (TELESAR VI))	[220]
Search and rescue (avatar robot)	Follower	Momentum based whole-body QP controller (Atlas))	[101]
Spacecraft maintenance (avatar robot)	Follower	Not specified (G1)	[1]
Dance show (avatar robot)	Follower	ID based QP controller (HRP-2)	[186]
Agriculture Robot: autonomous pesticide giver (avatar robot)	Follower	Not specified	[235] [23]

Table 1.3: Examples of human-robot interactions classified by task/application: role assigned to the robot w.r.t. to the human partner, robot type and its control strategy.

protective cages [3]. To this end, they should also exhibit advanced interpersonal communication skills and be able to learn new operations and new tasks through social interaction [255].

Human-robot collaboration studies focused on tasks necessary for the introduction of robots into industry [119]. Similarly to [110], Rapetti *et al.* proposes to improve human ergonomics by extending their controller to try to minimize the estimated torque and joint velocities from a human partner [225]. Palunko *et al.* [168] proposed a HR co-manipulation scenario in which they modeled the physical properties of the suspended object. The collaborative robot KUKA lightweight robot arm has been used in Erden *et al.* [67] for welding. Peternel *et al.*proposed robotic solutions for polishing, object handover, sawing and drilling [176, 177, 180]. The authors proposed a method where the robot uses the learned skills to substitute the human in the physically demanding task, letting the human recover. Human-Robot cooperative blasting operation [44, 227]. Kim *et al.* [112] presented a HRC framework that aims to improve human ergonomics and the reconfigurability of the production/assembly processes in industrial environments. The proposed framework enabled a cobot to simultaneously adapt to user states (pose, overloading torques, variations in the workspace, and task condition) by detecting the tools and parts in the workspace.

Collaborative robots find their place also outside laboratories and Industries. In agriculture, human and robots work together for fruit harvesting [194]. Robotic solutions have also been proposed for assistive walking and for improving standing balance [193]. Wearable robots [54, 108] and exoskeletons [7, 33] should also be mentioned among the assistive technologies. In particular, the latter are finding wide use in assistance in both industrial and hospital settings. In fact, they can be used both to assist workers during tasks that require great strength as well as for the elderly and weak to increase their capabilities. For instance, Zhang *et al.* [259] developed a method for identifying the exoskeleton assistance that minimizes human energy costs during walking. Optimized torque patterns from an exoskeleton worn on one ankle reduced metabolic energy consumption compared to no torque. The approach was effective with exoskeletons worn on one or both ankles, during a variety of walking conditions, during running, and when optimizing muscle activity. Poggensee *et al.* [181] studied the importance of training and adaptation for human wearing exoskeletons. Song *et al.* [211] used human-in-the-loop optimization for identifying exoskeleton characteristics that maximize the benefits of assistance, which has been critical to achieving large improvements in energy economy.

Humanoid robots can also be used as co-workers [14]. They are perceived differently than robotic manipulators [234], which could have a beneficial impact depending on the application. In a recent work, Bolotnikova *et al.* presented a human-friendly humanoid that is able to approach a person in need and establish multimodal interactions for human assistance, including initiating physical contact [27]. Even though there was no shared task in [27] it gives a prime example of how leveraging the human perception could be used for assistance in the future.

1.6 Conclusion

To guarantee proficient and adequate cooperative behaviors, robots need to advance their cognitive, social and physical interaction skills. This chapter reported on the current work in these areas of research, acknowledging the main limitations due to the real-time nature of the interaction and the complexity of modeling and identifying the human state. We started with the high-level aspects that the robot has to fulfil, namely the socialy aspects. After that, we showed how these aspects are reduced at an intermediate level to the definition of cost functions and the type of interaction that the human and the robot accommodate. Finally, we presented how this intermediate level is implemented at a low level in the robot by using control laws that consider the forces acting on the robot. Human-aware robot collaborators capable of long-term interactions in real situations are the next grand challenge. This is why a key

aspect of collaboration is the real-time estimation of the human state. In this chapter (Sec.1.4) we have presented which tools are generally used to estimate it. In the next chapter (chapter 2) we present two methods using a motion caption suit to estimate the quality of human motion online and display it via two easy-to-use frameworks. The proposed tools were created to be used during human-robot physical interaction.

2

Ergonomic assessment during pHRI

Improving the ergonomy of working environments is essential to reducing work-related musculo-skeletal disorders. We consider real-time ergonomic feedback a key technology for achieving such improvements. To this end, in this chapter, we review state of the art technologies for ergonomic assessment and we present novel tools for online ergonomics assessment and visualization. As we showed in the previous chapter, a key aspect of human-robot collaboration is real-time estimation of human state. Precisely, we design modules that return an online evaluation and visualization of strenuous efforts and postures of a worker, specifically when physically interacting with a robot. A digital human model(DHM) is used to estimate human kinematics and dynamics and visualize non-ergonomic joint angles, based on the on-line data acquired from a wearable motion tracking device.

In addition to the article hal-03684130v1, we extended the state of the art in ergonomic assessment including some examples in different domains (like agriculture), we amplified the part in how to evaluate the human posture. The chapter presents two main contributions already presented in the paper: internal torque estimation and latent ergonomic map. For both the contributions we extended the formalization better declaring the parameters used and clarifing steps that we had covered in the paper quickly due to space constraints. The robotic part has been better clarified to give a better view of how we assessed to the human internal torque.


sensors

MDPI

Article

Latent Ergonomics Maps: Real-Time Visualization of Estimated Ergonomics of Human Movements

Lorenzo Vianello 1,2,*,†, Waldez Gomes 3,4,*,†, Frenk Stulp 3, Alexis Aubry 2, Pauline Maurice 1 and Serena Ivaldi 3

Video is available at: video Latent Ergonomics Map.

2.1 Ergonomics Evaluation

Poor ergonomics conditions in work environments may lead to serious work-related musculoskeletal disorders (WMSDs), including severe disabilities [243]. The development of WMSDs is an issue not only for the workers' health and well-being but also represents an important cost for companies and society [182, 201]. Poor ergonomics conditions are also present in agriculture, where operators are subject to awkward postures while performing tasks of harvesting, load carrying, pruning, planting, and other ordinary manual operations [24]. Not only manual operations but also highly mechanised jobs subject workers to physical stress [25].

In recent years, there has been a surge in robotic solutions for ergonomics interventions, notably using industrial manipulators conceived for collaboration with humans (i.e., cobots) and exoskeletons [205, 229]. To plan appropriate collaborative actions, collaborative robots need to have an estimation of the current human posture [143, 152]. They must be able to calculate the physical, physiological, and/or cognitive state of the human to act accordingly. The perception of the human state relies on sensors that can be placed in the environment, embedded in the robot, or worn by the human. State-of-the-art motion capture techniques based on infrared cameras and reflective markers, or more recently on inertial technology, remain widely used to provide high-fidelity and high-frequency measurements of human kinematics [145]. The captured data are fitted to a DHM designed to have similar properties to the human operator (height, weight, and structure). Ergonomics scores typically rely on kinematics and dynamics information about the human's movement, which are extracted from the DHM. As explained in Chapter 1 there are two main types of DHMs: musculoskeletal models, they have many degrees of freedom, and allow the analysis of the human movement by simulating the muscular efforts [18]; rigid-body models, which are simplified models with fewer degrees of freedom, where the human is represented as made of rigid body links [148]. While musculoskeletal models can be very accurate on a biomechanical standpoint, less accurate rigid-body models are much faster to simulate. As such, they are better suited for real-time applications such as model-based prediction, control, and ergonomics assessment [148].

The need to reduce musculoskeletal disorders in the industry leads to extensive research into measures of ergonomics. Many ergonomics assessment tools use the kinematic of a given worker to evaluate, and score a given task execution [114]. For instance, RULA [150] and REBA [92] evaluate the upper-body and full-body posture by scoring how far the worker's current joint angle positions are from a neutral and safe position. The Rapid Upper Limb Assessment (RULA) tool [150] is often used by ergonomists to evaluate work activities involving upper-body motion. It consists of a score ranging from 1 to 7, calculated based on the joint positions (posture), the known force/load applied to the worker's arm, and how many times the activity is repeated. The time evolution of RULA during a work activity is likely to have discontinuities and plateaus that make it inconvenient to use for motion optimization or continuous postural assessment. To alleviate this problem, we define a continuous version of RULA: RULA-C ($\varepsilon_{rc} \in \mathbb{R}^+$). To compute RULA-C, we fit a second-degree polynomial function to calculate intermediate scores for the RULA joints. The joint scores for each limb are combined with weighted sums, where the weights are computed from linear regressions of the standard RULA tables. Some works have also used assessments typically used in robotics, such as manipulability measures that can be associated with the user's operational comfort at executing the task [65, 223].

Postural-based approaches, however, do not consider the dynamics properties of the human model nor any dynamics interactions with the environment. In many ergonomics scoring sheets, external forces and loads can be considered (e.g., in EAWS it is possible to account for manipulated weights), but a more general approach considering efforts due to physical interaction with loads and robots is required to inform the human. For this reason, many works in human-robot collaboration use DHMs to estimate the status of human dynamics. Latella et al. [121, 122] estimate the balance, and the internal force distribution of the human during a human-robot collaboration using F/T sensors at the robot's end-effector, force plates at the feet, and/or sensorized insoles. Peternel et al. [177] estimate the human joint overloading torque, a quantification of the effect an external load has on a given body joint. Maurice et al. [147] estimate the human body joint torques by solving an optimization problem where the objective function encodes the human posture and the optimization variables include torques and wrenches of the human model.

The data relevant for assessing ergonomics is tipically high-dimensional, including kinematic and dynamic state variables related to posture and efforts. This high-dimensional data is difficult to interpret, even for experts. Physiological sensors such as surface EMG or EKG often measure critical information for ergonomics assessment, but they require considerable post-processing and are difficult to interpret

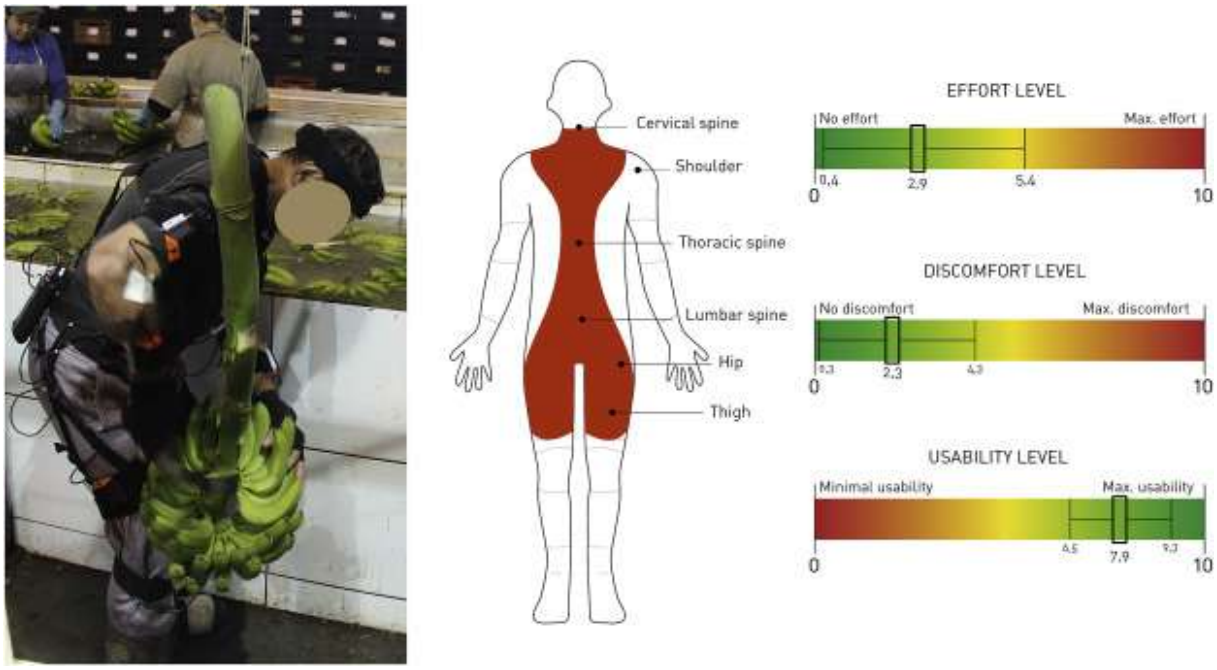

Figure 2.1: In [154] the authors evaluate the risk of musculoskeletal injuries in a banana processing task.

promptly. They are mostly used for post-experimental analysis [149], while few applications of online use in human-robot collaboration exist [180]. Also, the dimensionality of the data may become a bottleneck real-time computation and interpretation. For this reason, many works proposed to reduce the dimensionality of a data set, reducing it to a set of representative principal features [142]. The reduced human representation has been used to execute for instance activity recognition and prediction [48] or ergonomic optimization [143].

2.2 Dimensionality Reduction for Human State Representation

DHMs typically have many degrees of freedom. A depiction of the human status, therefore, requires high-dimensional vectors, which in turn increase the computational cost of the ergonomics status evaluation [141]. To reduce the dimensionality of a data set, a solution is to extract a reduced set of representative principal features from the original data set [82]. This procedure is usually applied to reduce the amount of data necessary to train a model and to reduce the risk of overfitting during the training [61]. Recent works have applied this concept to compactly represent human motion. For instance, Mandery et al. [142] were able to reach high accuracy in a human motion classification task using only four features. Human models with a high number of degrees of freedom impact the time performance of motion analysis. To improve speed in the motion processing of the DHM data, recent works have used a representation of the human motion in a **latent space** [56, 143]. A latent space is an embedding of a set of items in which items which resemble each other more closely are positioned closer to one another. In other words, neighboring objects in the latent space are similar while distant objects are different. In this case the similarity meter is highly dependent on the features chosen to construct the latent space. In most cases, the dimensionality of the latent space is chosen to be lower than the dimensionality of the feature space from which the data points are drawn, making the construction of a latent space an example of dimensionality reduction, which can also be viewed as a form of data compression. Marin et al. [143] showed that the use of a latent space human representation improved the performance of their

application. Ikemoto et al. [97] use principal components analysis (PCA) to reduce the dimensionality of the postures of a humanoid robot, which has a similar description to the DHM.

Dimensionality reduction techniques applied to human poses are also used in movement planning or prediction [135]. This type of approach uses latent space representations for selecting points that complete a given path (movement prediction) or for joining two extremes (movement planning). By inverting the relationship which maps the high-order dimensional to the latent space, it is possible to recover the poses having the latent space representations. For instance, variational autoencoders have been used to predict the next pose given the current one [128, 133].

Among dimensionality reduction techniques, autoencoders (AEs) and variational-AEs (VAEs) have high reconstruction ability and produce compact latent spaces. For this reason, they have been widely used for reducing the dimensionality of the human state and for movement generation [48]. Dermy et al. [56] address the problem of predicting future human whole-body movements given prior observations. They map high-dimensionality trajectories into a reduced latent space using AE. Then the prediction is based on a probabilistic description of the movement primitives in the latent space, which reduces the computational time for the prediction to occur.

To the best of our knowledge, the state of the art lacks a unified simple and intuitive visualization tool built specifically for industrial and human-robot collaboration tasks. In this chapter we present a framework for online visualization of human posture quality consisting of a simulation of the human and a two-dimensional mapping method of this posture. Our framework was built using demonstrations taken from industrial and robot collaboration tasks.

2.3 A supportive tool for Human-Robot Collaboration

In this chapter, we present intuitive visualization tools to provide online ergonomic feedback to industrial operators. Our contribution is twofold:

- Online visualization of joint angles and torques for ergonomic feedback. Given a human posture, the framework calculates the ergonomic assessment and an estimation of the human effort. This latter estimation is derived from inversion of the Lagrangian model using variables (e.g., Intertia, Coriolis) extracted from a simulated DHM. This enables to quickly verify a body posture, captured online using a motion capture suit. This visualization consists of a DHM with color-coded visual cues that express specific locations and joints of the body postures that are particularly non-ergonomic, further facilitating the ergonomics assessment.

- Latent Ergonomic Maps (LEMs) for immediate overall 2D visual feedback on RULA and RULA-based (RULA-continuous) scores. The algorithm uses a state-of-the-art method for dimensionality reduction and generative network, namely Variational Auto-Encoders (VAE). VAE allows us to encode high dimension postures and to sample and decode variations of the same postures. The latter allows creating a LEM by sampling the latent space, decoding the posture, and applying ergonomic assessment to the posture.

The system is designed to be applicable to diverse industrial scenarios in which a human operator may execute non-ergonomic movements, either working alone, or in interaction with a robot. The intuitive visualization tools enable the human to easily visualize the risks of their posture even if they are not ergonomic experts. The human operator could visualize the latent maps and the DHM along with ergonomics suggestions on a display during a training session, where time can be dedicated to analyzing and improving the gestures and the postures associated with a workstation. Looking at the display is hardly possible during the regular work because the display could divert the attention of the worker,

cause distractions and increase the risk of accidents; however, the display can be used for post-hoc analysis immediately after a gesture if the production time allows for it. The visual feedback could be also displayed to the worker using augmented reality glasses [160]. Interestingly, the visual feedback can be used directly by the human workers, as well as by colleagues and ergonomics experts that evaluate the worker's activity at a workstation. The only requirement of our system is that it requires a real-time human motion tracking system like wearable or environmental sensors. In this work, the human posture is tracked using an Xsens MVN motion tracking suit, but in a real application scenario it could be tracked by another lighter sensing device or extracted from video.

Digital Human Model

Our DHM is a rigid multi-body system, similar to a humanoid robot, with anthropometrics properties of the human (height, weight) to mimic their kinematic and dynamics. It has 66 segments and is based on the Xsens MVN model (Figure 2.2). Using such a model, it is possible to reproduce the human movement as recorded by the Xsens MVN motion tracking system, a wearable set of 17 sensors distributed along the human body.
We modeled the human spherical joints collected by the motion capture suit as a series of 3 one-dimensional revolute joints, where each DoF is controlled by a single actuator. The resulting DHM posture is represented by the 66 joints: the links are modeled with geometric shapes (parallelepiped, cylinder, sphere) scaled with the human height. The dynamic properties (e.g., mass) are computed from anthropometric data available in the literature [148], assuming a homogeneous density of the links and scaling with the human body mass.

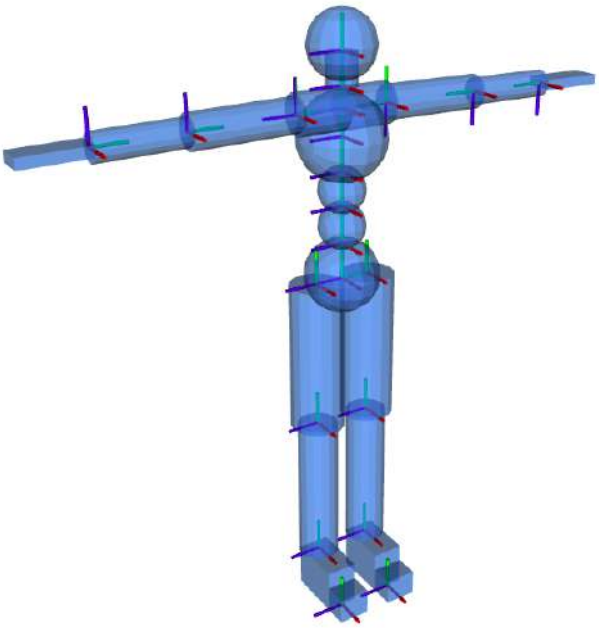

Figure 2.2: Digital Human Model (DHM) with 66 degrees of freedom. For each DHM's link, its origin axis (x in red, y in blue, and z in green) is displayed.

The posture of the DHM is calculated using a one-to-one mapping from the original human poses, which are measured in our case by a human skeleton or motion tracking system. The position of the floating base of the DHM is calculated using the position of the pelvis, which is provided by the motion

tracking system.

The DHM enables the estimation of the human internal torques, as described in previous works [147]. However, here we do not use force plates to retrieve feet wrenches: instead, we approximate the wrench acting on the human feet with the weight force generated by the body. This approximation introduces an error in the joint torque estimation, but it is tolerable for our visualization purposes as long as the joint torques are not used in a control loop. This allows transporting easily the framework while having an issue with the movement quality, especially for upper-body movements.

The internal torques are calculated starting from the classical Lagrangian formulation:

$$\boldsymbol{M}(\bar{\boldsymbol{q}})\ddot{\bar{\boldsymbol{q}}} + \boldsymbol{C}(\bar{\boldsymbol{q}}, \dot{\bar{\boldsymbol{q}}})\dot{\bar{\boldsymbol{q}}} + \boldsymbol{G}(\bar{\boldsymbol{q}}) = \boldsymbol{S}^{\top}\boldsymbol{\tau} + \sum_{i=1}^{n_k} \boldsymbol{J}_{p_i}(\bar{\boldsymbol{q}})^T \boldsymbol{f}_i \tag{2.1}$$

where $\bar{\boldsymbol{q}} = (\boldsymbol{x}_F, \boldsymbol{q})$ is the DHM extended posture composed by the floating base pose ($\boldsymbol{x}_F \in \mathbb{R}^6$) and the joints angles ($\boldsymbol{q} \in \mathbb{R}^{66}$), $\boldsymbol{M}, \boldsymbol{C}, \boldsymbol{G}$ are respectively the inertia, the Coriolis and the gravity matrices, $\boldsymbol{S}$ is the actuation selection matrix due to the free-floating base and $\boldsymbol{\tau}$ is the vector of the DHM joint torques. Concerning the computation of the external wrenches acting on the i-th link ($\boldsymbol{f}_i$), we consider the force sensed by the robot through the torque sensors ($\boldsymbol{f}_{RH} = \boldsymbol{J}_F(\boldsymbol{q})\boldsymbol{\tau}_{F,ext}$, where $\boldsymbol{J_F}$ is the robot Franka's Jacobian matrix and $\boldsymbol{\tau_{F,ext}}$ are the robot external torques) and the gravitational forces acting on the feet. The external wrenches acting on the ith link are multiplied by the Jacobian matrix from the world frame to the i-th link frame ($\boldsymbol{J}_{p_i}$). The choice of using only the gravitational forces acting on the feet helps to improve the speed of the algorithm and facilitates the deployment of our tools for ergonomics feedback to situations where only the human skeleton information is accessible. We solve the Eq.2.1 for $\boldsymbol{\tau}$.

Display Ergonomics Scores on the DHM

The DHM is used to display in real-time the ergonomics information associated with human movement. The real-time information about the human posture is used to update the DHM pose and compute the local ergonomics score, where "local" indicates the specific body location. We use scores based on kinematics information (RULA, RULA-C, manipulability) and dynamics information (joint torques). To account for the comfort of movement, especially in presence of physical interaction, we consider the arm manipulability: it provides information about the velocity and force production capacity of the limb endpoint in different configurations [177]. It provides a piece of complementary information about the human posture to RULA and RULA-C about the capacity of the human to produce forces. Each score is calculated using the partial scores presented in the RULA table. In the case of RULA-C, these have continuous values because they are the result of polynomials that approximate the RULA values. The local ergonomic scores are then visualized on the DHM to provide intuitive feedback about the current posture. Specifically, we color some spheres placed at relevant joints (knees, ankles, back, torso, shoulders, and elbows) with colors that are proportional to the ergonomic score. The latter is normalized in the range $[0, 1] \rightarrow$ [GREEN, RED], using the maximum score value that is set after the maximum score registered for that body part on the dataset used for training the LEM in the offline phase. The reason for the latter normalization is to better spot the difference in ergonomic scores between similar movements. Normalizing the values enables to highlight for a specific task the differences in the ergonomics while executing the same movement in different ways. We are aware that this normalization has some limitations (e.g., encountering new movements that are particularly risky). For this reason, at the time of the writing of this manuscript, we are trying to overcome these limitations and integrate activity recognition [140] into our framework, to change normalization values according to the current activity and movement. In our setup, it is possible to select the ergonomic score to visualize on the DHM by interacting with an easy-to-use

	RULA Local scores
Torso	$+1$ if $q = 0°, +2$ if $0° < q < 20°, +3$ if $20° < q < 60°, +4$ if $q > 60°$ $+1$ if twited, $+1$ if side bending
Neck	$+1$ if $0° < q < 10°, +2$ if $10° < q < 20°, +3$ if $20° < q, +4$ if $q < 0°$ $+1$ if twited, $+1$ if side bending
Shoulder	+1 if $-20° < q < 20°$, +2 if $q < -20°$ or $20° < q < 45°$, +3 if $45° < q < 90°$, +4 if $q > 90°$ $+1$ if shoulder raised, $+1$ if shoulder abducted
Elbow	+1 if $60° < q < 100°$, +2 if $0° < q < 60°$ or $100° < q$,
Wrist	$+1$ if $q = 0°, +2$ if $-15° < q < 15°, +3$ if $15° < q$ or $-15° > q$

Table 2.1: Local scores associated to the RULA score. Each score is normalized by the maximum score registered for the given task.

GUI (some examples in the video attachment). Figure 2.9 shows the DHM displayed during a manipulation task, together with the RULA LEM: while the LEM provides a synthetic visualization of the overall ergonomics score, the spheres on the DHM enable to visualize the individual scores on the different body parts. This is convenient to identify the body parts that are more at risk, from the ergonomics standpoint, which are colored in red; those that are not at risk are colored in green, and the intermediate values in yellow. Figure 2.12 shows more examples of the DHM during a pick and place movement where the human takes on different body postures: back joints are red when the human is bent forward, the knees are red during squats, while shoulders are red during over-head work.

Latent Ergonomics Maps (LEMs)

Latent Ergonomics Maps (LEMs) project an ergonomics score on a 2-dimensional latent space that is trained to represent the human posture (note that this means that each ergonomics score listed in Section 2.3 leads to a different map). In this Chapter, we propose a synthetic representation of the human postures using a 2D latent space created by a Variational Auto-Encoder, and then we project ergonomics scores of sampled human postures on the latent space, in the form of a map. The resulting map is the Latent Ergonomics Map. This representation allows us to visualize in an immediate way when a person is in a non-ergonomic (associated with red color) or ergonomic (associated with green color) posture.

The LEM is created in an offline phase, requiring a dataset of human movements and the definition of the ergonomics score. Training LEM proceeds in two steps. The first step is to create and train a Variational Auto-Encoder (VAE) to represent human postures. A schematic of the training procedure is shown Fig.2.3. A VAE is an auto-encoder based on variational inference [95]. Let $[\boldsymbol{x}_k]_{k=1}^K$ be a dataset of K independent and identically distributed samples of some continuous observation variable $\boldsymbol{x}$ of unknown distribution. It is assumed that $\boldsymbol{x}$ is generated by some process involving the latent variable $\boldsymbol{z}$ and the parametric functions of distribution $p_{\boldsymbol{\theta}^*}(\boldsymbol{x}|\boldsymbol{z})$ and $p_{\boldsymbol{\theta}^*}(\boldsymbol{z})$: $\boldsymbol{x} \sim \int_z p_{\boldsymbol{\theta}^*}(\boldsymbol{x}|\boldsymbol{z}) p_{\boldsymbol{\theta}^*}(\boldsymbol{z}) d\boldsymbol{z}$ where $\boldsymbol{\theta}^*$ is a set of parameters. In a VAE, the so-called *decoder* neural network tries to fit the function which maps

$\boldsymbol{z}$ to $\boldsymbol{x}$, and so learns from data the values of the weights $\boldsymbol{\theta}$. The distribution is assumed to be Gaussian: $p_{\boldsymbol{\theta}}(\boldsymbol{z}) = \mathcal{N}(\mathbf{0}, \boldsymbol{I})$ and $p_{\boldsymbol{\theta}}(\boldsymbol{x}|\boldsymbol{z}) = \mathcal{N}(\boldsymbol{\mu}_x, \boldsymbol{\sigma}_x^2)$. However, the transition function $p_{\boldsymbol{\theta}}(\boldsymbol{z}|\boldsymbol{x})$ is not known. A recognition model $q_{\boldsymbol{\phi}}(\boldsymbol{z}|\boldsymbol{x})$ is used to approximate true posterior $p_{\boldsymbol{\theta}}(\boldsymbol{z}|\boldsymbol{x})$. In our case, the distribution is also assumed to be Gaussian for simplicity, but without loss of generality: $q_{\boldsymbol{\phi}}(\boldsymbol{z}|\boldsymbol{x}) = \mathcal{N}(\boldsymbol{\mu}_z, \boldsymbol{\sigma}_z^2)$, where $\boldsymbol{\phi}$ is represented by weights and biases of a neural network (*encoder*). Training the VAE aims at recovering values of the parameters $(\boldsymbol{\theta}, \boldsymbol{\phi})$ in such a way to approximate as much as possible the optimal parameters $(\boldsymbol{\theta}^*, \boldsymbol{\phi}^*)$.

We choose a relational VAE to define a loss function which represents both the reconstruction loss and a loss on the relation reconstruction [151]:

$$L = (1-\alpha)D_{kl}(q_\phi(\boldsymbol{z}|\boldsymbol{x})||p_{\boldsymbol{\theta}}(\boldsymbol{x}|\boldsymbol{z})) + \alpha D_{kl}(q_{\boldsymbol{\phi}}(\boldsymbol{z}|\varepsilon(\boldsymbol{x}))||p_{\boldsymbol{\theta}}(\varepsilon(\boldsymbol{x})|\boldsymbol{z})) \tag{2.2}$$

where $D_{kl}(.)$ is the Kullback-Leibler divergence, $\varepsilon(.)$ is the relation function (in our work corresponding to the ergonomic loss function RULA-C) and, finally, the parameter α is a scale parameter to control the weights of the data reconstruction loss and the relationship reconstruction loss. This enables us to obtain a latent space that not only represents the postures but also tries to encode the space to minimize the error in reconstructing the correct ergonomics score for the compressed posture.

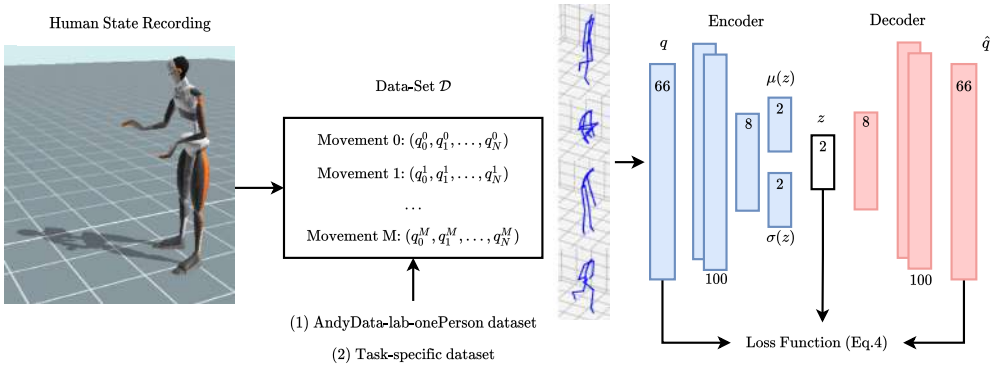

Figure 2.3: Training the VAE of the LEM requires a dataset of human postures. For each posture an ergonomics score exists. In our experiments, as a dataset, we used: (1) the AnDy dataset [145] and (2) a task-specific dataset acquired for each experiment. The training is done to find the VAE weights which simultaneously minimize the reconstruction error of the postures and the associated ergonomics score.

Training the VAE requires a dataset of human movements. For example, the AnDy dataset [145] contains many examples of human activities, recorded with the Xsens motion tracking suit, which can provide both wearable sensing data and estimated postural data. To simplify, let us assume that we input human postures fitted to the DHM ($\mathbb{R}^{66}$). We train the VAE with batches of human postures from the training dataset to find the parameters of the encoder-decoder networks, to minimize the loss function Equation (2.2) via back-propagation. The VAE architecture consists of 5 layers with 66 inputs, 200 hidden neurons, 2-dimensional latent space, and 66 outputs, where rectifier, *tanh* and identity activations are used for the hidden layers and the output layer. The hyperparameters of the VAE are chosen based on the reconstruction error and the training time by grid search. To train the latent space, we perform first a pre-training with a large human motion dataset (*AndyData-lab-onePerson dataset* [145], containing more than 5 h of recorded data), then a fine-tuning with smaller task-specific datasets acquired for each experiment (see below). This latter step is optional. The first training with a large dataset is sufficient to generate a LEM, in particular, it enables to obtain a generic LEM that is task-independent and that captures a variety of different postures. In our experiments, however, the fine-tuning enables us

to obtain a task-specific LEM that is more specialized to represent the postures of a specific task, while maintaining the generalization capabilities. All the datasets were normalized between zero and one and augmented using intermediate and mirrored poses before training. During training, we optimized both the weight of the *encoder* and the *decoder*. The weight optimization was done on an Intel Core^{TM} i7-8850H with 6 cores at 2.6GHz, requiring about 20 min. The trained *encoder* can be used to visualize example movements in the latent space. This can be useful for preliminary insights into the postures for different activities. For example, Figure 2.10 shows the sequence of postures, projected in the 2D latent space, associated with the movements from the dataset of [140], which contains activities such as bending, kicking, lifting objects, and walking. Some postures are also displayed to clarify that each 2D point is representing a different posture. Some 2D points belong to different activities, and this is normal since the same body posture can be observed in different activities. It is also possible to display ergonomics information in this activities representation: as shown in Figure 2.5, it is possible to color-code the points associated with a movement according to the ergonomics scores. In this case, the activity information is lost, but it is possible to inspect one or more movements.

Once the VAE is trained, the second step consists in creating the ergonomics landscape projected on the latent map. The procedure is illustrated in Fig.2.4. We uniformly sample in the latent space a set of *2D* vectors ($\boldsymbol{z}_{i,j} = [z_i, z_j] \in \mathbb{R}^2$). We reconstruct the samples using the decoder. Then, for each reconstructed human posture ($\hat{\boldsymbol{q}}_{i,j} \in \mathbb{R}^{66}$) we calculate the ergonomic score $\varepsilon(\hat{\boldsymbol{q}}_{i,j})$ (e.g., RULA or RULA-C) from the estimated human joint angles, following the method presented in Section 2.1. Note that one map is created for each ergonomics score (for instance, one map for the standard RULA score, and another map for the RULA-C score). If the data used for the training are subject to a normalization function ($f_n(.)$), it is necessary to invert the normalization ($\varepsilon(f_n^{-1}(\hat{\boldsymbol{q}}_{i,j}))$) before calculating the ergonomic scores. The result is a height-map composed by the *2D* coordinated in the latent space and the ergonomic score ($[z_i, z_j, \varepsilon(\hat{\boldsymbol{q}}_{i,j})] \in \mathbb{R}^3$). In Figure 2.11, we show the LEMs for RULA and RULA-C. The triadic color code (green, yellow, red) is applied to the postures classified according to the RULA recommendations, while a continuous color coding based on the triad is used for RULA-C. The LEM created using the RULA-C score creates, by definition, a latent space that is similar to that of the RULA but continuous. While there is no immediate advantage in using one of the two LEMs for ergonomics visual feedback, the continuous LEM can be used in future work as a reduced model for planning ergonomics movements using gradient-based methods [86].

The LEM can be used online to display the movement that the human operator is executing, which appears as a trace on the landscape: since every point is a posture, the height of each point indicates the ergonomics evaluation associated with the corresponding human posture. The human posture is recorded with wearable sensors (e.g., in our case the Xsens MVN motion tracking suit) and retargeted into the DHM ($q_c \in \mathbb{R}^{66}$). The *encoder* neural network reduces the input to its *2D* representation ($z_{i,j}$), the ergonomics score is then retrieved. We adopt a triadic color code to make the height map more intuitive to read: we associate low ergonomic scores (e.g., ergonomic postures, with low risk) with green; high ergonomic scores (e.g., non-ergonomic postures, with high risk) are associated with red; middle scores are associated with yellow. This kind of representation allows to visualize in an immediate way when a person is in a non-ergonomic (and therefore associated with red color) or ergonomic (associated with green color) posture space. Similarly, different variations of the same movement (and therefore different postures) can be mapped in the latent space, as it was done in Figure 2.5, to visualize which trajectory is better from an ergonomic point of view.

2.4 Experiments

In this section, we elaborate on the structure of the VAE and the specific training procedure for the ex-

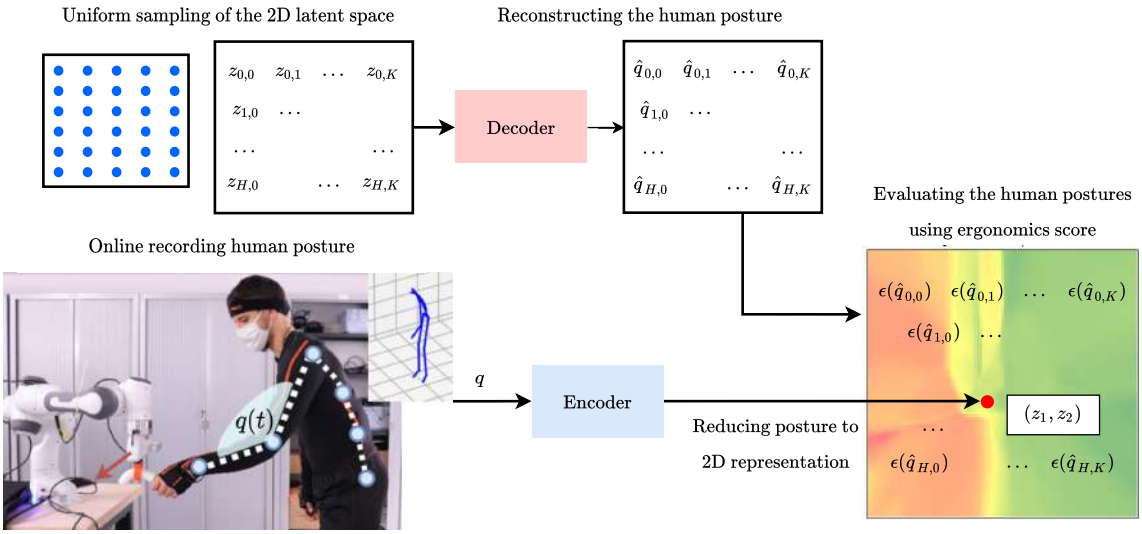

Figure 2.4: Creation of the LEM: the 2D latent space of the VAE is sampled. The decoder reconstructs sampled latent points. The reconstructed postures are used to compute the ergonomics scores. The ergonomics score is therefore associated with the original 2D points, thus creating a heightmap.

periments. We then describe the use of the trained LEM to provide online ergonomics feedback in two different experiments, where a human executes pick and place activities with and without robot assistance.

2.4.1 Setup and Scenarios: Experiment 1

We demonstrate our ergonomics visualization tools to evaluate human movements executed in two experiments, with two work-related scenarios. In the first experiment, the human performs a pick and place task. The task is inspired by packaging tasks on assembly lines in the manufacturing industry and consists of picking, carrying, and placing a 6 kg bar. One male participant performed 8 sequences of the task, with each sequence consisting of 6 to 8 pick-and-place actions. Each sequence started and ended in the same neutral pose. The bar was initially placed at a height of 45 cm on a 100 $\times$ 50 cm flat support. The participant was instructed to take the bar with both hands, carry it to the other side of the support, place the bar there and return to the initial position to perform the next iteration. Each sequence lasted around one minute. To add variability to the data, the participant was instructed to change the position of his hands on the bar and to follow two different paths when going to and coming from the bar's final position.

2.4.2 Setup and Scenarios: Experiment 2

In the second experiment, the human carries loads in collaboration with a robot. They move a box together from a point A to a point B and then backward, along a trajectory that lasts about one minute. The box is initially placed at a height of 85 cm on a table. The box is fixed to the robot end-effector which carries the majority of its weight; the human grasps the object through a handle as shown in Figure 2.6. Each sequence lasts around one minute. At the beginning of the activity, the robot and the human grasp the object, and each sequence starts and ends in the same neutral pose. The robot control is based on a Cartesian impedance controller:

$$\boldsymbol{\tau} = \boldsymbol{J}(\boldsymbol{q})^\top (\boldsymbol{D}(\dot{\boldsymbol{x}}_d - \dot{\boldsymbol{x}}) + \boldsymbol{K}(\boldsymbol{x}_d - \boldsymbol{x})) + g(\boldsymbol{q}) \tag{2.3}$$

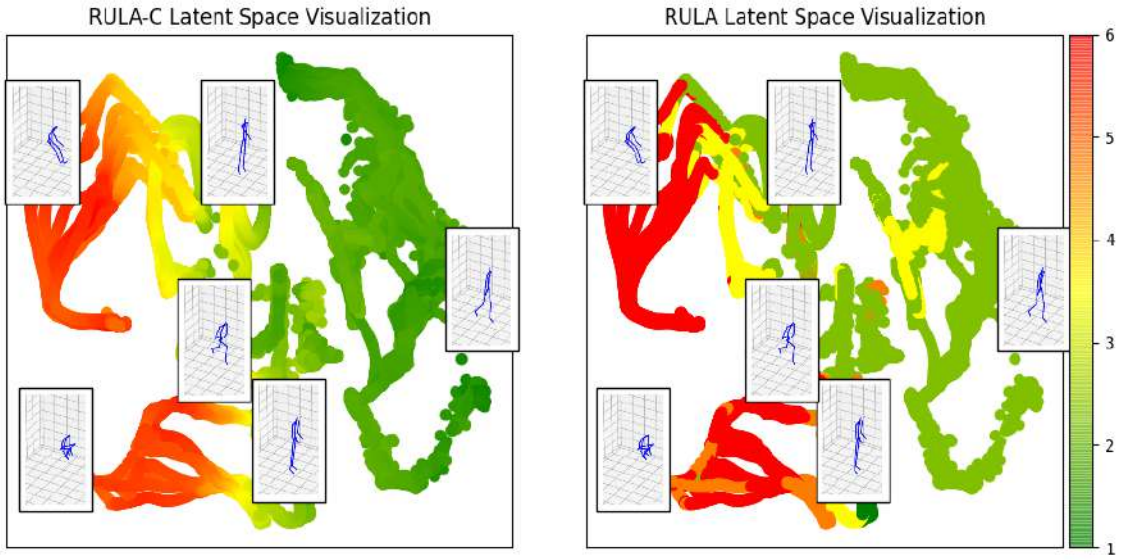

Figure 2.5: Latent space representation: in this plot, some examples of movements from the dataset of [140] colored according to the ergonomic evaluation. The postures associated with some 2D points in the latent space are shown. On the right, the scale of the colors corresponds to the ergonomic scores where: 1 (green) corresponds to the safer postures while 7 (red) represents the postures less safe.

where $\boldsymbol{K} \in \mathbb{R}^{6\times6}$ and $\boldsymbol{D} \in \mathbb{R}^{6\times6}$ are respectively the stiffness and the damping matrices and $g(.)$ is the gravity compensation term. Cartesian impedance control generates a torque proportional to the error between the end-effector pose and the desired end-effector pose ($\boldsymbol{x}, \boldsymbol{x}_d \in \mathbb{R}^6$) and their derivatives ($\dot{\boldsymbol{x}}_d, \dot{\boldsymbol{x}} \in \mathbb{R}^6$).

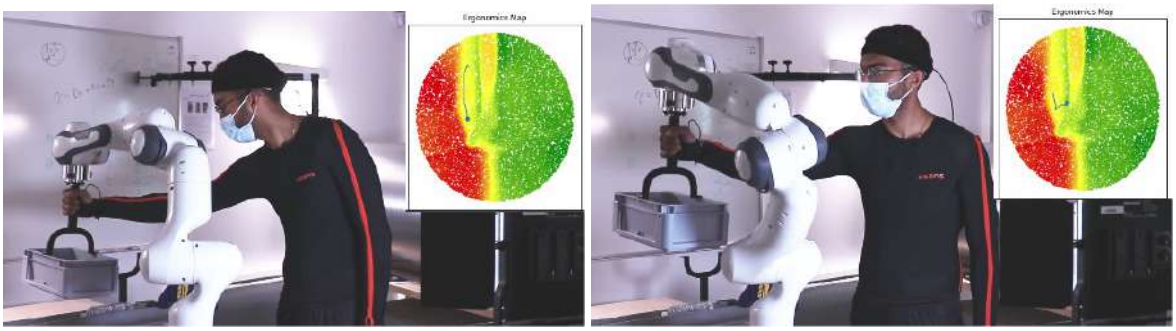

Figure 2.6: Experiment 2: collaborative object transportation. The human is physically interacting with the Franka robot. On the right of each photo, the Latent Ergonomic Map. The current human posture is a point on the map while the line that is attached to it represents the previous human posture.

We implemented two Cartesian impedance behaviors changing the values of the stiffness matrix: in the first, the robot was more compliant ($\boldsymbol{K} = 500$ N/m) and in the second the robot was stiff ($\boldsymbol{K} = 1000$ N/m). The desired Cartesian damping $\boldsymbol{D}$ was calculated proportional to $\boldsymbol{K}$ using factorization design as in [8]. The robot's trajectory is predefined by the robot planner, the latter selects a trajectory of Cartesian points using a parabolic curve passing through the initial and final points while the orientation is maintained constant. A participant repeated the movements 15 times, with 3 different robot trajectories (5 times for each trajectory) to add variability to the movement; in particular, we de-

signed different robot trajectories in such a way to induce a variety of human postures and ergonomics. Some movement examples are shown in the video attachment. The robot used is the Panda (Franka Emika) robot controlled using *libfranka* and *FrankaROS* libraries.

In both experiments, the human is equipped with an Xsens MVN motion tracking suit, which provides real-time (240Hz) information about the current human pose: joint angles and link's positions, orientations, velocities, and accelerations. Both the human's and the robot's sensors measurements are streamed online to the module, to visualize and simulate their movements in the simulation (Dart [126]) as shown in Figure 2.7.

An overview of the main modules used in the two scenarios is shown in Figure 2.8, which details as well the flow of information from the Xsens sensors and the Franka robot. The simulation receives the sensed information from both humans and robots, and their corresponding models are updated. All the items in the scene are modeled (i.e., a Unified Robotic Description Format (URDF) is available for all the elements: robot, experimental setup—table, object, etc.—as well as human) and simulated. Precisely, the robot communicates the following information to the simulation: (1) Robot joint configuration, (2) Robot end-effector pose, (3) External measured torques, and (4) Internal torques. The robot pose (joint angles, end-effector pose, and torque) are used to update the simulated robot. Meanwhile, the measured external torques are used to calculate the wrenches that the human is applying to the robot and then used to calculate the effort estimation Equation (2.1) Similarly, the motion tracking suit communicates: (1) the human posture expressed as the joint angles, and (2) the positions of the human links. The human joint angles are used to generate the LEM and to simulate the DHM; the links' poses are used to locate the DHM in the reference frame of the simulation.

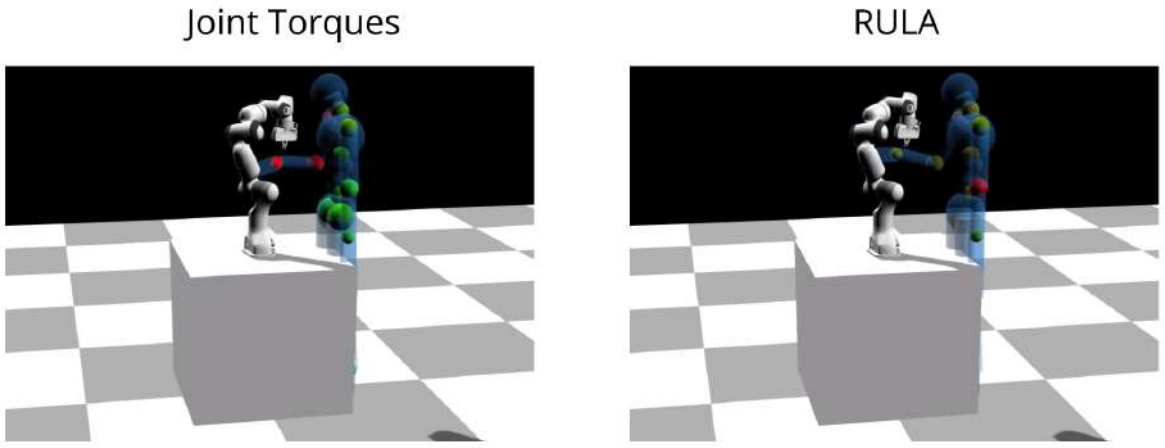

Figure 2.7: Experiment 2: collaborative object transportation. The DHM with the colored spheres indicating non-ergonomic joint values.

The main interest of the second scenario is to use a DHM with visual clues of the joint torques and efforts, to account for the physical interaction between the human and the robot. The contact wrenches are input in the DHM in real-time, using the Franka robot's sensor measurements, which enables a better representation of the ergonomics status of the human from the point of view of efforts.

In the online phase, the LEM is used to visualize the overall ergonomics score of a posture. Figure 2.9 shows the RULA LEM (center) corresponding to the human motion (left) tracked in real-time (240 Hz) by the Xsens MVN suit. During the execution of the movement, the current human posture is projected into the ergonomic map, after being encoded by the *encoder* into a 2D point in the latent space. The

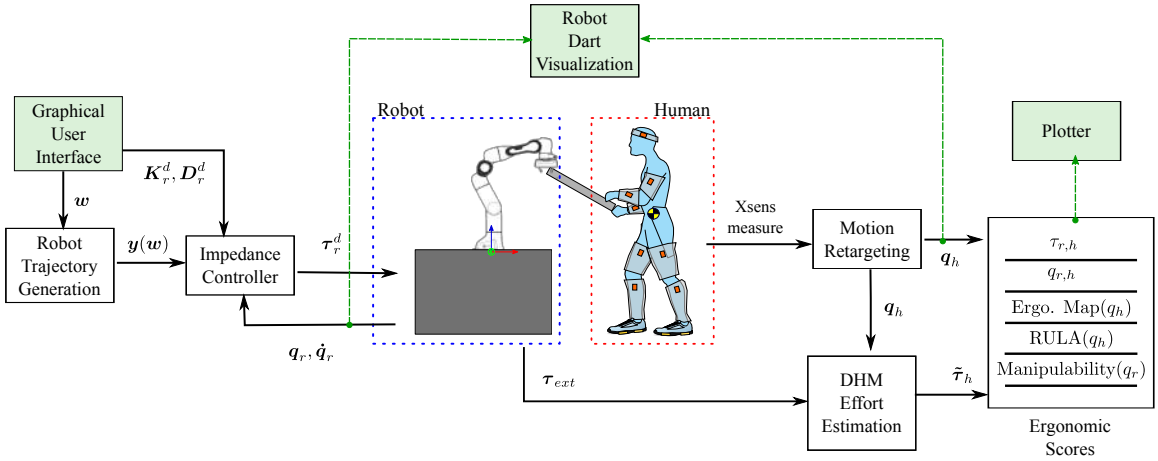

Figure 2.8: Overview of the system in a human-robot collaboration setting. In the left box: the robot modules that enable to control the robot and retrieve information about the contact forces exchanged with the human. The human-robot interaction force is measured on-line thanks to the joint torque sensors embedded in the robot. Each of the 7 axis is equipped with a torque sensor, and based on these torques measurements, the Franka API provides an estimation of the interaction force at the end-effector. In the right box: modules for online estimation of the human kinematics, dynamics, ergonomics scores, and visualization tools. Green boxes: the framework includes visualization tools to plot the online ergonomics scores and other relevant quantities, as well as visualizing the human and the robot interacting in a digital twin based on Dart physics engine.

result is a trace, i.e., a sequence of 2D points moving in the ergonomic map, representing the human motion and its ergonomics evaluation. Another example of the trace onto a LEM is shown in Figure 2.6.

2.5 Discussions and Conclusions

In this chapter, we presented a set of tools for providing online ergonomics feedback to human workers during their activities, also when they physically interact with robots. A Digital Human Model is used to visualize, with color-coded spheres, the body areas and joints that are subject to efforts and non-ergonomic postures according to state-of-the-art ergonomics scores, such as RULA.

Our contribution, Latent Ergonomics Maps, are synthetic representations of the overall ergonomics scores projected onto a bidimensional latent space that maps human postures. The result is an intuitive color-coded map where the human posture is a point, a movement is a line, and their associated color is an estimation of the ergonomics score of choice. LEMs can be used for bio-feedback or self-correction, as a visual tool for teaching, or simply to inform the human. Their potential goes beyond the online feedback for the human, as they can be used to inform the robot as well, which can find applications in planning ergonomically optimal collaborative motions. A limitation of projecting the map on a 2D latent space, which is necessary for visualization purposes, is the information loss that may result from such a strong dimensionality reduction. However, the error is tolerable for ergonomics scores based on postural information, and otherwise acceptable if coupled with the visualization of efforts on the Digital Human Model.

Another limitation of our method is the use of an inertial tracking method. This type of technology is difficult to integrate into all-day industrial activity compared to more common video-type sensors. Nevertheless, it has many advantages, one of which is its robustness in the case of obstructions (such

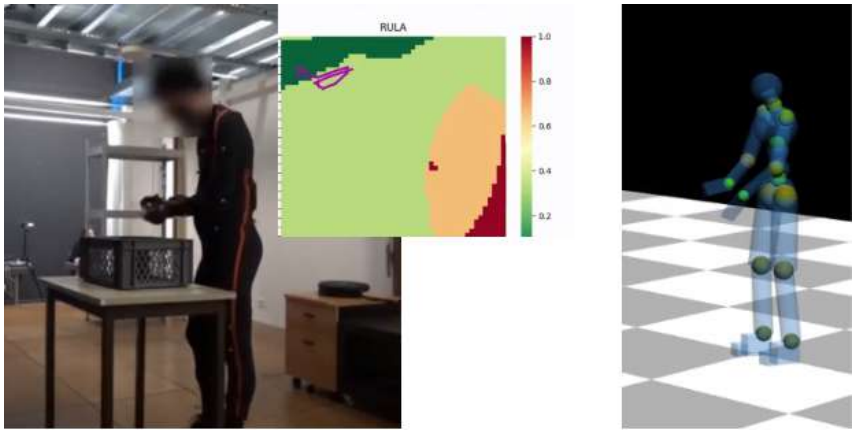

Figure 2.9: The ergonomics visual feedback tools used to measure the executed motion in real-time. Left: the human movement is tracked with the Xsens MVN motion tracking suit. At the same time, the RULA Latent Ergonomics Map is calculated with the visualization of the current human movement (the magenta-colored line). Right: the DHM with colored spheres showing the RULA scores at relevant body locations.

as robots). In addition, we think that it can be used for occasional checks of the quality of work. In any case, our method is independent of the type of technology used so for greater integration into future industry we propose to test the methods presented using video sensors in future work.

In future works we would like to combine the prediction of intended movement [56] with LEMs, therefore predicting future ergonomics scores for the intended movement. This, we think, will enable us to alert the human of possible risks associated with ergonomics in particular during human-robot collaboration. The idea is to inform the robot about the ergonomics risk associated with planned collaborative robot trajectories. In fact, we think that an estimation of future movements can give crucial information to the robot, which can then avoid harmful movements before they occur. For this reason, in the next chapter (Chapter 3) we present a tool for human state prediction while physically interacting with a robot.

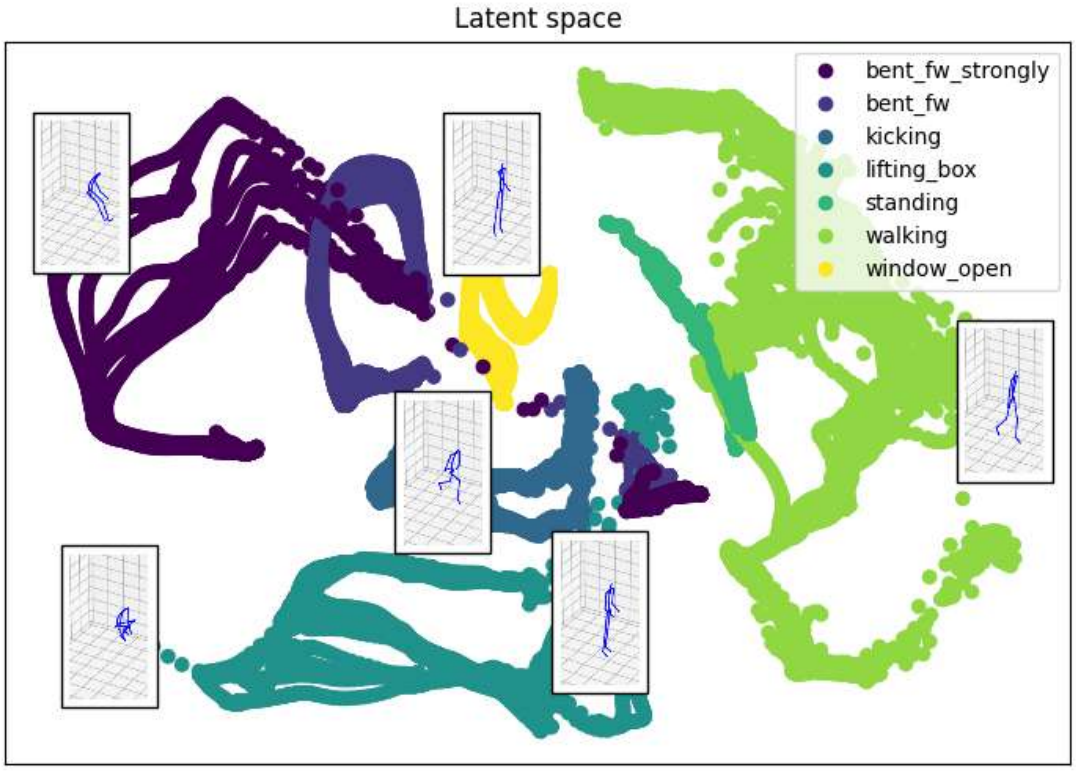

Figure 2.10: Latent space representation of the human movement during some activities from the dataset of [140]. The movements presented in this latent space are: bent forward (strongly), kicking, lifting a box, standing, walking, open a window. A movement is a sequence of points in the latent space. A color code enables to distinguish the 2D path associated with each sequence. The postures associated with some 2D points in the latent space are shown.

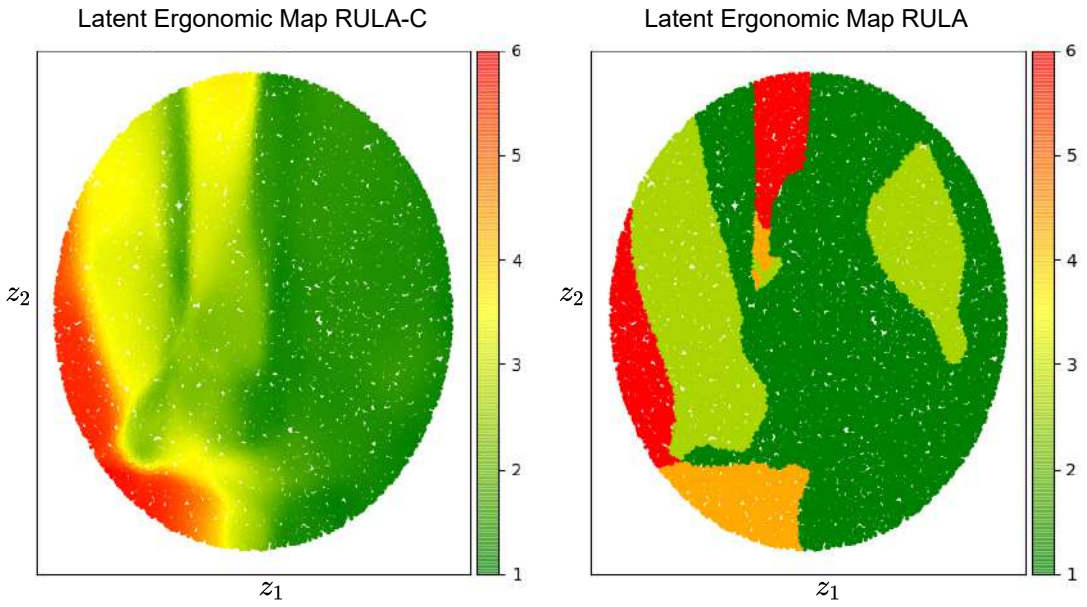

Figure 2.11: Latent Ergonomics Maps (LEMs): one for RULA, one for RULA-C. The figure visualizes the ergonomic data generated by the decoder network of a variational autoencoder. Here, we've sampled a grid of values around the origin with a radius of size 1 from a two-dimensional Gaussian and displayed the output of our decoder network. The distinct ergonomic scores which exist in different regions of the latent space smoothly transform from one to another.

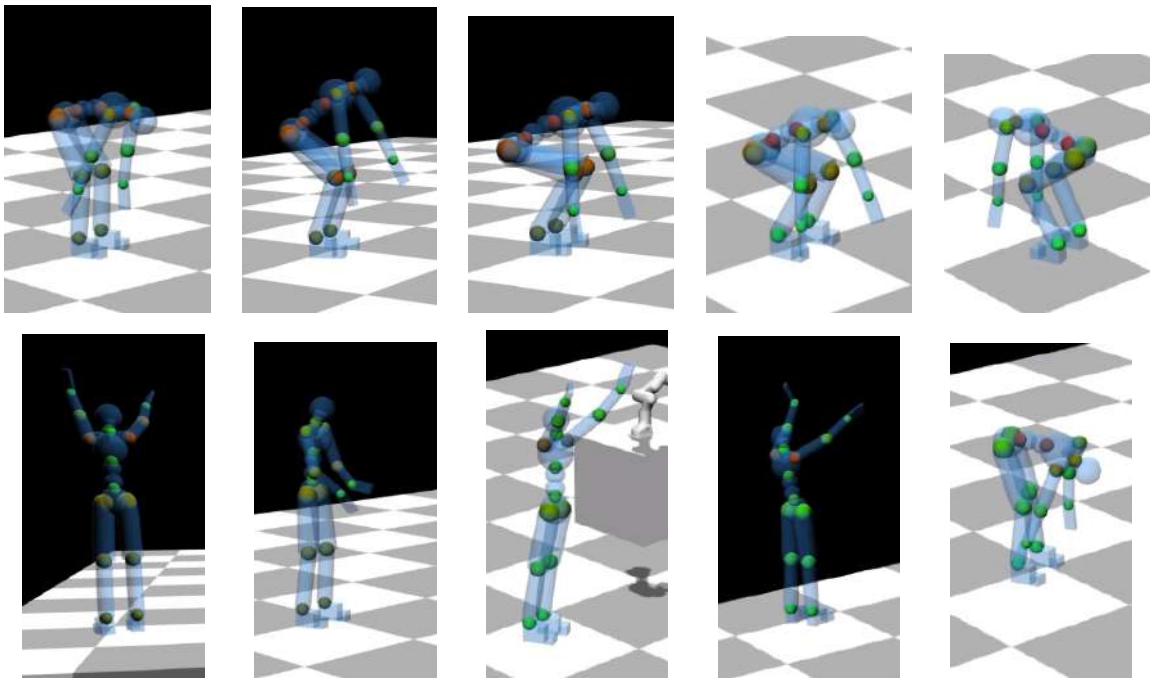

Figure 2.12: Experiment 1: pick and place. Across the pick and place task, the human takes on different postures. In particular, some are usually classified as non-ergonomic (e.g., hands over shoulders, bent back, squat). The color-coded spheres on the DHM show the body parts that have a high risk (ergonomics score: RULA) during these postures.

3

Human state prediction during pHRI

When a human is interacting physically with a robot to accomplish a task, his/her posture is inevitably influenced by the robot movement. Since the human is not controllable, an active robot imposing a collaborative trajectory should predict the most likely human posture corresponding to a trajectory imposed by the robot. This prediction should possibly consider individual differences and preferences of movement execution, as it is necessary to evaluate the impact of the robot's action from an ergonomics point of view. In this chapter, we review state of the art methods for human state prediction, in particular during collaboration with collaborative robots. Moreover, we propose a method to predict, in probabilistic terms, the human postures of an individual for a given robot trajectory executed in a collaborative scenario. We formalize the problem as the prediction of the human joints velocity given the current posture and robot end-effector velocity. Previous approaches to solve this problem relied on the inverse kinematics but did not consider the human body redundancy nor the kinematic constraints imposed by the physical collaboration, nor any prior observations of the human movement execution. We propose a data-driven approach that addresses these limits. The key idea of our approach is to learn the distribution of the null space of the Jacobian and the weights of the weighted pseudo-inverse from demonstrated human movements: both carry information about human postural preferences, to leverage redundancy and ensure that the predicted posture will be coherent with the end-effector position. We show in a simulated toy problem and on real human-robot interaction data that our method is able to improve model-based inverse kinematics prediction, sample-based prediction, and regression methods that do not consider geometric constraints. We validate our approach in a simulated toy problem and on two real human-robot interaction experiments where a human is physically interacting with a Franka robot.

This chapter is based on the article hal-03115242v2. In addition to the contributions of the article, in this chapter we presented more results to better validate our method: the mathematical formulation of the method has been better clarified; we display the differences in predicting the null space of directly the joint space of a simulated 5R; we showed the results we obtained for each experiment done with two different tasks and two different participants; finally, we displayed the data diversity for both training set and test set. Moreover, we extended the state of the art better clarifing what are the contributions of our work in the litterature.


Human Posture Prediction during Physical Human-Robot Interaction

Lorenzo Vianello[1,2], Jean-Baptiste Mouret[1], Eloise Dalin[1], Alexis Aubry[2], Serena Ivaldi[1]

Video is available at: video posture prediction.

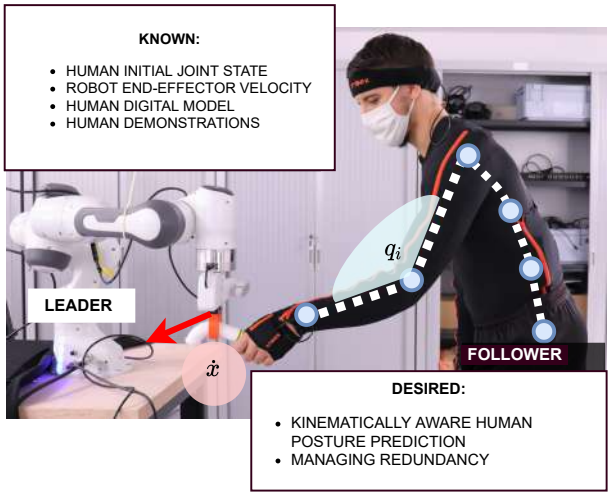

Figure 3.1: The human posture is influenced by the robot's trajectory during physical interaction, but the human may adopt different postures during each task execution. In this paper we want the robot to predict the human posture given a known Cartesian trajectory of its end-effector and prior observations of the task executed by the human. The human posture is measured online by a wearable Xsens MVN suit.

3.1 Human Posture Prediction as an Inverse Kinematics Problem

Collaborative robots need to estimate of the current human posture and its future intended evolution to plan appropriate collaborative actions. The human posture can be retrieved in real-time essentially using cameras or wearable motion tracking sensors [145]. However, robots often do not have access to the human posture measurement in real-time, and the only information they have is the fact that human is physically attached to their end-effector in some tasks. In such cases, Inverse Kinematics (IK) is used to predict the human pose starting from the end-effector position using simplified human models as in [206].
The problem is that the human posture is not uniquely defined by its end-effector position because of the intrinsic human body redundancy but also task preferences and other individual factors, many HRC scenarios can be seen as a redundant setup where the human can potentially perform the task without the assistence of the robot [108]. Thus, it is hard to predict the human posture given only the task description. Indeed, IK alone cannot solve this problem given the overactuated nature of the human.
To address this kind of problem, a common approach is to sample in the space of the possible solutions and to evaluate them accordingly to the kinematic properties [254] and to task-specific loss functions [184]. We refer to these kinds of methods as sampling based approaches. These kinds of methods are computationally expensive and highly dependent on the choice of parameters. Moreover, they are not well designed to integrate human demonstrations that capture human preferences of movement.

The problem becomes even more difficult if we wish to estimate future poses. In fact, predicting the human intention, i.e., the future intended movement [57] is an active field of research, where, traditionally, movements are represented by trajectories or movement primitives issued with a probabilistic description. The prediction with motion primitives is most often done in the task space, e.g., the Cartesian space, and IK is used to find the most appropriate corresponding joint trajectories to fulfill the robot task. Motion primitives can also be learned in the joint space. However, each joint primitive cannot be learned independently as all the primitives must be kinematically consistent, and conditioning may not

(a) Subject leans backward to create an upward motion at the end-effector of the prosthetic arm.

(b) Subject eans forward to create forward motion at the end-effector of the supernumerary arm.

Figure 3.2: In [108] the authors exploit human kinematic redundancies for minimizing posture-related cost functions.

be sufficient to properly ensure this property [169]. In [170], this problem was solved using Probabilistic Motion Primitives (ProMPs), by conditioning the motion primitive in the joint-space with the one in the operational space. A limit of this approach is that it requires the knowledge of the ProMP for each possible movement, which only makes sense for specific applications and gestures.

Recurrent neural networks have also been proposed for predicting future human postures [118, 258]. One of the main challenges of these methods is to encode the multi-value behaviour of the human, coming by its redundant structure, and to evaluate the different solutions [51]. Data-driven methods are, in general, time efficient and they do not require hard coded evaluation functions because they learn directly from demonstrations. The main limit of these algorithms is the loss of the kinematic consistency in the prediction: it was demonstrated that applying regression for mapping from task space to joint space using standard regression can lead to inconsistent predictions [224]. In [231] the human pose is predicted using learned models (e.g. nearest neighbour); but, then, an IK correction is required to fix the hand positions to match the kinematic constraints imposed by the collaborative robot. Also, authors reported it was too computationally expensive to be used for online planning.

The estimation of the operator's future posture is crucial information for ergonomic optimisation [231]. Ergonomics scores typically rely on kinematics and dynamics information about the human's movement, which are often extracted from simulations of Digital Human Models. We refer the reader to Chapter 2 for a more in-depth discussion of these topics.

3.2 Problem formulation

Notation: In our study, the human is represented by a DHM, a rigid body model with n degrees of freedom. The notation presented in Table 3.2 is used for the DHM. The robot state is determined by $\boldsymbol{x}_R, \dot{\boldsymbol{x}}_R$, i.e., the Cartesian position and velocity of its end-effector (EE).

We consider a cooperating human-robot interaction scenario, where a human and a robot manipulator interact to perform a joint task. The robot's task trajectory at the EE is known at each time step, in the following, we drop the time dependence t in the equations, unless necessary, to improve the readability of the equations: $\{\dot{\boldsymbol{x}}_R(t)\}_{t=0}^{T-1}$. The two agents are physically coupled at their EEs; the robot is leading (leader role), while the human (follower role) is guided by the robot; hence, we assume $\dot{\boldsymbol{x}} = \dot{\boldsymbol{x}}_R$. We assume a rigid, constant roto-translation between the two frames. Given the current human joint

$\boldsymbol{q} \in \mathbb{R}^n$	vector of joints values
$\boldsymbol{x} \in \mathbb{R}^m$	hand Cartesian pose
$k = n - m > 0$	degrees of redundancy
$f(.) : \mathbb{R}^n \rightarrow \mathbb{R}^m$	forward kinematics function
$\dot{\boldsymbol{q}}$ and $\dot{\boldsymbol{x}}$	joint and Cartesian velocities
$\boldsymbol{J}(\boldsymbol{q}) \in \mathbb{R}^{m \times n}$	Jacobian Matrix
$\boldsymbol{y} \in \mathbb{R}^k$	null space of the Jacobian $\boldsymbol{J}(\boldsymbol{q})$
$\mathcal{D} = \{(\boldsymbol{q}_i, \dot{\boldsymbol{x}}_i), \dot{\boldsymbol{q}}_i\}_{i=1}^{N_D}$	Dataset of N_D demonstrations

Table 3.1: Notation

configuration q (known, we suppose its measure is accessible to the robot) and the robot EE velocity $\dot{\boldsymbol{x}}_R$, we want to predict the human joint velocity $\dot{\boldsymbol{q}}$. Since the human is over-actuated, we want to predict a distribution of solutions that capture the "preference" of human movement (i.e., analogously to the concept of most likely solutions [184]); such solutions must be kinematically feasible, i.e., they must verify that $\dot{\boldsymbol{x}} = \boldsymbol{J}(\boldsymbol{q})\dot{\boldsymbol{q}}$. The problem can be formalized as computing the conditional probability:

$$p(\dot{\boldsymbol{q}}|\boldsymbol{q}, \dot{\boldsymbol{x}}) \quad \text{s.t.} \quad \dot{\boldsymbol{x}} = \boldsymbol{J}(\boldsymbol{q})\dot{\boldsymbol{q}}\,, \tag{3.1}$$

where the second term is the kinematic constraint which determines the set of possible solutions.

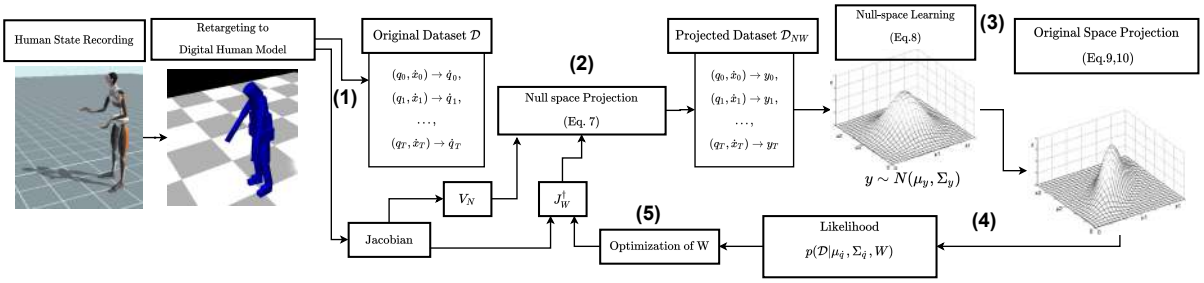

Figure 3.3: Flowchart of the offline training: (1) We collect human movements using a motion capture suit. The joint states are passed to a digital human model and they are used to calculate the Jacobian at each joint configuration. From the digital human model we also record the dataset $\mathcal{D}$. (2) We project the joint velocities $\dot{\boldsymbol{q}}$ on the null space of the Jacobian; at the first iteration of the algorithm, the matrix $\boldsymbol{W}$ used for the pseudo-inverse is an identity matrix. (3) The projected dataset is used to train k independent GP. (4) We invert the projection to obtain a distribution over $\dot{\boldsymbol{q}}$ and we calculate the likelihood; (5) We optimize the $\boldsymbol{W}$ matrix accordingly to the likelihood using a gradient-free optimizer and we repeat from point (2).

3.3 Background

3.3.1 Kinematics for redundant DHMs

A redundant DHM is a DHM that has more degrees of freedom than the number nominally required to perform a given set of tasks ($n > m$). The reader may notice that "redundant DHM" is equivalent to "redundant robot", since the DHM is modeled essentially as a robot with rigid bodies. Redundancy

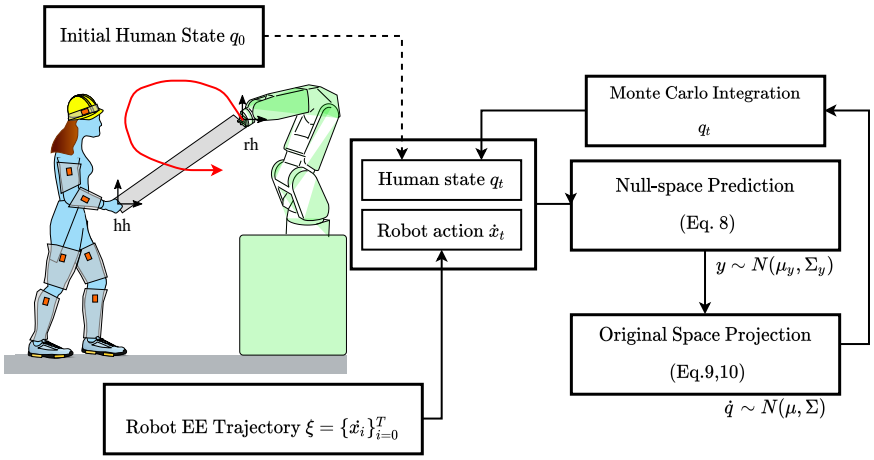

Figure 3.4: Flowchart of the online prediction: Given an EE trajectory imposed by the robot and the knowledge of the initial human state we can predict a distribution over the future human states. To do that, we sample on the human joint velocity $\dot{\boldsymbol{q}}$ calculated with our method (MI-NsGP) then we integrate the current human state, in this way, we could propagate the uncertainty to the next human state. We repeat this procedure throughout the EE trajectory, in this way, we create a probabilistic estimation of the human joint trajectory (Monte Carlo rollout).

yields increased dexterity and versatility for performing a task due to the infinite number (∞^{n-m}) of joint motions which produce the same EE motion. Given an EE pose $x \in \mathbb{R}^m$, the space which contains all the solutions of the IK equation $\{\boldsymbol{q} : \boldsymbol{x} = f(\boldsymbol{q})\}$ is defined as the inverse kinematics's manifold $\mathcal{M}_x$. It is considered a union of more simple and continuous manifolds, called "self-motion manifold" ($\mathcal{M}_s$) [39]. Any change of joint configuration ($\dot{\boldsymbol{q}}_s$) along a self-motion manifold is called "self-motions" and it does not change the position of the EE ($\boldsymbol{J}(\boldsymbol{q})\dot{\boldsymbol{q}}_s = 0$). The space containing these joint velocities is the null-space of the Jacobian matrix evaluated in q, which is the set of vectors $\dot{\boldsymbol{q}}_s$ which satisfy $\boldsymbol{J}(\boldsymbol{q})\dot{\boldsymbol{q}}_s = 0$ and with $\dot{\boldsymbol{q}}_s \neq 0$. A basis for the null space of $\boldsymbol{J}(\boldsymbol{q})$ is composed of the columns of the matrix $V_N = [\mu_1, ..., \mu_{n-m}]$; this matrix can be obtained by singular value decomposition:

$$\boldsymbol{J} = \boldsymbol{U}\boldsymbol{S}\boldsymbol{V}^\top = \boldsymbol{U}(\boldsymbol{S}_R \quad 0)\begin{pmatrix}\boldsymbol{V}_R^\top \\ \boldsymbol{V}_N^\top\end{pmatrix} \tag{3.2}$$

where $\boldsymbol{V}_R$ and $\boldsymbol{V}_N$ are the range and the null-space components, respectively [224]. Thus, each self-motion velocity could be represented by a linear combination of the columns of $\boldsymbol{V}_N$:

$$\dot{\boldsymbol{q}}_s = \boldsymbol{V}_N(\boldsymbol{q})\boldsymbol{y}, \tag{3.3}$$

where $\boldsymbol{y} \in \mathbb{R}^k$ is the vector of the coefficients of the linear combination. This consideration is particularly useful for interpreting local redundancy resolution technique: each movement in the joint state can be seen as the sum of the minimal velocity needed to match $\dot{\boldsymbol{x}}$ plus a movement in the joint space which has no effect in the workspace. In the literature, this approach is usually referred to as the dual projection method: the joint velocity is computed as

$$\dot{\boldsymbol{q}} = \boldsymbol{J}_W^\dagger(\boldsymbol{q})\dot{\boldsymbol{x}} + [\boldsymbol{I} - \boldsymbol{J}_W^\dagger(\boldsymbol{q})\boldsymbol{J}(\boldsymbol{q})]\, z(\boldsymbol{q}) \tag{3.4}$$

$$\boldsymbol{J}_W^\dagger(\boldsymbol{q}) = \boldsymbol{W}\boldsymbol{J}^\top(\boldsymbol{q})[\boldsymbol{J}(\boldsymbol{q})\boldsymbol{W}\boldsymbol{J}^\top(\boldsymbol{q})]^{-1} \tag{3.5}$$

that instantaneously minimizes the symmetric weighted quadratic form $\dot{\boldsymbol{q}}^\top \boldsymbol{W}^{-1}\dot{\boldsymbol{q}}$, and $z(\boldsymbol{q}) \in \mathbb{R}^n$ is a joint velocity projected onto the null space of the manipulator Jacobian and thus on the tangent space of the self-motion manifold. Typically, $z(\boldsymbol{q})$ is designed as a potential function that minimizes a desired cost function $\mathcal{C}(.)$ [59] [208].

3.3.2 Gaussian Processes

A Gaussian Process (GP) [188] is a collection of random variables such that any finite collection has a joint Gaussian distribution. In regression the random variables represent the value of the function $f(x) \in \mathcal{Y}$ for the given input $x \in \mathcal{X}$.

A GP, denoted by $f(x) \sim \mathcal{GP}(m(x), k(x, x'))$, is entirely characterized by the mean $m(x) = E[f(x)]$ and covariance $k(x, x') = E[(f(x) - m(x))(f(x) - m(x))]^\top$, which is symmetric and positive semi-definite.

Let $\mathcal{D} = \{(x_i, y_i) | x_i \in \mathcal{X}, y_i \in \mathcal{Y}\}$ be a training set and (x_*, y_*) a point we did not observe in $\mathcal{D}$. The GP predictive distribution for the output y_* at the test input x_*, given in vector form, is

$$
\begin{aligned}
p(y_*|\mathcal{D}, x_*) &= \mathcal{N}(\mu_*, \Sigma_*), \\
\mu_* &= k_*^\top (k + K_{err})^{-1} y, \\
\Sigma_* &= k_{**} - k_*^\top (k + K_{err})^{-1} k_*
\end{aligned}
$$

where, given a kernel function $k(.,.) : \mathbb{R} \times \mathbb{R} \to \mathbb{R}$ we use the notation $k = k(x, x), k_* = k(x, x_*), k_{**} = k(x_*, x_*)$ and K_{err} is the measurement error variance. In this work, we use the radial basis function (RBF) kernel: $k_{\sigma^2,\lambda}(x, y) = \sigma^2 exp(-\frac{||x-y||^2}{2\lambda}), \lambda > 0$, where, the parameters (σ^2, λ) are chosen by maximizing the marginal likelihood $P(y|(\sigma^2, \lambda))$.

3.4 Proposed Method

We consider a DHM with n degrees of freedom. We assume that the human/DHM follows this classic control law from robotics (section 3.3.1, [59, 208]):

$$
\dot{\boldsymbol{q}} = \boldsymbol{J}_W^\dagger(\boldsymbol{q})\dot{\boldsymbol{x}} + (\boldsymbol{I} - \boldsymbol{J}_W^\dagger(\boldsymbol{q})\boldsymbol{J}(\boldsymbol{q}))z(\boldsymbol{q}) \tag{3.6}
$$

where $z(\boldsymbol{q})$ is an unknown vector of null-space velocities, often, it is calculated as the gradient of a cost function $\mathcal{C}(.)$. The weights $\boldsymbol{W}$ of the weighted pseudo-inverse $\boldsymbol{J}_W^\dagger$ are also unknown. The EE velocity $\dot{\boldsymbol{x}}$ is known. Our objective is to learn $z(\boldsymbol{q})$ and $\boldsymbol{W}$ from data. In this way, the solutions we find must always satisfy the kinematic constraint: $\dot{\boldsymbol{x}} = \boldsymbol{J}(\boldsymbol{q})\dot{\boldsymbol{q}}$.

3.4.1 Learning the null-space velocity with Gaussian processes

Let us consider a dataset $\mathcal{D}$ of DHM motions, composed of N_D pairs: a tuple with the current joint state $\boldsymbol{q} \in \mathbb{R}^n$ and the EE velocity $\dot{\boldsymbol{x}} \in \mathbb{R}^m$, and the joint velocity $\dot{\boldsymbol{q}} \in \mathbb{R}^n$: $\mathcal{D} = \{(\boldsymbol{q}_i, \dot{\boldsymbol{x}}_i), \dot{\boldsymbol{q}}_i\}_{i=1}^{N_D}$. Such a dataset can be generally acquired via human motion tracking (see (1) in Fig. 3.3).

At this stage, we consider the values of the weight matrix $\boldsymbol{W}$ of Eq. 3.6 to be known, for example $\boldsymbol{W} = \boldsymbol{I}$, where $\boldsymbol{I}$ is the identity matrix (see section 3.4.2 for learning $\boldsymbol{W}$).

Instead of directly learning the value of $z(\boldsymbol{q})$, we notice that we can write [232]:

$$
\boldsymbol{V}_N(\boldsymbol{q})\boldsymbol{y} = (\boldsymbol{I} - \boldsymbol{J}_W^\dagger(\boldsymbol{q})\boldsymbol{J}(\boldsymbol{q}))z(\boldsymbol{q}) \tag{3.7}
$$

where $\boldsymbol{V}_N(\boldsymbol{q})$ is the basis of the null space of the Jacobian $\boldsymbol{J}(\boldsymbol{q})$, which is computed using Singular Value Decomposition (SVD), and $\boldsymbol{y} \in \mathbb{R}^k$ represents the coordinates of the self-motion joint velocity in the null space.

We learn $\boldsymbol{y}$ instead of $z(\boldsymbol{q})$ because it is the minimal size representation for a self-motion joint velocity (see (2) in Fig. 3.3). Therefore, we project every joint velocity $\dot{\boldsymbol{q}}$ of our dataset to the null space of the Jacobian $\boldsymbol{J}(\boldsymbol{q})$ evaluated in the current joint configuration $\boldsymbol{q}$ by applying:

$$\boldsymbol{y}(\boldsymbol{q}, \dot{\boldsymbol{x}}) = \boldsymbol{V}_N^{\dagger}(\boldsymbol{q})\Big(\dot{\boldsymbol{q}} - \boldsymbol{J}_W^{\dagger}(\boldsymbol{q})\dot{\boldsymbol{x}}\Big) \tag{3.8}$$

Thus, given the dataset $\mathcal{D} = \{(\boldsymbol{q}_i, \dot{\boldsymbol{x}}_i), \dot{\boldsymbol{q}}_i\}_{i=1}^{N_D}$, we apply Eq. 3.8 to obtain $\mathcal{D}_{NW} = \{(\boldsymbol{q}_i, \dot{\boldsymbol{x}}_i), \boldsymbol{y}_i\}_{i=1}^{N_D}$.

We learn $\boldsymbol{y}(\boldsymbol{q}, \dot{\boldsymbol{x}})$ using GPs (section 3.3.2) that map the current joint state and the EE velocity to the joint velocity:

$$\boldsymbol{y}|(\boldsymbol{q}, \dot{\boldsymbol{x}}) \sim \mathcal{GP}\Big(m(\boldsymbol{q}, \dot{\boldsymbol{x}}), k((\boldsymbol{q}, \dot{\boldsymbol{x}})_i, (\boldsymbol{q}, \dot{\boldsymbol{x}})_j)\Big) \tag{3.9}$$

After experimental testing and, following [46], we train k independent GP, one for each dimension of $\boldsymbol{y}$. We choose this approach to keep the method simple, but we expect that the performance of our method could be improved with the right choice of multidimensional GP, and we will investigate this improvement in future work. Since Eq. 3.8 is linear, given the Gaussian distribution $p(\boldsymbol{y}) \sim \mathcal{N}(\boldsymbol{\mu}_y, \boldsymbol{\Sigma}_y)$, we can get the Gaussian distribution of $p(\dot{\boldsymbol{q}}) \sim \mathcal{N}(\boldsymbol{\mu}_{\dot{q}}, \boldsymbol{\Sigma}_{\dot{q}})$ by inverting it:

$$\boldsymbol{\mu}_{\dot{\boldsymbol{q}}}(\boldsymbol{q}, \dot{\boldsymbol{x}}) = \boldsymbol{J}_W^{\dagger}(\boldsymbol{q})\dot{\boldsymbol{x}} + \boldsymbol{V}_N(\boldsymbol{q})\boldsymbol{\mu}_y \tag{3.10}$$

$$\boldsymbol{\Sigma}_{\dot{\boldsymbol{q}}}(\boldsymbol{q}, \dot{\boldsymbol{x}}) = \boldsymbol{J}_W^{\dagger}\boldsymbol{\Sigma}_{\dot{\boldsymbol{x}}}(\boldsymbol{J}_W^{\dagger})^{\top} + \boldsymbol{V}_N(\boldsymbol{q})\boldsymbol{\Sigma}_y\boldsymbol{V}_N(\boldsymbol{q})^{\top} \tag{3.11}$$

where $\boldsymbol{\Sigma}_{\dot{\boldsymbol{x}}}$ is the covariance matrix of the noise of $\dot{\boldsymbol{x}}$ learnedfrom the data (see (4) in Fig. 3.3).

3.4.2 Learning the parameters W

We want to find the values of $\boldsymbol{W}$ that maximizes the likelihood of the $\dot{\boldsymbol{q}}$ of the training set (see (5) in Fig. 3.3). To do so, we introduce a score function $S(\boldsymbol{W})$ that is maximized with a non-linear optimizer:

$$S(\boldsymbol{W}) = \frac{1}{N_D}\sum_{i=1}^{N_D}\mathcal{L}(\dot{\boldsymbol{q}}_i|\boldsymbol{W}), \tag{3.12}$$

where $\mathcal{L}(\dot{\boldsymbol{q}}_i|\boldsymbol{W})$ is the likelihood of $\dot{\boldsymbol{q}}_i$ given a particular value of $\boldsymbol{W}$ and $\boldsymbol{N}_D$ is the size of the training set. For a given $\boldsymbol{W}$ and $\dot{\boldsymbol{q}}$, $\mathcal{L}(\dot{\boldsymbol{q}}|\boldsymbol{W})$ can be computed using $\boldsymbol{\mu}_{\dot{\boldsymbol{q}}}$ and $\boldsymbol{\Sigma}_{\dot{\boldsymbol{q}}}$ from Eq. 3.11 (since $\boldsymbol{\mu}_{\dot{\boldsymbol{q}}}$ and $\boldsymbol{\Sigma}_{\dot{q}}$ define a multivariate Gaussian distribution and we know $\dot{\boldsymbol{x}}$ and $\boldsymbol{q}$ from the training set):

$$\mathcal{L}(\boldsymbol{W}|\dot{\boldsymbol{q}}) = \frac{1}{\sqrt{(2\pi)^k|\boldsymbol{\Sigma}_{\dot{q}}|}}\exp\left(-\frac{1}{2}(\dot{\boldsymbol{q}} - \boldsymbol{\mu}_{\dot{q}})^{\top}\boldsymbol{\Sigma}_{\dot{\boldsymbol{q}}}^{-1}(\dot{\boldsymbol{q}} - \boldsymbol{\mu}_{\dot{q}})\right)$$

where $|\boldsymbol{\Sigma}_{\dot{q}}|$ denotes the determinant of $\boldsymbol{\Sigma}_{\dot{q}}$, $\boldsymbol{\mu}_{\dot{q}} = \boldsymbol{\mu}_{\dot{q}}(\boldsymbol{q}, \dot{\boldsymbol{x}})$, and $\boldsymbol{\Sigma}_{\dot{q}} = \boldsymbol{\Sigma}_{\dot{q}}(\boldsymbol{q}, \dot{\boldsymbol{x}})$.

Any non-linear optimizer can be used to maximize $S(\boldsymbol{W})$. For simplicity and robustness, we used BIPOP-CMA-ES [91], which is a gradient-free stochastic optimizer available in the "pycma" Python library.In each iteration of the algorithm new candidate solutions of $\boldsymbol{W}$ are generated by variation. Then, some solutions are selected to become the parents in the next generation based on the score function $S(\boldsymbol{W})$ evaluated after learning $\boldsymbol{y}(\boldsymbol{q}, \dot{\boldsymbol{x}})$ using GPs as explained in the previous section.

3.4.3 Prediction Phase

Once the model is trained, it can be used to predict the human joints' trajectories given the current configuration $\boldsymbol{q}_t$ and the expected EE trajectory executed by the robot $\{\boldsymbol{x}_1^d, \ldots, \boldsymbol{x}_T^d\}$. At each time step we can sample the EE velocity as: $\dot{\boldsymbol{x}}_t \sim \frac{1}{\Delta_t}\left(\boldsymbol{x}_{t+1}^d - f(\boldsymbol{q}_t) + \mathcal{N}(0, \boldsymbol{\Sigma}_{\dot{x}})\right)$, where Δ_t is the distance between two time-steps, $\boldsymbol{\Sigma}_{\dot{x}}$ is the robot repeatability when executing a trajectory (which we estimated empirically by executing a desired trajectory 10 times).

At each time-step, given the current configuration $\boldsymbol{q}_t$, we can get $\boldsymbol{\mu}_{\dot{q}}(\boldsymbol{q}_t, \dot{\boldsymbol{x}}_t)$ and $\boldsymbol{\Sigma}_{\dot{\boldsymbol{q}}}(\boldsymbol{q}_t, \dot{\boldsymbol{x}}_t)$ by querying the model (Eq. 3.11). From this multivariate Gaussian distribution, we can sample $\dot{\boldsymbol{q}}_t$, which allows us to compute the value of $\boldsymbol{q}_{t+1} \sim \boldsymbol{q}_t + \Delta_t \, \mathcal{N}(\boldsymbol{\mu}_{\dot{q}}(\boldsymbol{q}_t, \dot{\boldsymbol{x}}_t), \boldsymbol{\sigma}_{\dot{q}}(\boldsymbol{q}_t, \dot{\boldsymbol{x}}_t))$. To sample a whole trajectory, we repeat this procedure by propagating the sampling over time from $t = 0$ to $T - 1$. If we repeat this sampling procedure many times for a given trajectory, we get a Monte-Carlo estimation of the distribution over the human joint trajectories according to our model [47]. A schema of the prediction phase is depicted in Fig. 3.4.

3.5 Experiments

To evaluate our method (denoted as MI-NsGP), we compare it experimentally to alternative approaches that use only subsets of our elements (i.e., we make several ablation experiments):

1. **MI-NsGP**: Null-Space Gaussian Process with weight identification: our method, which learns both $\boldsymbol{W}$ and $\boldsymbol{y}(\boldsymbol{q}, \dot{\boldsymbol{x}})$ (section 3.4): $\dot{\boldsymbol{q}}|(\boldsymbol{q}, \dot{\boldsymbol{x}}) \sim \boldsymbol{J}_W^\dagger(\boldsymbol{q})\dot{\boldsymbol{x}} + \boldsymbol{V}_N(\boldsymbol{q})\mathcal{GP}(\boldsymbol{q}, \dot{\boldsymbol{x}})$
2. **GP**: learning directly from data: $\dot{\boldsymbol{q}}|(\boldsymbol{q}, \dot{\boldsymbol{x}}) \sim \mathcal{GP}(\boldsymbol{q}, \dot{\boldsymbol{x}})$.
3. **W-IK**: learning $\boldsymbol{W}$ but not $\boldsymbol{y}(\boldsymbol{q}, \dot{\boldsymbol{x}})$ (i.e., $\boldsymbol{y}(\boldsymbol{q}, \dot{\boldsymbol{x}}) = 0$)

   $\dot{\boldsymbol{q}} = \boldsymbol{J}_W^\dagger(\boldsymbol{q})\dot{\boldsymbol{x}}$
4. **NsGP**: learning $\boldsymbol{y}(\boldsymbol{q}, \dot{\boldsymbol{x}})$ but not $\boldsymbol{W}$ (i.e., $\boldsymbol{W} = \boldsymbol{I}$)

   $\dot{\boldsymbol{q}}|(\boldsymbol{q}, \dot{\boldsymbol{x}}) \sim \boldsymbol{J}_I^\dagger(\boldsymbol{q})\dot{\boldsymbol{x}} + \boldsymbol{V}_N(\boldsymbol{q})\mathcal{GP}(\boldsymbol{q}, \dot{\boldsymbol{x}})$
5. **Sb-M**: fitting a normal distribution $\mathcal{N}(\boldsymbol{\mu}_y, \boldsymbol{\Sigma}_y)$ on the training set for $\boldsymbol{y}(\boldsymbol{q}, \dot{\boldsymbol{x}})$ and not learning $\boldsymbol{W}$:

   $\dot{\boldsymbol{q}}|(\boldsymbol{q}, \dot{\boldsymbol{x}}) \sim \boldsymbol{J}_I^\dagger(\boldsymbol{q})\dot{\boldsymbol{x}} + \boldsymbol{V}_N(\boldsymbol{q})\mathcal{N}(\boldsymbol{\mu}_y, \boldsymbol{\Sigma}_y)$

where $\mathcal{GP}(\boldsymbol{q}, \dot{\boldsymbol{x}})$ denotes the distribution that corresponds to the GP model learned from data. The same training set and test set were used for all the methods.
Moreover, we compared our method with a state-of-the-art method for predicting joint trajectory while satisfying a task space motion primitive:

6. **ProMP** [170]: We fit both the joint space and operational space using probabilistic movement primitive. And then we use Bayesian task prioritization to condition the joint space using the operational space.

All methods were evaluated in three experiments. The first (**5R**) consists of predicting the joint state of a simulated 5R planar robot controlled by a biased IK function. The second (**EXP1**) and third (**EXP2**) consist in predicting the human posture (i.e., joints) during a co-manipulation trajectory, where a human is physically attached to the Franka robot to do a task.

3.5.1 Toy problem: 5R Manipulator

We simulate an overactuated planar robot with 5 degrees of freedom. Like a human, this 5R planar robot is overactuated for the two-dimensional position of its EE.

The robot controller is conceptually similar to the (unknown) human controller (Eq. 3.6), except that the ground truth is known ($\boldsymbol{W}, z(\boldsymbol{q})$). The 5R robot is controlled using the control law from Eq. 3.6, with:

$$z(\boldsymbol{q}) = \frac{\nabla \mathcal{C}(\boldsymbol{q})}{\nabla \boldsymbol{q}} + \mathcal{N}(0, \boldsymbol{\sigma}_z) \tag{3.13}$$

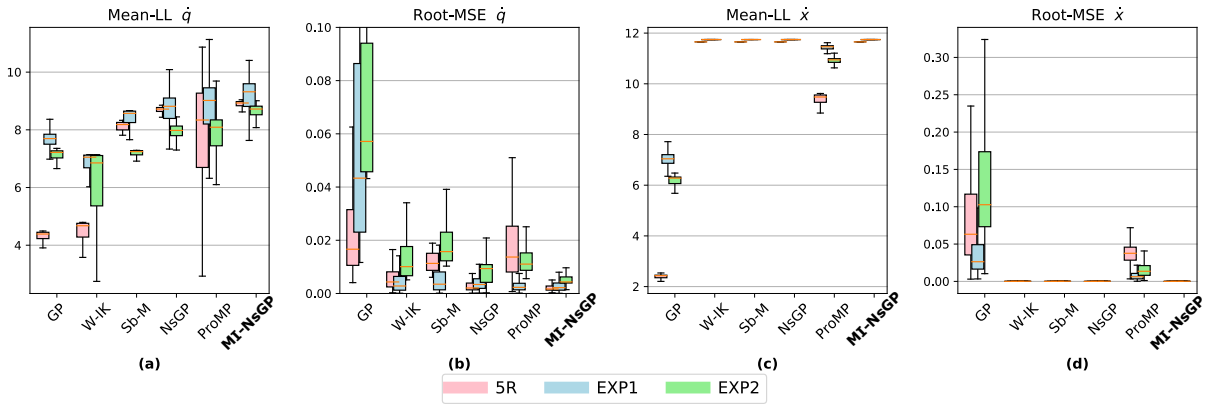

Figure 3.5: Comparison of methods for joint velocity prediction: (a) Mean-Log-Likelihood of the predicted joint velocity (b) R-MSE between the mean of the predicted joint velocity and real value (c) Mean-LogLikelihood of the EE velocity (d) R-MSE over the EE velocity. The methods were evaluated in three experiments: (red) simulated 5R planar robot controlled by a biased IK function; (blue) human posture prediction during a human-robot collaboration task; (green) human posture prediction during a human-robot collaboration task using different tasks in the training-set and in the test-set).

To define $z(\boldsymbol{q})$ similar to the human model, we hypothesized, as in [184], that the joint velocity minimizes an ergonomic cost function $\mathcal{C}(\boldsymbol{q})$ that depends on the joint configuration. We designed a cost function similar to the RULA continuous ergonomic score [40]. It is composed of the sum of a second order polynomial: $\mathcal{C}(\boldsymbol{q}) = \sum_{j=1}^{n}(p_{2,j}q_j^2 + p_{1,j}q_j + p_{3,j})$ where (p_1, p_2, p_3) have been calculated by fitting a second degree polynomial within the RULA score.

$(p_1, p_2, p_3)_{j=0}$	$(1.1 \times 10^{-03}, 0.0, 0.0)$
$(p_1, p_2, p_3)_{j=1}$	$(9.8 \times 10^{-04}, 0.0, 1.0)$
$(p_1, p_2, p_3)_{j=2}$	$(1.6 \times 10^{-04}, -2.5 \times 10^{-02}, 2.0)$
$(p_1, p_2, p_3)_{j=3}$	$(1.2 \times 10^{-04}, 0.0, 0.0)$
$(p_1, p_2, p_3)_{j=4}$	$(2.1 \times 10^{-03}, 0.0, 1.0)$

Table 3.2: Values of the parameters of the cost function $\mathcal{C}(q)$ similar to the RULA continuous ergonomic score.

To define $\boldsymbol{W}$, we assumed that some joints have more contribution than others (for example, in humans, the shoulders and elbows are typically more involved than lumbar's joints, but any musculoskeletal disorder can change this distribution drastically). To model these situations, we choose a weight matrix $\boldsymbol{W}$ that has non-uniform values (e.g., a low value for the first joint means that it is not used much). Specifically, we selected a diagonal and positive definite matrix with values bounded in $[0+\epsilon, 2-\epsilon]$. We choose to bound the values otherwise we risk falling into a singular configuration in which a joint never moves or always moves, which appears far from a human-like behavior.
Starting from a configuration $\boldsymbol{q}_0$, we apply $\boldsymbol{N}_D$ times the control law specified in Eq. 3.6 and 3.13, with a random EE velocity $\dot{\boldsymbol{x}}_i \in [-u_{max}, u_{max}]$. The successive joint state is then updated as $\boldsymbol{q}_t = \boldsymbol{q}_{t-1} + \dot{\boldsymbol{q}}_{t-1}\Delta_t + \omega_a\Delta_t^2$, where $\omega_a \sim \mathcal{N}(0, \boldsymbol{\Sigma}_a)$ is a Gaussian noise. If the robot falls in a singular configuration, the data collection stops and restarts from the $\boldsymbol{q}_0$ configuration. At each time step t, we collected $\{(\boldsymbol{q}, \dot{\boldsymbol{x}}), \dot{\boldsymbol{q}}\}_t$ to create the training set $\mathcal{D}$. The dataset, composed of $N_D = 10^3$ points, was normalized and divided into a training and a validation set following the proportion 70/30. We trained

the models using the training set. Each GP was implemented in Python using *gpytorch* library, with a constant mean and the RBF kernel. The optimization was done on an Intel Core^{TM} i7-8850H with 6 cores at 2.6GHz, requiring about 10 hours. We repeated the experiment 10 times, varying the starting point and the parameters of the control model (W).

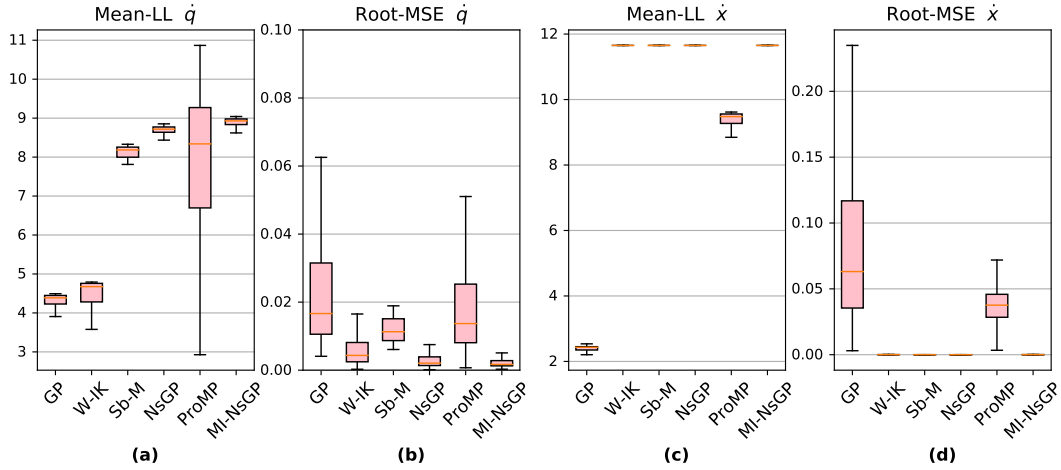

Figure 3.6: Comparison of methods for joint velocity prediction for 5R manipulator: our method (MI-NsGP), learning directly from data using Gaussian Process (GP), learning W and apply pseudo-inverse (W-IK), learning null space (NsGP), motion primitives based method (ProMP), sampling in the null space (Sb-M). The criteria: (a) Mean-Log-Likelihood of the predicted joint velocity (b) R-MSE between the mean of the predicted joint velocity and real value (c) Mean-LogLikelihood of the end-effector's velocity obtained applying the methods (d) R-MSE of the end-effector's velocity.

	M-LL $\dot{q}$	R-MSE $\dot{q}$	M-LL $\dot{x}$	R-MSE $\dot{x}$
GP	4.39 [4.23, 4.45]	(16.98 [10.34, 30.90])$\times 10^{-3}$	2.43 [2.35, 2.45]	(6.31 [3.54, 11.68])$\times 10^{-2}$
W-IK	4.67[4.28, 4.76]	(4.33 [2.46, 8.13])$\times 10^{-3}$	**11.65 [11.65, 11.65]**	**(3.57[1.47, 4.25])**$\times 10^{-5}$
Sb-M	8.18[8.00, 8.26]	(11.30 [8.69, 15.10])$\times 10^{-3}$	**11.65 [11.65, 11.65]**	**(2.96 [1.73, 3.22])**$\times 10^{-5}$
NsGP	8.72[8.64, 8.77]	(2.06 [1.36, 3.91])$\times 10^{-3}$	**11.65 [11.65, 11.65]**	**(1.27 [0.63, 2.35])**$\times 10^{-5}$
ProMP	8.34[6.70, 9.27]	(13.69 [8.07, 25.29])$\times 10^{-3}$	9.47[9.27, 9.55]	(3.76 [2.84, 4.58])$\times 10^{-2}$
MI-NsGP	**8.93[8.83,8.97]**	**(1.69 [1.26, 2.80])**$\times 10^{-3}$	**11.65 [11.65, 11.65]**	**(2.41 [1.05, 3.81])**$\times 10^{-5}$

Results: We first analyze the quality of the predicted distribution by computing the mean log-likelihood over the test set (red box-plots in Fig. 3.5a). Overall, our method (MI-NsGP) leads to significantly better likelihood values than all the other control approaches. The worst likelihoods are obtained by the methods that do not use the null space. Among the methods that use the null space, learning W makes a significant difference. The low likelihood for ProMP is due to the lack of a primitive for the movements, which results in a large variance for the solution obtained using ProMP. We then focused on the mean prediction by computing the root mean square error on $\dot{\boldsymbol{q}}$ (red box-plots in Fig. 3.5b) (we ignored the variance). As before, the best results are obtained with our method, and using the null space makes a significant difference. However, learning a simple Gaussian model instead of a GP leads to very bad mean square errors, whereas it corresponds to high likelihood values (red box-plots in Fig. 3.5a). This means that this method has a very large variance, which makes the test set likely (high likelihood score) but the predictions very inaccurate. Also in this case, the solutions found using the ProMP are inaccurate.

Last, we computed the mean log-likelihood and the root-MSE for the EE position (red boxplots in Fig. 3.5c and Fig. 3.5d). As expected, perfect scores are obtained with the methods that exploit the

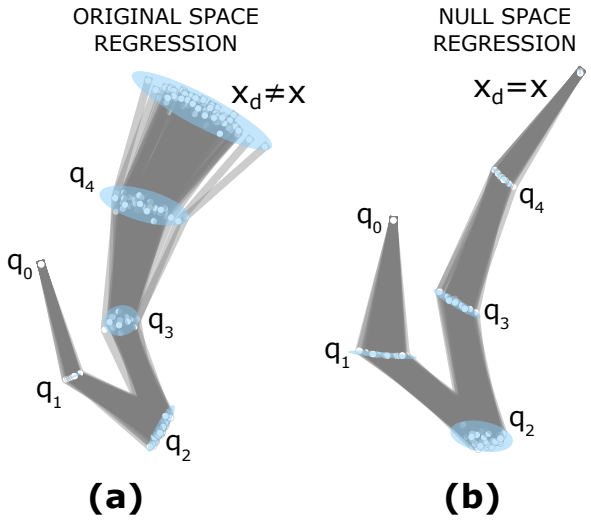

Figure 3.7: Example of how regression in the null space guarantees the kinematic constraint while regression in the original space is not able to satisfy the kinematic constraint in the toy problem.

null space (W-IK, Sb-M, NsGP, MI-NsGP), but learning directly a GP that predicts $\dot{\boldsymbol{q}}$ directly leads to significant errors in the EE position. The solutions obtained using ProMPs have lower score since the task space has large variance trying to fit a ProMP to trajectories that are not related to a movement primitive. These results suggest that if the human's IK model is similar to the one we used for the 5R robot, our method is likely to improve the quality of posture prediction, returning only solutions which satisfy the kinematic constraint.

3.5.2 Human IK prediction

We then evaluated our method in three experiments (**EXP1**, **EXP2**, and **EXP3**), where a human interacts with the Franka Emika Panda robot. The human is facing the robot, his/her right hand is in physical contact with the robot's EE (see Fig. 3.1 and video attachment). The Xsens MVN suit is used to capture the human posture (and to have the ground truth of the posture prediction). The human poses are fitted (retargeted) to a DHM of 66 segments (Fig. 3.14a), based on the Xsens MVN model. The segments are scaled with the human height, while the dynamic properties (e.g., mass) are computed from anthropometric data available in literature [148]. We modeled the human spherical joints collected by the motion capture suit as a series of 3 one-dimensional revolute joints, where each DoF is controlled by a single actuator. The resulting DHM posture is represented by the 66 joints. A URDF (Universal Robot Description Format) model is then created to represent the kinematics and dynamics of the DHM, and used by the Pinocchio library [45] to calculate the Jacobian going from the human pelvis to the right hand for a given human joint configuration.

In this paper, we predicted only the joints that belong to the active kinematic chain, i.e., joints that connect segments from the pelvis to the right hand. The reason is twofold: first, a simpler model speeds up the computation; second, it is the set of joints that are used to compute ergonomics score (e.g., RULA, back angle), which is our final objective. The human posture is thus characterized by 24 revolute joints and the resulting dataset $\mathcal{D} = \{(\boldsymbol{q}_i, \dot{\boldsymbol{x}}_i), \dot{\boldsymbol{q}}_i\}_{i=0}^{N_D}$ contains $\boldsymbol{q} \in \mathbb{R}^{24}$, i.e., the joints which link the human pelvis to the right hand, and $\boldsymbol{x} \in \mathbb{R}^6$, i.e., the EE position and orientation. We evaluated our method in three experiments:

In **EXP1** the training set used to train the algorithm consists of human postures recorded during the

repeated execution of similar co-manipulations (for which we can compute a movement primitive).The robot executes four "pick and place" trajectories spanning 50cm, and its orientation is maintained constant. Each trajectory is repeated 10 times: during the first experiment (EXP1) the first five trajectories comprise the training set, and the five remaining ones, the test set. Fig. 3.15a shows the intrinsic variability of the human repetitions (for the same EE movement, the joint trajectories change).

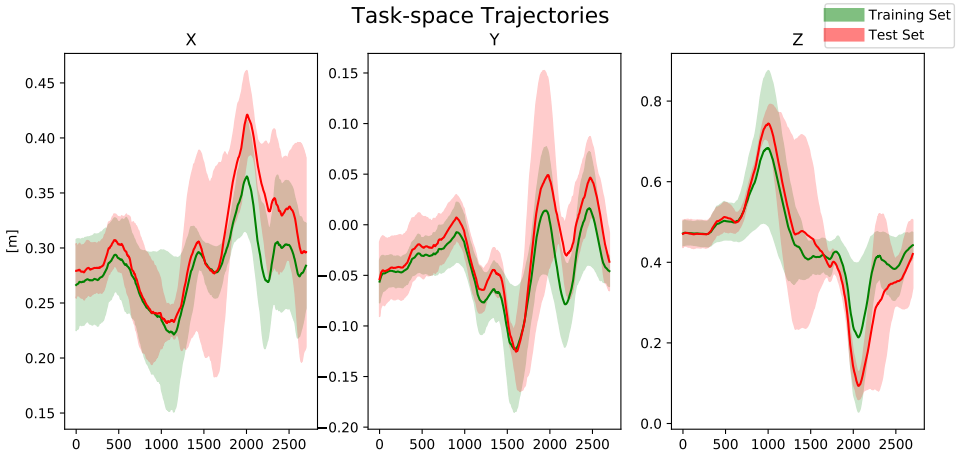

Figure 3.8: End-effector's trajectories used in the first human-robot interaction scenario (**EXP1**): in this case, the training set and the test set belong to the same movement primitive.

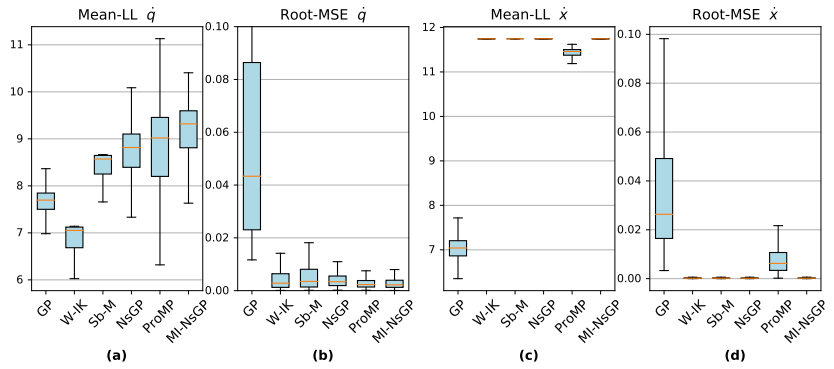

Figure 3.9: Comparison of methods for joint velocity prediction in Human Joint Velocity Prediction: (a) Mean-Log-Likelihood of the predicted joint velocity (b) R-MSE between the mean of the predicted joint velocity and real value (c) Mean-LogLikelihood of the EE velocity (d) R-MSE on the EE velocity.

In **EXP2** the training set consists of pseudo-random trajectories that do not necessarily refer to motion primitives. With this second experiment, we tested the ability of our method to generalize to new movement primitives. To do that, we collected a not pre-defined training set of "pick and place" movements controlling the robot using a Joystick. We trained our algorithm on this dataset and we tested on the same test-set as EXP1.

In **EXP3** we record ten trajectories during a human-robot collaboration scenario (Fig. 3.12): we chose another human operator to test if the algorithm could be used for a different person with different body shape (in the first experiment, the operator is a male subject of height $1.84m$ and weight $90kg$, in the second experiment the operator is a female subject of height $1.68m$ and weight $64kg$). We record ten

Figure 3.10: Set-up for **EXP2**: the robot executes pseudo-random movements while it is controlled by a second operator using a joystick.

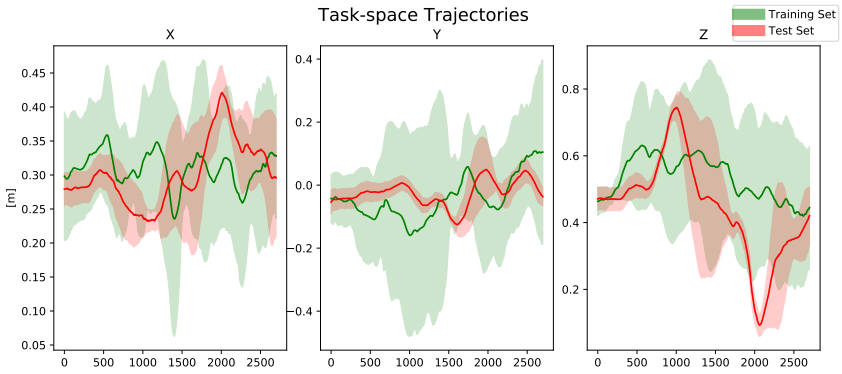

Figure 3.11: End-effector's trajectories used in **EXP2**: in this case, the training set and the test set belong to different movement primitives.

trajectories while the human is collaborating with the robot in a seated position; each trajectory consists of a combination of three pick and place gestures over a table.

Figure 3.12: Set-up for **EXP3**: Human and robot are coupled, the robot executes the same trajectory ten times while the human follows its movements.

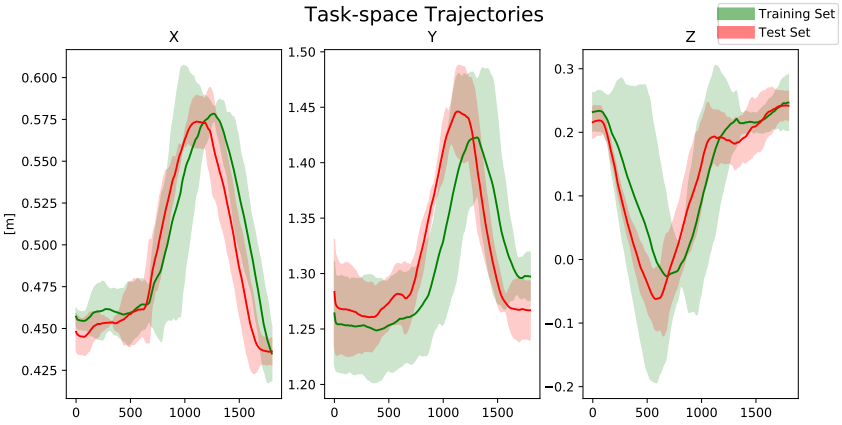

Figure 3.13: End-effector's trajectories in **EXP3**: in this case, the training set and the test set belong to the same movement primitive, a different human operator executes the movements with respect to the other scenarios.

In the prediction phase we sampled 10 trajectories using the Monte-Carlo approach and for each of them we calculated four different ergonomics scores from the state of the art in human ergonomics [148]: RULA, REBA, RULA continuous and cumulative back angle (Fig. 3.14b). The purpose is to show that the probabilistic IK also impacts the prediction of ergonomics scores, which is critical information for a collaborative robot.

Results: We evaluate the performance of our method in predicting the human posture when both, the training set and the test set, are considered the same movement primitive (EXP1). We analyze the quality of the predicted distribution by computing the mean log-likelihood over the test set (blue in Fig. 3.5a). Overall, our method (MI-NsGP) leads to significantly better likelihood values than all the control approaches. Moreover, its performance is comparable with the state-of-the-art method for human posture prediction (ProMP). In fact MI-NsGP performs better in the median and max value of the 95^{th} percentile (MI-NsGP: $9.32[8.81, 9.59]$, ProMP: $9.02[8.20, 9.46]$). Regarding the the root-mean-square error on $\dot{q}$ (Fig. 3.5b), our method is comparable with the SoA method (MI-NsGP: $(2.19[1.24, 3.38]) \times$

10^{-3}, ProMP: $(2.30[1.37, 3.83]) \times 10^{-3}$) and presents better results with respect to the other model-based methods (W-IK, Sb-M, NsGP) and with respect to using the GP in the original space (Fig. 3.5b). Regarding the ability to satisfy the kinematic constraint, we observed a behavior similar to the toy-problem. In fact, model based methods (W-IK, Sb-M, NsGP, MI-NsGP) always have bigger likelihood and smaller root-mean-square error with respect to GP regression. ProMP results are also accurate in this case because the training set and the test set belong to the same movement primitive. The superiority of model based methods is even more evident at trajectory level: if we use the GP alone to predict the DHM postures while the prediction horizon is growing, the R-MSE between the EE of the DHM and the robot's EE (the red progression in Fig. 3.15b) grows too fast to be used in a safe human-robot collaboration scenario while if we use MI-NsGP (the green progression in Fig. 3.15b) the error is acceptable. In the case of the human, W is unknown; thus, it is not straightforward to evaluate the resulting values from model identification. Nonetheless some considerations are possible: even considering different training-sets, the optimization converges to the same values of W; these values agree with our expectations regarding the distribution of the joint velocity. In fact, the joints which move less (e.g. lumbar joints) have a smaller value with respect to those which are more involved in the execution of the movement (e.g. shoulder and elbow).

In EXP2 we evaluate the ability of our method to generalize the information learned for one trajectory to another. The results show that our method outperforms the others both the likelihood (MI-NsGP: $8.72[8.52, 8.81]$, ProMP: $8.0[7.44, 8.34]$) and the root-mean-square error (MI-NsGP: $(4.34[3.93, 6.22]) \times 10^{-3}$, ProMP: $(11.04[8.70, 15.25]) \times 10^{-3}$) while continuing to satisfy the kinematic constraint (green in Fig. 3.5). The results suggest that our method could be used to have a probabilistic estimation of the human posture also for trajectories which do not share the same movement primitive.

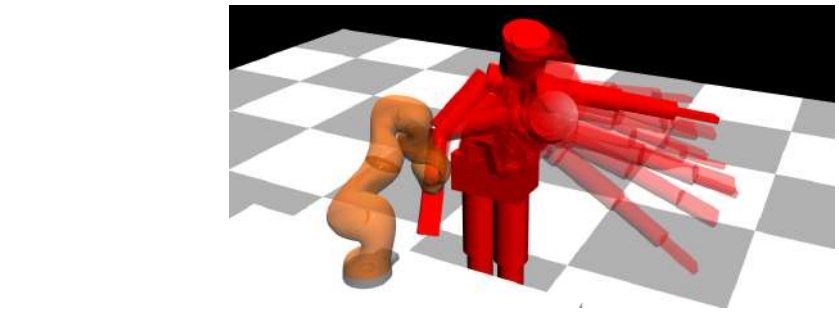

(a)

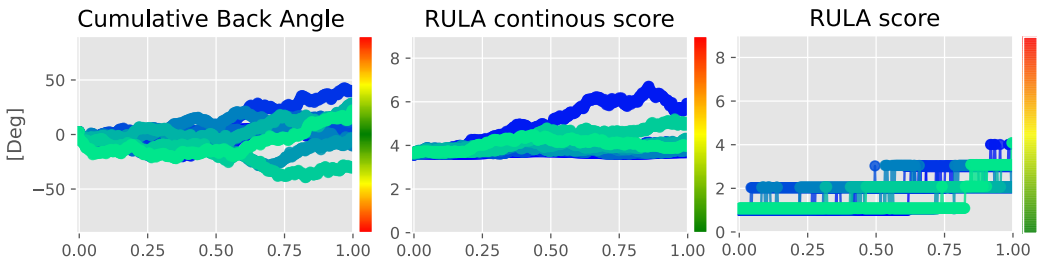

(b)

Figure 3.14: (a) The DHM in Simulation, showing the variance of the solutions calculated via Monte-Carlo integration. (b) Ergonomic scores computed on different sampled trajectories: RULA, REBA, RULA continuous, cumulative back angle.

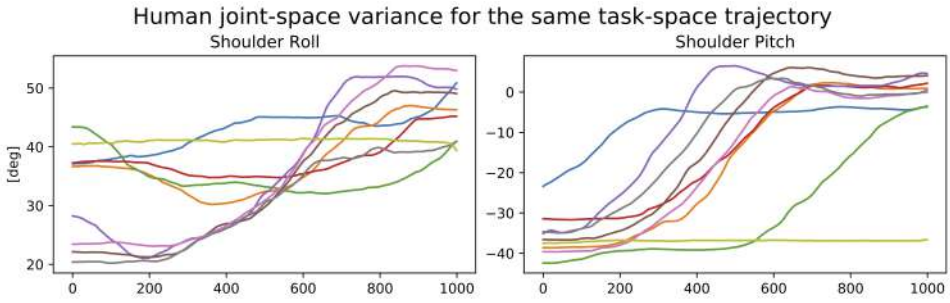

(a)

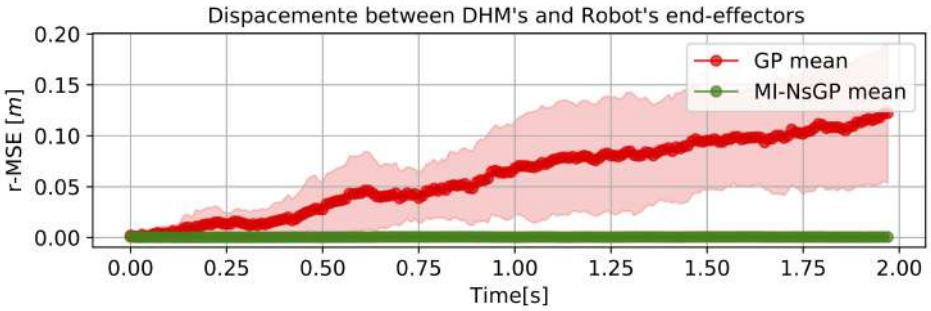

(b)

Figure 3.15: (a) Human joint trajectories (shoulder roll and pitch) in response to the same EE movements. (b) MSE in offline prediction with GP and MI-NsGP.

3.6 Conclusions

In this chapter we presented a method for predicting human posture in a Human-Robot Collaboration scenario where the human hand motion is constrained by the robot's end-effector. We propose a two-phase method: in the first phase, we leverage a dataset of human demonstrations to learn a distribution over the null-space of the human Jacobian using a Gaussian Process; in the second phase, we optimize the weights of the weighted pseudo-inverse of the Jacobian. Our method computes a probabilistic estimation of the future postures that satisfy the kinematic constraints imposed by the physical link between the human and the robot and, at the same time, it is coherent with the human preferences of movement.

In the future, we want to consider the full human model in posture prediction and integrate the algorithm into our framework for ergonomics control, which aims to optimize a collaborative robot's motions to maximize the comfort and the ergonomics of the human collaborator. A byproduct of our method is the probabilistic computation of ergonomics scores for a given robot's EE trajectory, which is a critical element for planning the robot's trajectories. Further, we want to remove the leader/follower hypothesis and address the case where the leadership role may vary over time. In fact, we wonder how human behavior may vary depending on the control law implemented in the robot. To try to give an initial answer to this question in the next chapter (Chapter 4) we propose a study in which we analyze the motor behavior of subjects performing a co-manipulation task with a robot.

4

Design of Cooperative and Collaborative strategies using Impedance control

In previous chapters, particularly Chapter 1, we already pointed out that robotics solutions have the potential to improve the working conditions of human operators in industry [66]. In particular providing physical assistance to reduce the human physical workload [6] and intelligently adapting its assistance to each user and task. However, it has been pointed out that the acceptance of collaborative manipulators may not be straightforward for human workers [19, 144]: in particular, it could be easier to interact with a robot that has a fixed role in the interaction rather than with a robot with more complex behavior. This preference may not necessarily relate to better performance in task execution. This observation led to the current investigation of whether it is more convenient or efficient for a human to cooperate or collaborate with a robot to execute a co-manipulation task and whether this behavior has any relation with the way two humans cooperate or collaborate to solve the same task.

In this chapter, we address this problem by focusing on a human-robot co-manipulation task where an object has to be carefully extracted from a tube and inserted into another one, without touching the environment. This task requires precision, and we expect the stiffness of each agent to be critical to reject disturbances that may lead to task failure. In this context, we ask the following questions: is it more efficient and task-performing for the dyad to cooperate or to collaborate? When collaborating, should the robot behave as a human collaborator? Among the possible collaboration strategies, should the robot imitate or reciprocate the human's stiffness behavior?

To answer these questions, we conducted two co-manipulation experiments in the same setup/scenario: the first with a human-human dyad, the second with a human-robot dyad. In the first phase, we investigated the performance and the arm stiffness of human-human dyads when they were cooperating and collaborating [84]. Dyads were more accurate (i.e., fewer task errors) when there was no clear role allocation (i.e., when they were collaborating) at the expense of a higher effort. Indeed, during collaboration, both agents had similarly high levels of arm muscle co-contraction, therefore, higher levels of arm stiffness, as if they were both leaders. This study showed that collaborating humans mirror their stiffness: could this be a legitimate collaborative strategy also for a robotic collaborator?

In the second phase, we investigated the performance and arm stiffness of the human interacting with a robot (Franka) when the dyad is cooperating and collaborating, across four conditions. In cooperative conditions, the robot is either leader or follower, and vice-versa for the human. In the collaborative conditions, we implemented two possible collaborative impedance strategies: the first, inspired by the previous study, mirrors the human stiffness, while the second, inspired by [178], reciprocates the human stiffness.

Our human-robot study confirmed that in co-manipulation it is more convenient to collaborate be-

cause collaboration leads to fewer task errors. Both collaborative impedance strategies give similar results in terms of human effort (i.e., arm muscle co-contraction), however subjective evaluations indicate a clear preference of the human participants for the reciprocal impedance strategy.

In the following, we briefly overview the first study and report on the methodology and results of the second study, discussing the implications of the results for future collaborative robotics technologies.

This chapter presents the preliminary results of an experimental study we are conducting(hal-03589692v1). We tested the experimental conditions on 13 subjects, and here we present the results obtained with these participants. At the time of writing this thesis, 3 more tests were carried out on other subjects, and we plan to integrate the results by considering these latest results. Also, compared to the current writing of the paper, in this chapter we extended the background on human motor behaviour and we present the setup and control design of the robot more in detail. Also the results have been extended presenting the values of the index of co-contraction for the different participants.


Cooperation or collaboration? On a human-inspired impedance strategy in a human-robot co-manipulation task

Lorenzo Vianello[1,2], Waldez Gomes[1,3], Pauline Maurice[1], Alexis Aubry[2], Serena Ivaldi[1]

Abstract— We investigate whether a robot should behave as a collaborator or as a cooperator of a human partner in a co-manipulation task. In a previous study, we addressed the same question for a human-human dyad and found that collaboration is preferable to make fewer errors at the expense of increased arm stiffness for the humans, who behave as if they were both leaders. In this study, the human is coupled with a Franka robot and they jointly engage in the same co-manipulation task in different conditions. In the cooperation conditions, the robot is either a leader or a follower, exhibiting fixed impedance strategies. In the collaborative conditions, the robot exhibits either reciprocal or mirrored adaptive impedance strategies that vary according to an EMG-based online estimation of the human arm stiffness. Our results show that, for the co-manipulation task, a robot collaborator seems more preferable than a robot cooperator, leader or follower, and that the reciprocal strategy for impedance seems to be the most indicated.

Video is available at: video Human-Franka co-manipulation.

4.1 Cooperation vs. Collaboration

We adopt the distinction between cooperation and collaboration as defined by Jarrassé et al. [99]. If before the co-manipulation, the agents have been assigned, or have agreed upon, different roles (asymmetric responsibilities) to execute the task, then the interaction is classified as a *cooperation*. In contrast, during a *collaboration*, both agents form a "spontaneous" coalition to accomplish the task [60]: their "activity is synchronized and coordinated in order to build and maintain a shared conception of a problem" [192]. That is, in collaboration, the agents may deliberate and negotiate their roles in executing the task to accomplish the dyad's common goal.

Human-robot cooperation is often formalized by fixed roles determined by coordination between the agents. Typically, fixed roles such as leader and follower are determined by the endpoint impedance. The leader-follower role allocation approach in which the human is always the leader of the task is likely the most traditional coordination strategy in physical Human-Robot Interaction (pHRI) [138]. In co-manipulation, this is usually characterized by high stiffness profiles for the leader's arm endpoint, and low stiffness for the follower's [215]. In this case, the robot may be controlled to guarantee only certain aspects of the task execution, such as rejecting disturbances, or sustaining forces and positions in different axes from the ones controlled by the human [247]. Ficuciello *et al.* [73] uses a more sophisticated strategy that explores the null-space of a redundant robot to decouple the apparent inertia at the robot end-effector, reportedly improving the intuitiveness of the task for the leader. It is frequent to find this configuration in rehabilitation robotics, for example, when robotic arms (leaders) guide the patients' arms (followers) along desired trajectories [198]. Even though the leader-follower approach meets great success in some applications such as robotic surgery [166,183], and telemanipulation, there are instances in which adaptive or continuous roles could be preferred [100]. Cherubini *et al.* [52] alternates the leader and follower roles of a robot in a pHRI application for industry according to visual and haptic cues by

the human co-worker. Khoramshahi and Billard [107] propose a method to automatically detect when the human co-worker is physically trying to guide a robot that is executing an autonomous task. After the intent detection, the robot switches into a follower mode, and only goes back to leader mode when the human stops correcting the robot. Agravante *et al.* [3] interpolate between a humanoid robot's behavior from a total leader to a total follower (each behavior corresponds to a different walking pattern generator to the humanoid robot). During the leader behavior, the robot controller minimizes the errors for the desired trajectory (high-impedance), whereas for the follower behavior it minimizes the forces applied at the human operator (low-impedance).

Therefore, in the literature, it is often the case that either the roles are fixed (cooperation) or they are adapted according to a strategy (collaboration). However, to the best of our knowledge, little is known about the effect of the two approaches on the same joint task, to inform about the best strategy to adopt for humans. In this work, we compare both approaches in the same co-manipulation task, having in mind the outcome of a previous study that investigated human cooperative and collaborative behavior in the same task/scenario. Our rationale is that if collaboration is preferable for a joint task realized by a human dyad, there is a possibility that it would be preferable also for human-robot interaction in joint tasks. At the same time, we are aware that a robot cannot fully reproduce complex human behavior. We target the question of which impedance behavior the robot should exhibit to collaborate proficiently and whether this behavior should imitate the one of a human partner.

Transferable impedance from human signals to robot behavior is often referred to in the literature as *tele-impedance* [71]. Here, we use an index of co-contraction (Sec. 4.4.1) to estimate the modulation of human stiffness, and consequently, our tele-impedance profiles (Sec. 4.4.2). Peternel *et al.* [180] proposed a method for human-robot collaboration where the robot behavior is adapted online to the human motor fatigue. The same authors presented in [178] two control strategies (robot reciprocal and robot mirrored) based on the concept of tele-impedance. During Reciprocal tele-impedance the robot and the human operator execute two behaviors that are reciprocal in terms of phase of operation (e.g. sawing task). On the other side, during mirrored tele-impedance, both agents produce the same behavior in a certain phase of the task (e.g. valve turning). Their work led us to question whether this kind of adaptation could in any way be traced back to the collaboration observed during the human-human experiment.

4.2 Human Motor Control

A prerogative of control laws for robots to collaborate with humans is transparency. Transparent controllers must be easy to understand even for not expert people [252]. One way to do this is to construct control laws that refer to human motor control [253]. The human motor control system is light, its sensorimotor apparatus noisy and delayed. Despite these limitations, it can accomplish very accurately complex high-level tasks in presence of disturbances and unpredictable changes in the environment. Accuracy, in this case, is not based on high stiffness, but rather on anticipation and capability to adapt to perturbations, i.e. on a combination of feedback and feedforward control.

Feedforward control consists in applying a sequence of controls without monitoring the state during this sequence. This kind of control can yield suboptimal and unstable performances in unpredictable environments. Shadmehr and Mussa-Ivaldi [204] investigated how humans learn this feedforward component in different dynamical conditions. In their experiments, the environment in which the human performs a reaching task is subject to a force field. With practice, hand trajectories in the force field converged to a path very similar to that observed in free space. At this point, the authors suddenly removed the field. The resulting trajectories were approximately mirror images of those that were observed when the subjects were initially exposed to the field. This result suggested that humans gradually compose a

model of the environment and use that model to predict and compensate for external perturbations.

Feedback control becomes necessary to achieve high performance whenever the environment is unpredictable or unobservable. This explains the trial-to-trial variability of trajectories performed by humans during repetitive tasks: feedback controller tries to reduce global task errors and makes the controlled trajectory robust to perturbations by varying impedance through co-contraction. Burdet *et al.* [38] examined arm movements in an unstable dynamic environment. The results of the experiment proposed to suggest that humans learn to stabilize unstable dynamics by controlling mechanical impedance (resistance to imposed motion). However, fast and coordinated limb movements cannot be executed under pure feedback control alone, because biological feedback loops are too slow ($\geq 10ms$) and have small gains. The Feedforward loop anticipates the evolution of the system and accounts for a desired predicted trajectory.

So, the human motor control strength is the combination of the feedforward and feedback signal. The dominance of one component over another gradually changes from feedback control during the early stages of skill acquisition, to feedforward control in highly trained individuals [76]. With this in mind, in Gomez *et al.* [84] constructed an experiment to observe how human motor control functions in the presence of cooperation or collaboration between two subjects.

4.3 Previous study: Human-Human Dyad Experiment

Previously [84], the authors proposed an experiment with a task executed by two physically interacting human agents, i.e. a human-human dyad (Fig. 4.1a). The participants executed the task under two main conditions:

- **Cooperative**: Agent 1 is assigned the leadership while Agent 2 is the follower and vice-versa;
- **Collaborative**: there is no pre-assigned leadership.

During the task execution, they measured the participant's muscle activation, as well as their accuracy at executing the task for each trial. The results show that the human-human dyads made fewer errors without pre-assigned roles than when there was a leader. In addition, they also observed that when there was no pre-assigned leader, the agents had a muscle co-contraction level as high as when they were leaders of the task. Since muscle co-contraction is associated with arm stiffness, they hypothesize here that robots similarly modulating their end-effector stiffness could emulate the aforementioned human motor behavior.

Participants: the human-human dyad experiment was executed by 10 dyads, therefore 20 participants, of which 15 were male, and 5 were female. Their age ranged from 22 to 38 years old (M = 26.6 years, SD = 3.61 years). 17 participants were right-handed, and 3 were left-handed even though all manipulations were performed with the right hand.

Every participant provided written informed consent for their participation in the experiment. No participant claimed any chronic motor disease or health condition that could influence in the experiment's results. The experiments were approved by INRIA's ethical committee (COERLE).

Task description: the task consists in manipulating an object (pipe) to bring it from a start to an end point (Fig. 4.1a). The participants are instructed to avoid moving their backs during the task execution (they are not strapped). They hold the pipe with their right hand with a power grasp, placing their hand on one of the designated handles. In the start (Phase 1), the pipe is within Tube 1 (the one closest to Agent 1), then the pipe has to be taken out of Tube 1 while avoiding contact with Tube 1's front wall. After extracting the pipe from the tube (Phase 2, free movement), the pipe has to be moved around a cylindrical obstacle towards Tube 2 (the one closest to Agent 2). Then, the pipe has to be inserted into

Tube 2 (Phase 3), while avoiding contact with the front wall. By design, the task is always recorded and evaluated from Tube 1 to Tube 2, and the return motion is ignored.

In this experiment, a black curtain is placed between the participants to prevent visual eye-contact during the task execution. In addition, they are instructed not to talk during the task execution.

Experiment Description: in the human-human dyad experiment, two agents share the pipe manipulation. Each agent sits on one side of the table (Agent 1 and Agent 2 in Fig. 4.1a), then the dyad performs the task under the following conditions:

- *No specified roles:* Participants are only instructed to manipulate the pipe;
- *Agent 1 Leader and Agent 2 Follower:* Participants are instructed that Agent 1 must lead the movement;
- *Agent 1 Follower and Agent 2 Leader:* Participants are instructed that Agent 2 must lead the movement.

The order of the 3 conditions is randomized across dyads to counter-balance possible biases.

Before starting the recording for each condition the participants could practice for 2 trials. For each condition, 5 trials were recorded, resulting in a total of 15 trials. Since there were 10 recorded dyads, a total of 150 trials were recorded.

4.4 Human-Robot Dyad Experiment

In order to investigate how human-human dyads motor behavior transfers to human-robot dyads, we conducted an experiment in which human participants performed a co-manipulation task with a robot under different conditions. Namely, four profiles were defined for the robot end-effector impedance, to implement *cooperation* and *collaboration* conditions. The experiment is detailed hereafter.

4.4.1 Experimental set-up

The task consisted in co-manipulating an object ($0.2\,kg$ pipe of diameter $3\,cm$ and length $50\,cm$) with a collaborative robot, in order to bring it from a start to an end point (Fig. 4.2). The task was divided into 3 phases. In phase 1 the pipe is within a tube (tube 1, close to the robot) and is extracted from it while avoiding contact with its front wall (hole diameter: $4.5\,cm$). In phase 2, the pipe is moved in free space in a horizontal plane, from tube 1 to tube 2, around a cylindrical obstacle. In phase 3, the pipe is inserted in a second tube (tube 2, close to the human) while avoiding contact with its front wall. The return motion (from tube 2 to tube 1) was not part of the task. Performing the task once took between 15 and $25\,s$ on average, though there was no time instruction or limit. Participants were seated on a chair facing the robot and were instructed to avoid moving their backs during the task. They held the pipe with their right hand, on the designated handle while the other handle was attached to the robot end-effector with a dedicated 3D-printed part. The EMG sensors are placed on the subject following guidance rules from the European project SENIAM [216], as well as location cues from Perroto, 2011 [174]. After locating a muscle, the subject is asked to contract it to confirm the location of the "muscle belly", that is then marked with a pen. For each muscle, an EMG sensor is assigned, and annotated in our EMG acquisition software. Before placing a sensor on a muscle location, the area surrounding the pen mark is prepared accordingly. The subject's skin is cleaned with alcohol until it acquires red tones, which indicates good skin impedance. After the alcohol dryes out, the EMG sensor is placed on the skin at the muscle fibers direction with the help of a double-sided sticker provided by the sensor manufacturer. Prior to the task execution, each agent is asked to perform maximum voluntary contractions (MVC) during isometric

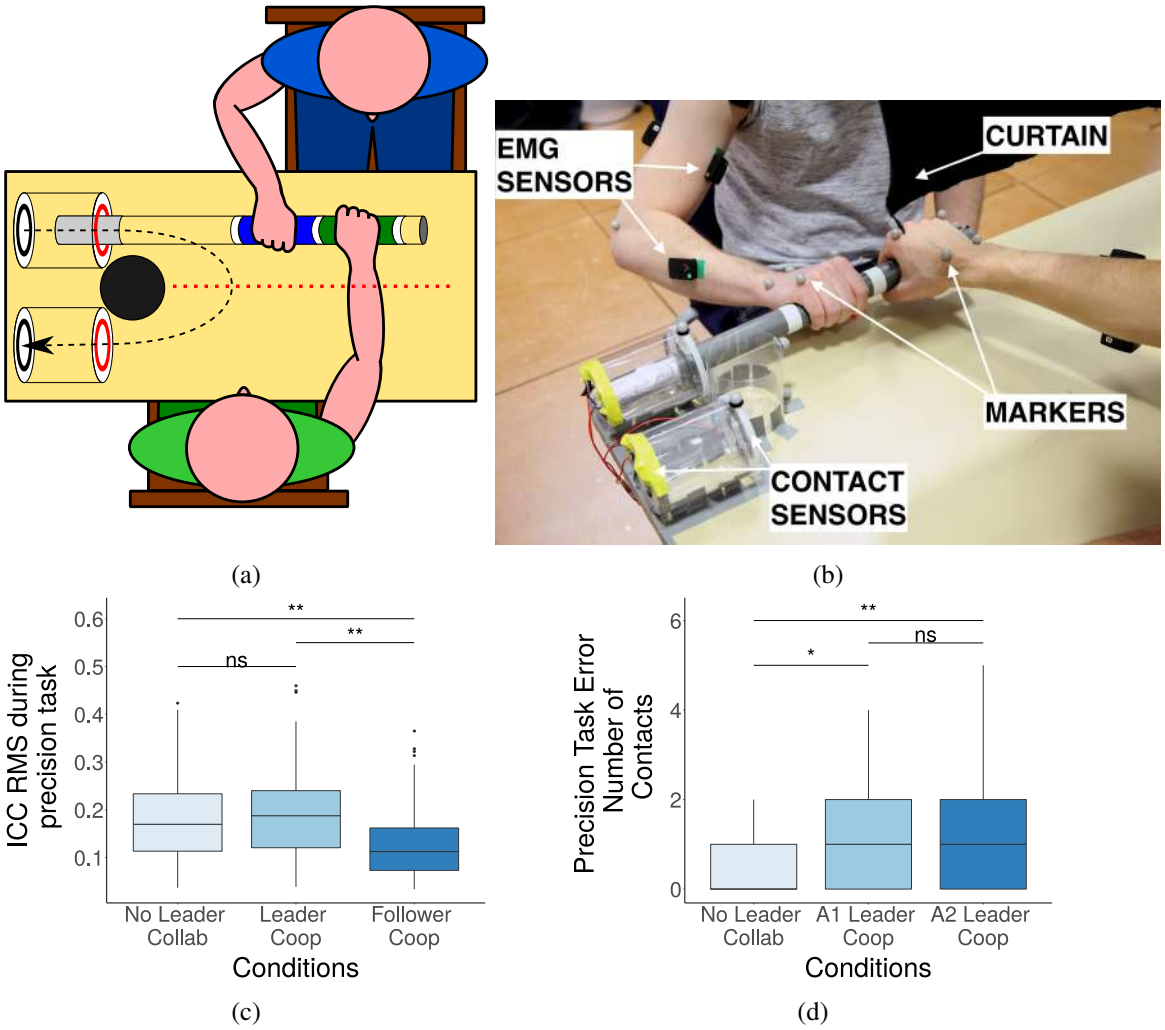

Figure 4.1: Human-Human co-manipulation study [84]: (a) Top-down view of the experiment set-up. The black dashed line approximates the pipe trajectory. The red circles are contact sensors used to detect any contact between the pipe and the tubes' front walls. The red dashed line represents a curtain placed between both agents to prevent visual eye-to-eye communication. (b) Experimental set-up. (c) Root Mean Square value of the index of co-contraction (ICC) during the extraction and insertion phases for each condition. (d) Number of contact between the pipe and the tubes' walls (errors) for each condition.

exercises for each selected muscle [216] for 3 s. The exercise is performed 3 times, with a 1 minute interval between them to decrease fatigue biases. After the 3 trials, the maximum EMG signal is then stored and used for posterior post-processing of the EMG signals during the task execution. The designed task requires the solo agent, or human dyad, to avoid contact between the pipe and the tube walls. We then use contact sensors to detect those contacts, and posteriorly use this information as a performance measure. To detect the contacts between the pipe and the tubes, we wrapped the end of the pipe with aluminum foil, and metallic rings were placed inside the walls of both tubes. It is important to note, that those contact sensors are essentially mechanical switches which are known for their bouncy signals, so to circumvent this issue we debounce the input through software. After we detect a signal onset (a contact) no other onset is stored as a contact for the next 100 ms window (roughly half of the average human simple reaction time [251]). The data collection taken from a Windows computer (EMG) and from a Linux computer (Robot control and contact sensor) is colleted and sincronized using ROSBAG.

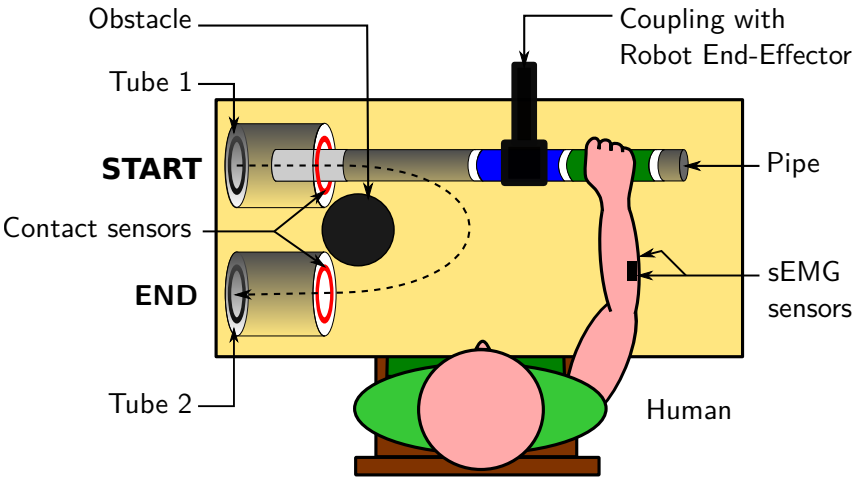

(a) Top-down view. The black dashed line approximates the pipe trajectory.

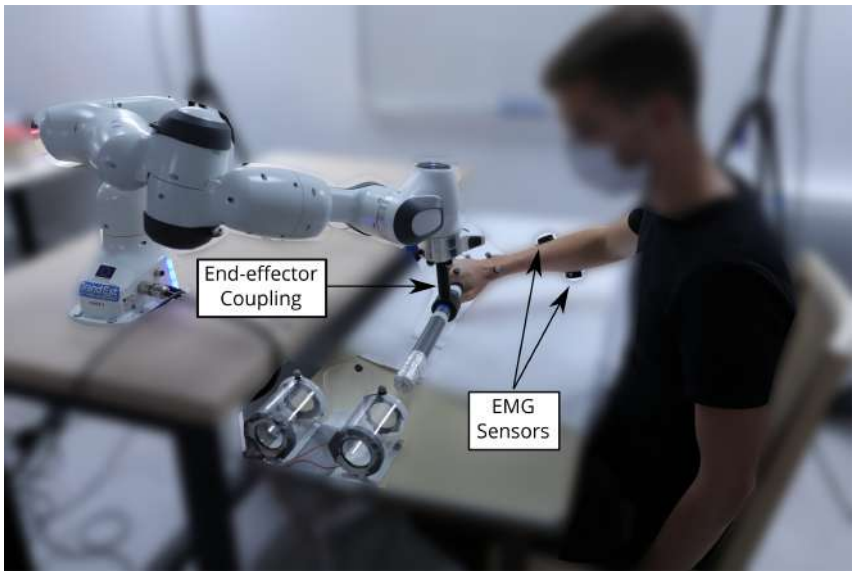

(b) A participant performing the task with the Franka Emika robot.

Figure 4.2: Experimental set-up for the human-robot co-manipulation study.

Twelve healthy adults took part in the experiment (4 females and 8 males, aged 24–55). All partic-

ipants performed the task with their dominant right hand. Participants were naive to the purpose of the study, and none reported any chronic motor disease or health condition that could influence the results. Participants signed an informed consent form prior to starting the experiment. The study was approved by INRIA's ethical committee COERLE, and was conducted in accordance with the Declaration of Helsinki.

Each participant performed the task in 4 different conditions, corresponding to different impedance behaviors of the robot (detailed in section 4.4.2):

- *Condition 1 – Robot Follower and Human Leader (RF):* Participants are instructed to lead the movement while the robot is compliant with the human movement;
- *Condition 2 – Robot Leader and Human Follower (RL):* The robot leads the movement, while participants are instructed to be compliant.
- *Condition 3 – Robot Collaborator with Reciprocal Stiffness (RR):* Participants are not given any fixed role and are instructed to simply collaborate with the robot, which modulates its end-effector stiffness inversely to the human end-point stiffness.
- *Condition 4 – Robot Collaborator with Mirrored Stiffness (RM):* Participants are not given any fixed role, and are instructed to simply collaborate with the robot, which modulates its end-effector stiffness proportionally to the human end-point stiffness.

According to the definition by Jarrassé *et al.* [100], conditions 1 and 2 correspond to a *cooperation* situation where the role of each agent (leader/follower) is pre-assigned, whereas conditions 3 and 4 correspond to a *collaboration* situation where agents have symmetric responsibilities.

Each participant performed 15 trials for each condition in a block manner, for a total of 60 trials. Participants were given a $30\,s$ break between each trial and a $5\,min$ break between each condition. Condition 1 (*robot follower*) was always performed first, as it was used to estimate scaling parameters needed for the implementation of the robot control in the two *collaboration* conditions (see Section 4.4.2). The order of 3 remaining conditions was randomized. Before starting the actual experiment, participants performed a few practice trials in *robot follower* condition to familiarize themselves with the task and the robot.

Human end-point stiffness Participants were equipped with 2 Delsys Trigno wireless sEMG sensors on antagonist muscles of their right forearm (FCU: Flexor Carpi Ulnaris and ECU: Extensor Carpi Ulnaris) to record muscle activity. EMG signals were recorded at $2\,kHz$, and filtered on-line using a $100\,ms$ RMS window followed by a low-pass 3rd order Butterworth filter with a $10\,Hz$ cutoff frequency. The filtered signal u^k (for muscle k) was then normalized by its maximum voluntary contraction value u^k_{MVC} measured prior to starting the experiment. Finally, a co-contraction index icc was computed based on the normalized EMG value of both muscles [87,90], which served to estimate the human end-point stiffness:

$$icc(t) = min\left(\frac{u^{FCU}(t)}{u^{FCU}_{MVC}}, \frac{u^{ECU}(t)}{u^{ECU}_{MVC}}\right). \tag{4.1}$$

Pipe-tube contact The main objective of the task was to extract/insert the pipe from/into the tubes without touching their front walls. Those walls were therefore equipped with custom contact sensors to detect contacts with the pipe. The contacts were recorded at $1\,kHz$ using a Raspberry Pi. Due to the reaction time of the human, contacts that were separated by less than $0.5\,s$ were counted as a single contact.

Task duration Even though there was no time objective or constraint in the experiment, the task duration (between the start and end points) was monitored to evaluate the efficiency of the interaction.

Questionnaires At the end of each experimental condition, participants were asked to fill a questionnaire including 2 questions: *Q1: From 1 to 10, how easy was it to do the task with the robot (1=not at all easy, 10=very easy)?*, *Q2: From 1 to 10, how much did the robot prevent you from doing the task the way you wanted (1=much prevented, 10=not prevented at all)?* At the end of the entire experiment, participants also reported their preferred condition orally.

4.4.2 Robot control and collaborative impedance strategies

The experiment was performed with a Franka Emika robot. The robot was controlled with an end-effector Cartesian impedance scheme that allowed it to easily implement different compliance behaviors. Let the robot equation of motion be:

$$\boldsymbol{M}(\boldsymbol{q})\ddot{\boldsymbol{q}} + \boldsymbol{C}(\boldsymbol{q}, \dot{\boldsymbol{q}})\dot{\boldsymbol{q}} + \boldsymbol{g}(\boldsymbol{q}) = \boldsymbol{\tau} - \boldsymbol{J}^{\top}\boldsymbol{F}_{ext} \tag{4.2}$$

with $\boldsymbol{M} \in \mathbb{R}^{n\times n}$ the inertia matrix, $\boldsymbol{C} \in \mathbb{R}^{n\times n}$ the matrix of Coriolis and centrifugal effects, $\boldsymbol{g}(\boldsymbol{q}) \in \mathbb{R}^n$ the vector of gravity forces, $\boldsymbol{J} \in \mathbb{R}^{6\times n}$ the end-effector Jacobian, $\boldsymbol{\tau} \in \mathbb{R}^n$ the joint torque vector, and $\boldsymbol{F}_{ext} \in \mathbb{R}^6$ the interaction wrench at the end-effector. Using feedback linearization, $\boldsymbol{\tau}$ can be computed to achieve a desired mechanical impedance at the end-effector, such that:

$$\boldsymbol{F}_{ext} = \boldsymbol{K}(\boldsymbol{x_{ee}} - \boldsymbol{x_d}) + \boldsymbol{D}(\dot{\boldsymbol{x}}_{\boldsymbol{ee}} - \dot{\boldsymbol{x}}_{\boldsymbol{d}}) \tag{4.3}$$

where $\boldsymbol{K} \in \mathbb{R}^{6\times6}$ and $\boldsymbol{D} \in \mathbb{R}^{6\times6}$ are the desired stiffness and damping matrices in Cartesian space, and $\boldsymbol{x}_{ee}$ and $\boldsymbol{x}_d$ are respectively the actual and desired end-effector poses. The four different robot behaviors described in section 4.4.1 were implemented by changing the values and profiles of the $\boldsymbol{K}$ and $\boldsymbol{D}$ matrices, as explained hereafter. Only the translational stiffness and damping were modified across conditions, whereas the rotational part remained identical to $200Nm/Rad$. To ensure the stability of the system we have the maximum force that can be exerted by the robot is limited. If the man-robot system reaches too high a level of torque/force the robot is forced to decrease its stiffness.

Cooperation conditions

The two cooperation conditions (RF: *robot follower*, RL: *robot leader*) were implemented using fixed values for $\boldsymbol{K}$ and $\boldsymbol{D}$ throughout the entire task execution. The diagonal coefficients of $\boldsymbol{K}$ were set to a low (resp. high) value in the RF (resp. RL) condition, as listed in Tab. 4.1 (all 6 coefficients have the same value). The coefficients of $\boldsymbol{D}$ were computed from $\boldsymbol{K}$ and the Cartesian mass matrix using factorization design [8, 178].

Collaboration conditions

The two collaboration conditions (RR: *reciprocal stiffness*, RM: *mirrored stiffness*) were defined and implemented based on the work by Peternel *et al.* [178]. In both cases, the robot Cartesian stiffness is adjusted on-line throughout the task depending on the human co-contraction index icc (Eq. 4.1). First, the human wrist stiffness trend $c_h(t)$ is estimated from the icc using a sigmoid function

$$c_h(t) = b_1 \frac{1 - e^{-b_2 icc(t)}}{1 + e^{-b_2 icc(t)}} \in [0, 1] \tag{4.4}$$

Table 4.1: Definition of the robot stiffness profile and reference trajectory for the four different conditions.

Robot role	**Stiffness Profile**	$\boldsymbol{K}_{\min}$ $\left(N.m^{-1}\right)$	$\boldsymbol{K}_{\max}$ $\left(N.m^{-1}\right)$	**Reference Trajectory**
Follower	$\boldsymbol{K} = \boldsymbol{K}_{\min}$	100	-	No
Leader	$\boldsymbol{K} = \boldsymbol{K}_{\max}$	-	1000	Yes
Reciprocal	$\boldsymbol{K}(t) \propto (1 - c_h)$	100	1000	Yes
Mirrored	$\boldsymbol{K}(t) \propto c_h$	100	1000	Yes

where $b_1, b_2 \in \mathbb{R}$ define the amplitude and shape of c_h, and are determined experimentally to reflect the actual operational range of the icc of a participant during the task execution.

For the *reciprocal stiffness* behavior (RR), $\boldsymbol{K}$ is:

$$\boldsymbol{K}(t) = \boldsymbol{K}_{cte} + \boldsymbol{S}\Big(\big(1 - c_h(t)\big)(\boldsymbol{K}_{\max} - \boldsymbol{K}_{\min}) + \boldsymbol{K}_{\min}\Big) \tag{4.5}$$

where $\boldsymbol{S}$ is a selection matrix that defines the axes where the stiffness is modulated, $\boldsymbol{K}_{min}$ and $\boldsymbol{K}_{max}$ contain the maximum and minimum desired stiffness for those axes, and $\boldsymbol{K}_{cte}$ contains a constant stiffness for the axes that are not modulated (the numerical values of these matrices' diagonal coefficients are summarized in Tab. 4.1). In this experiment, the translational stiffness in the horizontal plane was modulated, while the vertical translational stiffness was constant. In this condition, the robot behaves as a leader if the human is compliant, whereas it effectively cedes the autonomy of the task to the human when the human co-contracts.

For the *mirrored stiffness* behavior (RM), $\boldsymbol{K}$ is:

$$\boldsymbol{K}(t) = \boldsymbol{K}_{cte} + \boldsymbol{S}\Big(c_h(t)(\boldsymbol{K}_{\max} - \boldsymbol{K}_{\min}) + \boldsymbol{K}_{\min}\Big) \tag{4.6}$$

In this condition, the more the human co-contracts, the higher the robot stiffness.

Robot reference trajectory

The robot reference trajectory $\boldsymbol{x_d}$ was predefined offline for the RL, RR, and RM conditions. The desired end-effector orientation and the vertical position remained fixed for the entire task, while the trajectory in the horizontal plane was defined from straight lines and a parabolic curve (Fig. 4.2a). In the RF condition, $\boldsymbol{x_d}$ was set equal to the robot Cartesian pose at the previous timestep, which, associated with a low stiffness, made the robot very compliant. The duration of the reference trajectory was tuned experimentally and set to 25 seconds, which corresponded to a comfortable pace for users.

4.4.3 Statistical analysis

The dependent measures that were analyzed are: the RMS value over a trial of the human co-contraction index, the number of contacts between the pipe and the tubes, the duration of the task, and the score of each item in the questionnaire. The co-contraction index, task duration, and number of contacts were evaluated for every single trial. In order to get rid of any short-term learning effect that might happen in the early trials, we calculated linear regressions between the trial number and these dependent measures to identify when participants reached steady state performance. Regressions were calculated

for each of the four conditions, iteratively for the last 15, 14, 13 trials, and so forth until the slopes were not significantly different from zero (i.e. the 95 % intervals did include zero). This occurred when the regression was computed over the last 13 trials (i.e. excluding the first 2 trials). Hence, the first 2 trials of each condition were excluded from the subsequent analyses. In addition, since only steady-state performance was considered, each metric was averaged over the last 13 trials to obtain one single data point for each participant and condition.

Co-contraction index and task duration data were checked for normality with a Shapiro-Wilk test and then analyzed with a one-way repeated-measures analysis of variance (ANOVA) with *condition* as a within-subject factor and *participant* as a random factor. Pairwise multiple comparison post-hoc tests with Bonferroni corrections were conducted when a significant effect of *condition* was detected by the ANOVA. Questionnaire scores and number of contacts were analyzed with non-parametric Friedman tests given the nature of the data. Post-hoc tests were conducted when a significant effect of *condition* was detected. A significance level of 5 % was adopted for all statistical tests. Analyses were performed with the R software.

4.5 Results

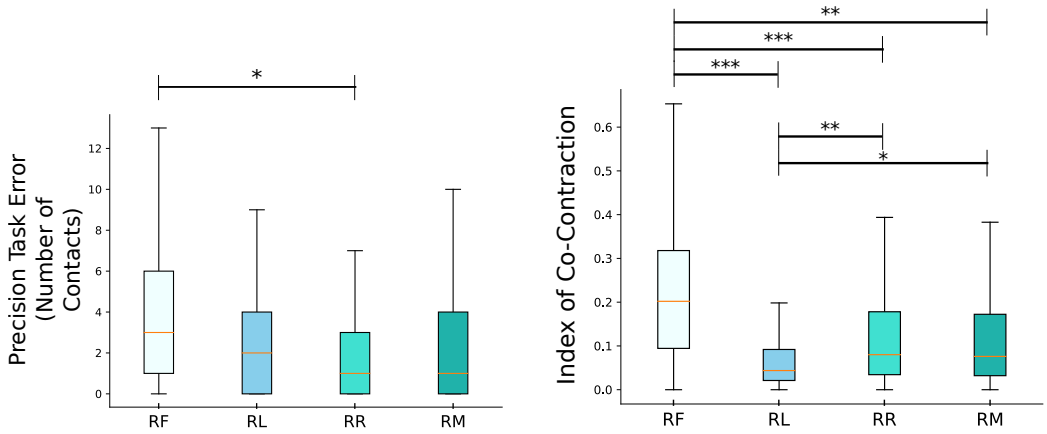

(a) Task errors (i.e., number of contacts).

(b) ICC of the participants.

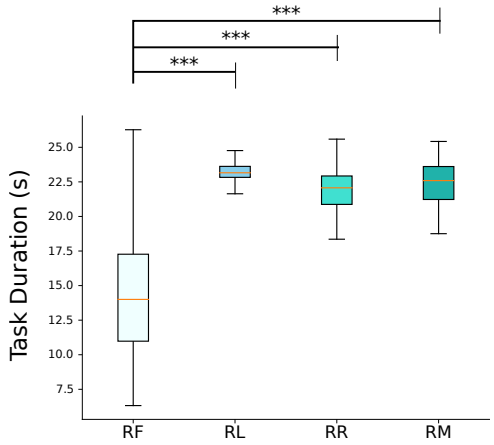

(c) Task duration.

Figure 4.3: Performance metrics across the 4 conditions.

4.5.1 Pipe-tube contacts

Fig. 4.3a displays the distribution of the number of contacts between the pipe and the tubes for all 4 conditions. The Friedman test revealed a significant effect of the *condition* factor ($\chi^2(3) = 13.22$, $p = .004$). Post-hoc tests indicated a significant difference only between the RF and RR conditions ($p = .031$). The other comparisons did not reach significance, though it was close for RF and RL ($p = .066$) and RL and RM ($p = .059$). The number of contacts (errors) was the largest when the human lead the task (RF condition) where s/he could not benefit from the robot position accuracy, and the smallest in the collaboration condition where the robot adopted a reciprocal behavior (RR condition).

4.5.2 Human co-contraction index

Fig. 4.3b displays the distribution of the co-contraction index for all 4 conditions. The ANOVA revealed a significant effect of the *condition* factor ($F(3, 33) = 28.1$, $p < .001$) on the co-contraction index. Post-hoc test revealed a significant difference between RF and RL ($p < .001$), RF and RR ($p = .001$), RF and RM ($p = .003$), as well as between RL and RR ($p = .012$) and RL and RM ($p = .049$). Other comparisons did not reach a significance level. Co-contraction was the largest when the human was leading the task (RF condition), and the smallest when the human was only following the robot (RL condition).

4.5.3 Task duration

Fig. 4.3c displays the distribution of the task duration for all 4 conditions. The ANOVA revealed a significant effect of the *condition* factor ($F(1.5, 16.7) = 38.0$, $p < .001$) on the task duration. Post-hoc test revealed a significant difference between RF and the 3 other conditions ($p < .001$ for all comparisons). Other comparisons did not reach a significance level. The task execution was the fastest when the human lead the task (RF condition), where the timing was not constrained by the robot reference trajectory, and the slowest when the robot was the leader (RL condition).

4.5.4 Questionnaire

Fig. 4.7 displays the distribution of the scores for the questionnaire. The Friedman tests revealed a significant effect of the *condition* factor for question Q1 (*How easy was it to do the task with the robot?*) ($\chi^2(3) = 15.3$, $p = .001$), but not for Q2 (*How much did the robot prevent you from doing the task the way you want?*) ($\chi^2(3) = 2.65$, $p = .44$). For Q1, post-hoc tests indicated a significant difference between RL and RF ($p = .009$) and RL and RM ($p = .005$), while the other comparisons did not reach significance. Participants felt the task was the easiest to perform when the robot leads the task (RL condition), followed by the robot reciprocal behavior (RR behavior). This result suggests that the reciprocal behavior RR was the preferred strategy among the 2 collaboration conditions (RR and RM). For Q2, trends in Fig. 4.7 suggest that participants had very diverse opinions on how the robot was hindering them in the 2 cooperation conditions (RF and RL), whereas the opinions where much more similar across participants in the 2 collaboration conditions (RR and RM).

4.6 Discussion

In this chapter, we focus on a human-robot co-manipulation task. In our previous work, we investigated the performance and the arm stiffness of human-human dyads when they were cooperating and collaborating [84]. We observed an improved performance using collaborative strategies over cooperative ones. In this context, we investigated if the same results are observable in the human-robot scenario.

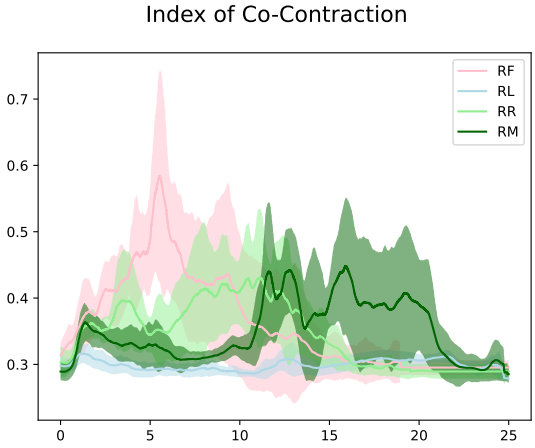

Figure 4.4: The graphs show how Subject 1 performed the task differently in the different trials. In particular, the mean of the movement (solid line) and the variance of the movement (shaded area) along the trials are shown.

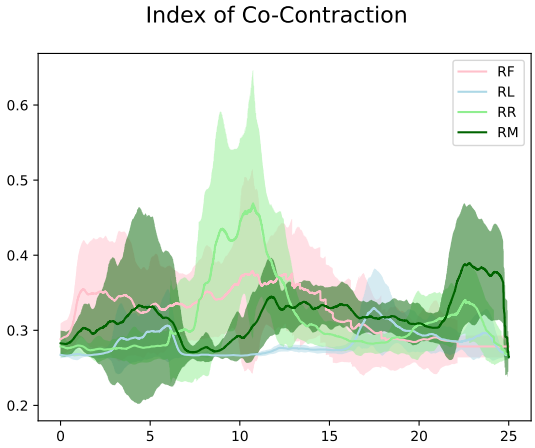

Figure 4.5: The graphs show how Subject 2 performed the task differently in the different trials. In particular, the mean of the movement (solid line) and the variance of the movement (shaded area) along the trials are shown.

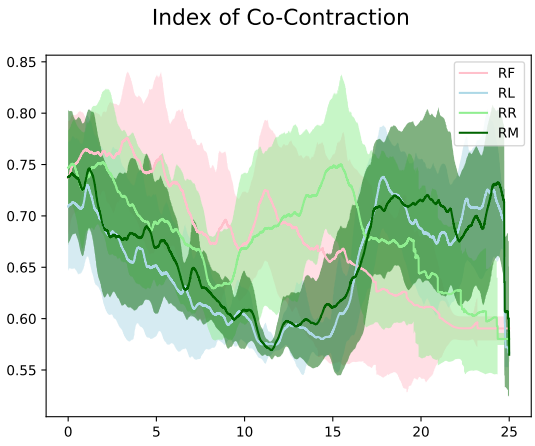

Figure 4.6: The graphs show how Subject 3 performed the task differently in the different trials. In particular, the mean of the movement (solid line) and the variance of the movement (shaded area) along the trials are shown.

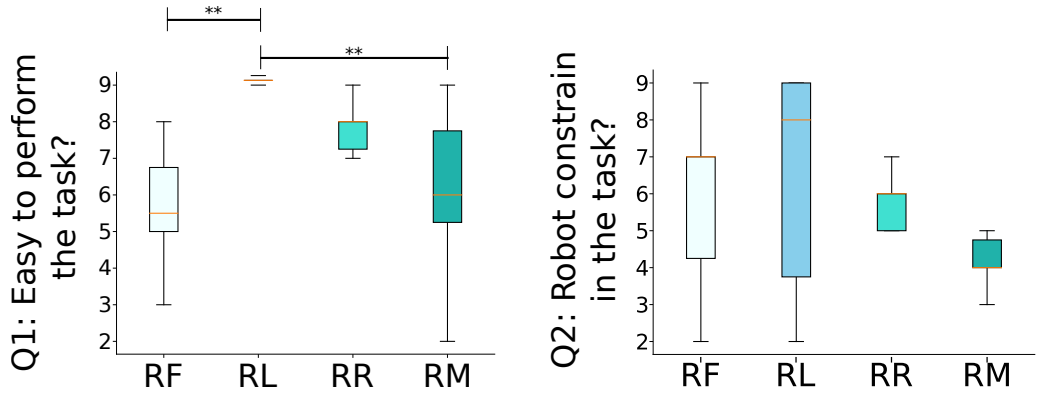

Figure 4.7: Subjective evaluation: questionnaire results. Q1: 1=not at all easy, 10=very easy. Q2: 1=much prevented, 10=not prevented at all.

4.6.1 Robot leader or Robot collaborator?

Fig. 4.3a reports on the task error, i.e. the number of pipe/tube contacts during the precision task. We expected the RL condition to be the most accurate in terms of task errors because the robot had a reference trajectory that could precisely accomplish the task. In this case, if the human complied with the robot's actions without adding perturbations, then the risk of task errors would be close to zero. In the human-human experiment, the collaboration condition delivered less errors (Fig. 4.1d). Meanwhile, in the human-robot experiment, the two collaboration conditions result in errors comparable to the cooperation condition when the robot is the leader (RL), and fewer errors than when the robot was follower (RF). Further, even though the distributions of RR and RM are not statistically different from the one of RL, the median of the task errors is lower in the collaboration conditions, similarly to what was observed in the human-human experiment. Thus collaboration does not worsen the task performance. On the contrary, when collaborating with the robot, the human seems to benefit from its accuracy.

Fig. 4.3b reports on the distribution of ICC values. The highest ICC values occur when the human is the leader (RF), as expected, since it is the condition where the human makes the greatest efforts to execute the task. In addition, even if the robot is following the human in a very compliant mode, it is, however, not entirely transparent, hence some human effort is also needed to compensate for the lack of transparency of the robot. In the RL condition, the ICC is at its lowest: this result is coherent with the subjective feedback from the participants, who reported that they "were just trying to relax and follow the robot doing a minimal effort. This is also aligned with our observations in the human-human experiment. However, these low ICC levels and their oral feedback point out a possible risk of "disengagement" from the task execution: if the human passively follows the robot across several repetitions of the task, s/he may risk progressively loosing awareness of the task and their surroundings. Should something unexpected occur, the limited awareness decreases the chance of a prompt reaction, and at the same time, the high robot stiffness of the RL condition strongly prevents the human to correct the robot or input changes in the task trajectory. The ICC values of the collaborative conditions (RR and RM) were in between RF and RL, having the advantage of avoiding disengagement while requiring only a limited physical effort.

If we consider both the task precision and the effort, the most convenient conditions are RL and RM (no statistical difference in contact errors and ICC). This result is partly close to the one of the human-human experiment, where collaboration was more convenient than cooperation, at the expense of larger ICC values. However, the experimental context is different: the human collaborators are not aware of the desired trajectory of their partner (which may vary across trials), nor they know if it is efficient or

accurate for completing the task. Conversely, in the human-robot experiment, the human participants are aware that the robot has a fixed reference trajectory that enables them to accomplish the task. In that sense, the comparison is not on equal terms, because the knowledge of the human is different in both cases. For a fair comparison, the robot should not have a reference trajectory and react to the intended human motion. This latter can be predicted from initial observations of the collaborative action, as we did in [56]. Studying the impact of this prediction on the collaborative strategies will be done in future studies.

We argue that giving some degree of autonomy to human is overall positive. The human can still benefit from the robot's assistance, especially if the robot has a reference task trajectory. Furthermore, in collaborative conditions, the robot compliance can leave the necessary degree of maneuver to the human to correct the task when needed, maintaining the task engagement without degrading the task performance (no difference in the task errors). Additionally, the human could exploit the compliance to accelerate or decelerate the task at their convenience: indeed Fig. 4.3c shows a tendency to accelerate the task execution in collaborative conditions. In fact, in the RF condition, the task duration was smaller, because the human could execute the task at their own pace (albeit probably "limited" by the robot). In our study, the robot reference trajectory and its duration were fixed: they were arbitrarily set to have a reasonable speed that would not challenge the participants. In future experiments, we will investigate whether the conditions other than RF can execute the task faster and whether the cooperative or collaborative conditions enable the dyad to be faster without being detrimental to performance or effort.

4.6.2 Preference for collaboration with reciprocal impedance strategy

Subjective evaluations suggest that it is easier to realize the task with a collaborating robot rather than with a cooperating robot. In Fig. 4.7, subjects indicated that the task was easier to perform in the RR condition. Regarding the question of whether the robot was interfering with them executing the task in their way, participants had very variable opinions for cooperative conditions, whereas they judged that the hindrance was relatively acceptable for the collaborative conditions. This is an important element in favor of collaborative robot behaviors for industrial applications: if robots must be used by a diverse population of workers, it is reasonable to expect a more consistent attitude towards collaborative rather than cooperative robots.

Interestingly, the majority of the participants reported preferring the reciprocal strategy, while the effort and errors do not show a significant different from the mirror strategy. The preference for the reciprocal condition contrasts with our expectation from the human-human study, where we found that collaborators exhibit high arm co-contraction as if they are both trying to lead. In hindsight, it is likely that humans prefer to interact with a "docile" robot that complies with human behavior, rather than competing with a robot that stiffens as the human does: lowering the stiffness when the human co-contracts may enforce the human feeling of being in control (empowerment), which has been frequently reported in the literature as one of the main drives for accepting and trusting a robot [19, 144, 202]. The reciprocal collaborative strategy also has the advantage of being more conservative concerning the passivity of the system, with notable safety implications [21].

In summary, for co-manipulation, a robot collaborator seems preferable to a robot cooperator (better than a robot leader, and definitely better than a robot follower), even if the way the human collaborates with the robot differs from when collaborating with another human. In addition, within the collaborative strategies, a reciprocal strategy for impedance seems the most indicated.

4.6.3 Limits of the study

Our results suggest that in a human-robot co-manipulation task, the robot should behave as a collaborator, adapting its impedance with a reciprocal stiffness law that relates to the human arm co-contraction. This control mode is efficient in terms of task accuracy and was also preferred by the participants.

However, our results should be considered carefully. First, the study was conducted with participants from the University environment, and while few participants were familiar with robots, the results cannot be generalized to a generic population, especially with industry workers that may have different attitudes when interacting with a robot [144]. Second, the co-manipulation task was very simple and the manipulated load was small and light. In this sense, we do not know if our results can be generalized to other co-manipulation tasks involving the manipulation of large and heavy loads, a situation that is often found in manufacturing where robots physically assist workers (e.g., manipulating car parts, such as wheels [145]). Third, the performance of each condition can possibly change with more training and expertise with the robot and the task. We already accounted for the source of bias due to learning by not including the initial trials in our analysis (see Section 5.3). However, the RF condition was always executed as the first (for the reasons explained in Section 4.4.1) and this might partly explain the lower performance of this condition in terms of task errors. At the same time, the participants reported that it was not easy to do the task with the robot in this condition, and our intuition is that this is mostly due to the fact that the robot was not entirely transparent. It is possible that interactions over hundreds of trials may lead to lower ICC levels and fewer errors. Future studies should investigate whether there is a significant learning effect for longer interactions and whether this learning process is user-specific: this knowledge will be critical to recommend suitable training to workers that collaborate with robots on a particular workstation.

4.7 Conclusion

We investigate whether it is preferable and more performing for a robot to behave as a cooperator (leader or follower) or collaborator (variable impedance) during a co-manipulation task with a human. Our study shows that with a robot leader informed of the task trajectory, the human makes less effort, but in terms of task accuracy and effort, a reciprocal collaborative strategy seems preferable for a human. Our results are relevant for the design of human-robot collaborative workstations. They also evoke new questions to further understand human behavior, precisely, the human arm impedance during joint work with humans and robots.

5

Adaptation in pHRI

In the advanced paradigm of Human-Robot collaboration, typical of Shared Autonomy (SA) [203], the collaborative robot is capable of adapting its level of autonomy based on its own understanding of human behaviour and of the environment. Several aspects of collaboration have been investigated in the literature: the communication channel between human and cobot [134], the experience of the operator in the task to be performed [67] and individual behavior characteristics [190]. Nevertheless, a fundamental question for this kind of collaboration is how the two agents adapt to each other across the tasks. In fact, if the robot was able to predict how a subject would adapt to a given policy, it could vary its policy with the intent of accelerating adaptation (in case the equilibrium condition was good) or conversely guide it to another equilibrium condition.

Human-machine adaptation is a widely studied field even beyond pHRI [78], implementing adaptive control schemes which conform to an unknown gain of the human [63]. Adaptation could be integrated by changing the cobot policy when thresholds of safety have been reached. For instance, Peternel *et al.* [180] proposed a method for human-robot collaboration where the robot behavior is adapted online to the human motor fatigue. In other situations, adaptation can be used to solve problems that in which neither the human nor the robot is able to solve the problem on their own [207].

Many of these works presented control algorithms that adapt and change the cobot policy during collaboration with the human. However, to the best of our knowledge, we lack knowledge of how humans perceive and react to changes in cobot behavior. Specifically, little is known on how humans adapt to changing roles and control strategies of collaborating robot during pHRI. We think this knowledge is important because it allows the robot to predict how a subject would perform in the short period (before adaptation) and in the long period (when the adaptation is reached). Knowing this the robot's policy can change to modify situations harmful to the subject

To fill this gap, we propose a human study in which 16 participants executed a collaborative human-robot sawing task where the cobot altered between three different control strategies(human-leader, human-follower, and reciprocal). In human-leader mode, the human guides the execution of the collaborative task, while the cobot follows. Viceversa, in human-follower mode, the cobot leads the execution, while the cobot follows. Finally, in reciprocal mode, the human and cobot behaviors are reciprocal in terms of phase of operation. We examined human adaptation when cobot suddenly changed the control strategy from one strategy to the other, resulting in six experimental conditions. The experiments were performed on the Kuka LBR iiwa robotic arm.

The aim of our study is to try to answer some of the questions not addressed in the literature. Our goal is to assess how switching is perceived, with both objective and subjective metrics. We also ask how collaboration performance is affected in the short and long term. Finally, we think it is interesting to assess how long subjects need to adjust to a strategy. We addressed the following questions:

(Th1) *How the switching between modes is perceived by the human? Is the task performance influenced in the first iterations of the task after the switching?*

(Th2) *Does a past transition influence the collaboration even after a steady state is reached?*

(Th3) *Do humans prefer some transitions with respect to others?*

We also observed the data collected before the mode switching happened and we used it to compare the three different modes. We addressed the following questions:

(Th4) *Does human adapt faster to some modes with respect to others?*

(Th5) *For the specific task studied in this work, is there a preferred mode of interaction among Human-Leader, Human-Follower, Reciprocal*

We tried to answer all these questions from both a point of view of objective measures and from a point of view of human perception (subjective scales).

This chapter presents the results of the study(hal-03890322v1) we conducted in collaboration with the Delft University of Technology, Netherlands. The human studies have been done in the Department of Cognitive Robotics in Delft. The paper we submitted to Journal of Intelligent Manufacturing contains less analysis of the results, in particular in this version of the manuscript we concentrate more on the adaptation. We display how the participants converge to the steady state solution over time giving a deeper analysis of the results. We describe more in detail the experimental setup and the control conditions, and elaborate more on the implications of this study in the human-robot adaptation literature.

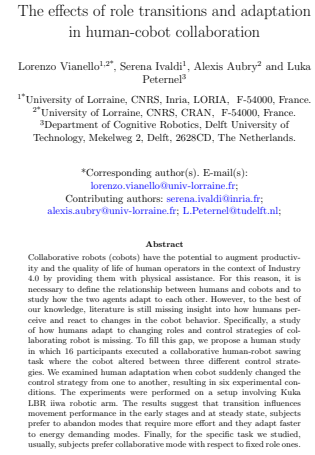

The effects of role transitions and adaptation in human-cobot collaboration

Lorenzo Vianello[1,2*], Serena Ivaldi[1], Alexis Aubry[2] and Luka Peternel[3]

[1*]University of Lorraine, CNRS, Inria, LORIA, F-54000, France.
[2*]University of Lorraine, CNRS, CRAN, F-54000, France.
[3]Department of Cognitive Robotics, Delft University of Technology, Mekelweg 2, Delft, 2628CD, The Netherlands.

*Corresponding author(s). E-mail(s): lorenzo.vianello@univ-lorraine.fr;
Contributing authors: serena.ivaldi@inria.fr; alexis.aubry@univ-lorraine.fr; L.Peternel@tudelft.nl;

Abstract

Collaborative robots (cobots) have the potential to augment productivity and the quality of life of human operators in the context of Industry 4.0 by providing them with physical assistance. For this reason, it is necessary to define the relationship between humans and cobots and to study how the two agents adapt to each other. However, to the best of our knowledge, literature is still missing insight into how humans perceive and react to changes in the cobot behavior. Specifically, a study of how humans adapt to changing roles and control strategies of collaborating robot is missing. To fill this gap, we propose a human study in which 16 participants executed a collaborative human-robot sawing task where the cobot altered between three different control strategies. We examined human adaptation when cobot suddenly changed the control strategy from one to another, resulting in six experimental conditions. The experiments were performed on a setup involving Kuka LBR iiwa robotic arm. The results suggest that transition influences movement performance in the early stages and at steady state, subjects prefer to abandon modes that require more effort and they adapt faster to energy demanding modes. Finally, for the specific task we studied, usually, subjects prefer collaborative mode with respect to fixed role ones.

Video is available at: video Human-Kuka adaptation.

5.1 Adaptation in pHRI

A classical Human-Robot Collaboration (HRC) strategy is to design cobot policies that adapts to humans (one-way adaptation). In [132], robot is able to adjust its own role according to the human's intention to lead or follow. Cherubini *et al.* [52] alternate the leader and follower roles of a robot in a pHRI application for industrial assembly tasks according to visual and haptic cues by the human co-worker. Peternel *et al.* [180] used tele-impedance to set the robot strategy and switch between roles when a given amount of fatigue is reached by the human. Other work proposes an adaptive control schemes in which the robot adapts its policy according to estimated forces [63]. Silimic considerations also apply with regard to exoskeletons. For this reason, Poggensee *et al.* [181] conducted experiments in which users learned to walk with ankle exoskeletons.

In more recent work, it was hypothesized that better collaborative approaches can be designed by also considering how humans change their policy by interacting with the robot [78]. Nikolaidis *et al.* [162] introduced a formalization for mutual adaptation between a robot and a human in a collaborative task. In

a similar way, the study in [207] present a reinforcement learning algorithm able to solve human-robot task in which neither the human nor the robot is able to solve the problem on their own. Ikemoto *et al.* [97] showed the importance of a bilateral learning process that takes place in both partners. Other works consider the evolution of the human trust in robot [50] and the robot's persuasive ability [196] to maximize long-term team performance.

To design the robot action which maximizes the expected reward, it is necessary to model the human behaviour [249] or, alternatively, the human-robot team behaviour [164]. Nikolaidis *et al.* [162] integrated the human ability to adapt to robot actions, defined as adaptability, to predict human actions in a human-robot collaboration scenario. Saunderson *et al.* [196] proposed to use Adaptive Persuasive Systems to acquire user information, update user models and adapt their persuasive approaches to the human operator. Chen *et al.* [49] use social projection theory to learn human models from human demonstrations. In addition, it should be considered that different individuals may have different behaviors. For this reason, Nemlekar *et al.* [161] divided into cluster subjects accordingly to their preferences.

All the aforementioned work rely on some human behaviour model that is used to determine the robot's policy of adaptation. However, these models lack information about how the human adapts to changes in the robot's behaviour. To create more accurate human models, we believe human studies in pHRI that compare different robot policies and observe how the human adapts to these given policies are critical [237]. In particular, the impact of changes in robot control policies during the collaboration were not yet examined. For this reason, we examine how humans adapt when the robot suddenly changes the collaborative control strategy.

5.2 Methods

We investigate how humans react and adapt to changes in cobot control modes during a collaborative task. Such changes are often necessary in collaborative robotics applications when different functionalities are required for the task execution.

To study how humans adapt to changing policy, we conducted an experiment in which human participants performed a collaborative sawing task with a cobot under different conditions. Three control strategies were defined for the cobot end-effector impedance: human-leader (**L**), human-follower (**F**) and reciprocal (**R**). In human-leader mode, the human guides the execution of the collaborative task, while the cobot follows. Viceversa, in human-follower mode, the cobot leads the execution, while the cobot follows. Finally, in reciprocal mode, the human and cobot behaviors are reciprocal in terms of phase of operation. The human intention is measured online using EMG sensors. The sensors are placed on the subject following guidance rules from the European project SENIAM [216]. Before placing a sensor on a muscle location, the area surrounding the pen mark is prepared accordingly. The subject's skin is cleaned with alcohol until it acquires red tones, which indicates good skin impedance. After the alcohol dryes out, the EMG sensor is placed on the skin at the muscle fibers direction with the help of a double-sided sticker provided by the sensor manufacturer. Prior to the task execution, each agent is asked to perform maximum voluntary contractions (MVC) during isometric exercises for each selected muscle [216] for 3 s. The exercise is performed 3 times, with a 1 minute interval between them to decrease fatigue biases. After the 3 trials, the maximum EMG signal is then stored and used for posterior post-processing of the EMG signals during the task execution. With respect to the previous experiment we used the muscles of the shoulder because more involved in the movement. The sensors comunicate with the robot controller via ros messages.

16 healthy adults took part in the experiment (4 females and 12 males, aged 24–30). Participants were naive to the purpose of the study, and none reported any chronic motor disease or health condition that could influence the results. Participants signed an informed consent form prior to starting the experiment.

The study was approved by TU-Delft's ethical committee and was conducted in accordance with the Declaration of Helsinki.

Each of the participants received instructions on the task to be performed, a description of the three modes, as presented in Sec. 5.2.1, and was informed about the presence of switch from one mode to another during each trial. However, they were not told what the two modes would be and when the switching would happen. They had to figure out which mode the cobot was executing, and how to adapt to the new one.

5.2.1 Experimental setup and Protocol

We selected a collaborative human-robot sawing task that requires both complex physical interactions and good coordination between the agents (Fig. 5.1). The task consists of alternating phases where the human pushes the saw (while the cobot pulls) and phases where the human pulls the saw(vice versa, the cobot pushes). The movement must be performed along the entire length of the saw ($45\,cm$). The blade used in the task has no teeth to simplify the task (less friction) and at the same time to ensure the safety of participants. Performing one trial takes $2\,s$ on average. A metronome is used to help the human to keep a constant frequency in the task execution. Constant frequency helps us to standardize the experiment among subjects, to make data comparable also in the case when human is leader and so no hint on the frequency comes from the cobot. Participants face the cobot and hold the saw with their dominant hand, while the other side of the saw is attached to the cobot end-effector. Fig. 5.1 shows the setup.

The cobot is controlled using three different control conditions (**F**, **L**, **R**) which are specifically adapted to the sawing task. In "Human-follower" (**F**), the human stabilizes the saw vertically, while the cobot does all the movement of the saw back and forth in the horizontal direction. In "Human-Leader" (**L**), the human moves the saw back and forth, while the cobot only stabilizes the saw at its own side. In "Reciprocal mode" (**R**), the robot replicates the standard way humans do the two-person sawing: both agents are only pulling the saw, and not pushing. The pulling is exchanged in the following manner. When humans pull the saw to their side, the cobot starts pulling it back to its side, and vice-versa. The reason not to pull is to not interrupt each other's activity (for example, in a two-person saw without the arc, the saw would bend, and the task would be interrupted). To express all the situations in which no previous mode has been executed (so the cobot is fixed), we used the terminology Nothing condition (**N**).

Each subject executed 6 trials; in each trial, two of the three cobot modes are executed. The first mode is executed for around $\sim$ 2 minutes, then the transition happens and the cobot switches to the second mode for other $\sim$ 2 minutes. Between each trial, the human rests and there is an allocated time to answer the questionnaire ($\sim$ 2 minutes) and time to recover ($\sim$ 3 minutes). The total amount of time fot the entire experiment is $\sim$ 1 hour. The acoustic sound of the metronome tells the human when the trial starts. The metronome frequency does not change for the full time of the task (even during the transition). The participant does not know which mode is executing nor when the transition happens. The six experimental conditions are presented in Tab. 5.1 and their order is presented randomly. One preliminary trial (in human-leader mode) of 1 minut is performed before each experiment to make the subject familiarize with the setup and the sawing task.

5.2.2 Cobot Controls

The experiment was performed with a KUKA iiwa robot. The robot was controlled with a mixed force-impedance scheme. Impedance control allows to move the saw and to easily implement different compliance behaviors. Force control allows the robot to maintain contact with the work-piece. Let the robot equation of motion be:

$$\boldsymbol{M}(\boldsymbol{q})\ddot{\boldsymbol{q}} + \boldsymbol{C}(\boldsymbol{q}, \dot{\boldsymbol{q}})\dot{\boldsymbol{q}} + \boldsymbol{g}(\boldsymbol{q}) = \boldsymbol{\tau} - \boldsymbol{J}^{\top}\boldsymbol{F}_{int} \tag{5.1}$$

Experimental Condition	Cobot Controls	Modes Conditions	Cobot Control
1	F → L	1b	N → F
2	F → R		
3	L → R	2b	N → L
4	L → F		
5	R → F	3b	N → R
6	R → L		

Table 5.1: Study design and experimented conditions: each subject performs the six experimental conditions, in which the cobot changes the mode from one to another. Three modes were tested: human follower (F), human leader (L), and reciprocal (R). To express all the situations in which no previous mode has been executed (so the cobot is fixed), we used the terminology Nothing condition (N). The experimental conditions are tested in random order.

with $\boldsymbol{M} \in \mathbb{R}^{n \times n}$ the inertia matrix, $\boldsymbol{C} \in \mathbb{R}^{n \times n}$ the matrix of Coriolis and centrifugal effects, $\boldsymbol{g}(\boldsymbol{q}) \in \mathbb{R}^n$ the vector of gravity forces, $\boldsymbol{J} \in \mathbb{R}^{6 \times n}$ the end-effector Jacobian, $\boldsymbol{\tau} \in \mathbb{R}^n$ the joint torque vector, and $\boldsymbol{F}_{ext} \in \mathbb{R}^6$ the interaction wrench at the end-effector. A hybrid force/impedance controller was implemented following [180]. The force behavior was defined as

$$\boldsymbol{F}_{int} = \boldsymbol{F}_{for} + \boldsymbol{F}_{imp} \tag{5.2}$$

where the term $\boldsymbol{F}_{for}$ is related to the force task (i.e., in sawing is keeping contact with the wood) controlled by a PI controller

$$\boldsymbol{F}_{for} = \boldsymbol{K}_P^F \boldsymbol{e}_F + \boldsymbol{K}_I^F \int \boldsymbol{e}_F dt, \tag{5.3}$$

$$\boldsymbol{e}_F = \boldsymbol{S}_F(\boldsymbol{F}_a - \boldsymbol{F}_d) \tag{5.4}$$

where $\boldsymbol{K}_P^F, \boldsymbol{K}_P^F$ are the gain of the PI controller, while F_a, F_d are respectively the actual and the desired force on the end-effector. The desired mechanical impedance at the end-effector is defined as:

$$\boldsymbol{F}_{imp} = \boldsymbol{K}(\boldsymbol{x_{ee}} - \boldsymbol{x_d}) + \boldsymbol{D}(\dot{\boldsymbol{x}}_{\boldsymbol{ee}} - \dot{\boldsymbol{x}}_{\boldsymbol{d}}) \tag{5.5}$$

where $\boldsymbol{K} \in \mathbb{R}^{6 \times 6}$ and $\boldsymbol{D} \in \mathbb{R}^{6 \times 6}$ are the desired stiffness and damping matrices in Cartesian space, and $\boldsymbol{x}_{ee}$ and $\boldsymbol{x}_d$ are respectively the actual and desired end-effector poses. The three different robot behaviors described in section 5.2.1 were implemented by changing the values and profiles of the $\boldsymbol{K}$ and $\boldsymbol{D}$ matrices, as explained in the next section. Only the translational stiffness and damping were modified across conditions, whereas the rotational part remained identical.

5.2.3 Robot role allocation

The two experiment conditions **L** and **F**, were implemented using fixed values for $\boldsymbol{K}$ and $\boldsymbol{D}$ throughout the entire task execution. The coefficient of $\boldsymbol{K}$ on the direction of the sawing was set to a zero value when the human leads the movement. When the human follows, the coefficient is set to high value. The coefficients of $\boldsymbol{D}$ were computed from $\boldsymbol{K}$ and the Cartesian mass matrix using factorization design [8].

The "Reciprocal mode" **R** was defined and implemented based on the work by Peternel *et al.* [178]. The robot's Cartesian stiffness is adjusted on-line throughout the task depending on the human shoulder

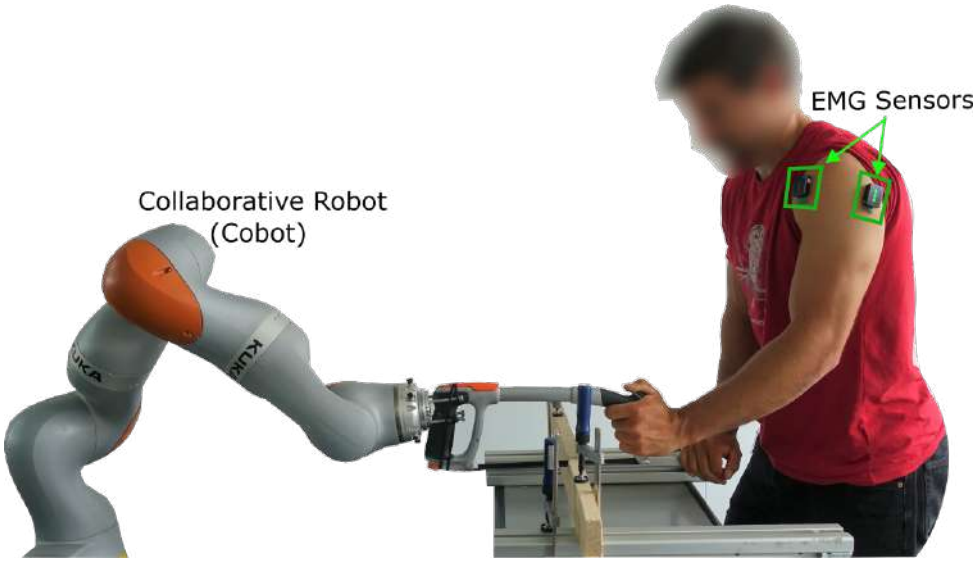

Figure 5.1: The experimental setup: the cobot is semi-rigidly attached to the saw, likewise the subject grabs the saw from the other end. EMG sensors are attached to the subject to measure muscle contraction during movement.

stiffness trend $c_h(t)$. The human stiffness profile is estimated as in [4] using the scaled mean of the shoulder muscles:

$$c_h = a\left(\frac{A_1 + A_2}{2}\right) \in [0, 1] \tag{5.6}$$

where $a \in \mathbb{R}$ defines the amplitude and shape of c_h, and is determined experimentally.

For the *reciprocal stiffness* behavior (R), $\boldsymbol{K}$ is:

$$\boldsymbol{K}(t) = \boldsymbol{K}_{const} + \boldsymbol{S}\Big(\big(1 - c_h(t)\big)(\boldsymbol{K}_{\max} - \boldsymbol{K}_{\min}) + \boldsymbol{K}_{\min}\Big) \tag{5.7}$$

where $\boldsymbol{S}$ is a selection matrix that defines the axes where the stiffness is modulated, $\boldsymbol{K}_{min}$ and $\boldsymbol{K}_{max}$ contain the maximum and minimum desired stiffness for those axes, and $\boldsymbol{K}_{const}$ contains a constant stiffness for the axes that are not modulated. In this experiment, the translational stiffness in the direction of the sawing was modulated, while the other components were constant. In this condition, the robot behaves as a leader if the human is compliant, whereas it effectively cedes the autonomy of the task to the human when the human co-contracts.

The robot reference trajectory has been designed in Cartesian space between two points based on the required saw movement in the experimental setup. When the robot reaches the end-point it comeback. The orientation of the saw is kept constant throughout the movement. The duration of the reference trajectory was tuned experimentally and set to 2 seconds, which corresponded to a comfortable pace for users and was comparable to the previous studies on human-robot collaborative sawing [178].

5.2.4 Performance metrics

To evaluate the performance of the task execution and of the collaboration, we observed the following **objective metrics**. These performance metrics were calculated at each iteration of the task, where as iteration is considered one round trip of the saw.

(M1) Length of the movement makes it possible to verify that the movement is performed along the entire length of the blade. The length is calculated as the difference between the maximum and minimum distance on the axis where the sawing is done.

(M2) Acceleration gives an estimation of the smoothness of the movement and it is calculated with double derivation from the movement. We considered the mean of the absolute value of the acceleration.

(M3) Co-Contraction index provides an estimation of the human effort. The value is calculated as the mean value of all the ICC over one trial.

(M4) Force applied to the robot is also a measure of human effort. It is calculated using the robot torque sensors ($F_{ext} = J\tau_{ext}$). We considered the mean value of the absolute value of the force only in the direction of the sawing (namely y axis) because we do not notice big forces in the other directions.

(M5) The **error on the reference position** gives us an idea of how much the subjects differ in motion from the trajectory proposed by the robot. The error is calculated as the sum of the differences between the desired position of the robot and the one actually executed. It is important to note that in the human leader mode (L) the subject has no clue what the trajectory indicated by the robot is. This justifies the use of the metronome as a tool to equalize the comparison between different modes.

(M6) Fourier: To compare the smoothness of each movement, we compute the sum of the frequencies minus the principal frequency using the Fourier transform of the movement [31].

Moreover, to evaluate the human adaptation to a given mode after the transition happens we calculate the number of transitions necessary to reach a steady state for the human. In the next section (Sec.5.2.5) will be presented how we consider that steady state is reached.

We also evaluate how the subjects perceived each experimental condition. This **subjective metric** is composed of a set of questions. After each trial, the subjects are asked to answer to three questions related to the transition between modes:

1. *Did you recognize the* 2 *modes?* This question was added to stimulate the subject to explore the experimental condition they are testing and thus engage more in the collaboration.
2. *The transition between the two modes was challenging.*
3. *I felt that the performance in collaboration improved after mode transitioning.*

After each experiment, they are additionally asked to fill in a questionnaire related to individual mode, with the following questions, with answers on a X-items Likert scale.

1. *The mode was engaging*
2. *The mode was demanding*
3. *The mode required high cognitive effort*
4. *The mode required high physical effort*
5. *The mode was boring*

Moreover, we included the Van der Laan questionnaire [230], which evaluates perceived usefulness and satisfaction for an experimental condition.

5.2.5 Statistical analysis

For each experimental condition, we analyzed two critical times: just after the mode-switching and when the steady state is reached. We decided to study the first trials after the transitions, because during pilot experiments we observed that these are the more critical moments for the collaboration.

To identify when participants reached steady state performance, we use linear regression. Regressions were calculated for each of the six experimental conditions ($F{\rightarrow}L$, $F{\rightarrow}R$, $L{\rightarrow}R$, $L{\rightarrow}F$, $R{\rightarrow}L$, $R{\rightarrow}F$) and the "nothing-to-something" conditions ($N{\rightarrow}L, N{\rightarrow}R, N{\rightarrow}F$), in a iterative way for the last n trials, where n goes from N(number of trials) to zero. We repeated this procedure until the slopes were not significantly different from zero (i.e. the 95 % intervals did include zero). Since different performance metrics have different convergence times to steady state, we decided to take the last one to converge.

The data (both for the first trials and for steady-state conditions) were checked for normality with a Shapiro-Wilk test and then analyzed with a one-way repeated-measures analysis of variance (ANOVA) with *condition* as a within-subject factor and *participant* as a random factor. Pairwise multiple comparison post-hoc tests with Bonferroni corrections were conducted when a significant effect of *condition* was detected by the ANOVA.

Questionnaire scores and number of contacts were analyzed with non-parametric Friedman tests, given the nature of the data. Post-hoc tests were conducted when a significant effect of *condition* was detected. A significance level of 5 % was adopted for all statistical tests. Analyses were performed with python software.

5.3 Results

This section is composed of three main parts. First, we look into transitions between modes. Second, we examine modes on their own. Finally, we check the results of subjective evaluation of both transitions and modes using questionnaires.

5.3.1 Transitions Evaluation

Transitions between modes are evaluated in terms of progress and in terms of reaching a steady state.

Progression

We noticed that the progress of the performance metrics varies accordingly to the current mode and the one experienced in the past. We could observe that the average number of iterations necessary for the participants to adapt (and so reach steady state) varies across the experimental conditions ($R{\rightarrow}L$: $7, F{\rightarrow}L : 10, L{\rightarrow}R : 13, F{\rightarrow}R : 10, L{\rightarrow}F : 14, R{\rightarrow}F : 17$).

Fig. 5.3 we display the distribution of the metrics on the first iterations of the task after the mode switching. The ANOVA revealed a significant effect for the length of the movement ($p = 0.02$), co-contraction index ($p = 0.04$) force ($p < 0.001$), error on the reference position ($p < 0.001$) and smoothness of the movement ($p < 0.001$). For these cases, we executed Post-hoc test. For the length of the movement, we observed differences between $F{\rightarrow}L$ and $L{\rightarrow}F$ ($p = 0.02$) and values close to differences between $F{\rightarrow}L$ and $L{\rightarrow}F$ ($p = 0.06$) and $F{\rightarrow}L$ and $R{\rightarrow}F$ ($p = 0.058$). For co-contraction index between $R{\rightarrow}L$ and all the last three conditions ($p < 0.001$ for all the conditions) and a similar thing for $F{\rightarrow}L$ and all the last three conditions ($p = 0.03, p = 0.004, p = 0.01$ respectively). Concerning the force, we found significant differences between $R{\rightarrow}L$ and all the last four conditions ($p = 0.02, p = 0.02, p = 0.001, p < 0.001$ respectively) and a similar thing for $F{\rightarrow}L$ and all the last

four conditions ($p = 0.012, p = 0.021, p = 0.003, p < 0.001$ respectively). Moreover there are significant differences between $R{\rightarrow}F$ and the two conditions ending with R ($p = 0.01, p = 0.04$ respectively). Error on reference position reported differences between the conditions having L after the transition and all the others ($p < 0.001$); moreover, the experimental condition $F{\rightarrow}R$ presents statistical differences with the experimental modes ending with F ($p < 0.001, p = 0.006$). The smoothness of the movement suggest statistical differences between $R{\rightarrow}L$ and $R{\rightarrow}F$ ($p = 0.02$), $F{\rightarrow}L$ and all the others ($p = 0.015$ for the first condition and $p < 0.001$ for the last three conditions) and $L{\rightarrow}R$ and $R{\rightarrow}F$ ($p = 0.01$).

In summary, we observe that the transition heavily influences the collaboration.

Steady state

Fig. 5.4 displays the distribution of the metrics on the steady state iterations of the task and after the mode switching. The ANOVA revealed a significant effect for acceleration ($p = 0.02$), co-contraction index ($p = 0.008$), force ($p < 0.001$), error on the reference position ($p < 0.001$) and smoothness of the movement ($p = 0.004$). For these cases, we executed Post-hoc test. For the acceleration, we observed differences between $R{\rightarrow}L$ and $F{\rightarrow}R$ ($p = 0.02$), $R{\rightarrow}L$ and $L{\rightarrow}F$ ($p = 0.001$). For the co-contraction index, between $R{\rightarrow}L$ and the last four conditions ($p = 0.018, p = 0.006, p = 0.004, p = 0.001$ respectively), for $F{\rightarrow}L$ there is significant differences only to the last three conditions ($p = 0.01, p = 0.001, p = 0.04$ respectively). Concerning the force, we measured significant differences between conditions ending with L and the other conditions. Error on reference position reported similar behavior; moreover, we found statistical differences between $F{\rightarrow}R$ and the experimental modes ending with F ($p = 0.01$ for both of them). About the smoothness of the movement, we found statistical differences only between the first two conditions and the last four.

In summary, we can observe that certain transitions influence collaboration even at steady state.

5.3.2 Modes Evaluation

Fig. 5.5 displays the distribution of the metrics described in Sec.5.2.4 for the three control modes after reaching steady state. The ANOVA revealed a significant effect co-contraction index ($p < 0.001$), force ($p < 0.001$), error on the reference position ($p < 0.001$), and smoothness ($p < 0.001$). For these cases, we executed Post-hoc test. For the co-contraction index, we notice significant differences between L and R ($p = 0.001$) and between L and F ($p < 0.001$). For the force, there are significant differences between L and R ($p < 0.001$) and between L and R ($p < 0.001$). Concerning the error on the reference position, there are significant differences between L and R ($p < 0.001$), between L and F ($p < 0.001$) and between R and F ($p = 0.001$). Also the Fourier showed differences between L and R ($p < 0.001$) and between L and F ($p = 0.002$). At steady state, we notice more statistical differences between L and R than between F and R. This may suggest that participants, at steady state, have a tendency to follow the movement of the cobot and supervise the movement. The only statistical difference between R and F is for the error on the reference position.

Regarding the number of iterations necessary for subjects to adapt, we observed that L mode generally converges faster to steady state (it takes around 12 iterations to converge) while R takes 20 iterations and F is generally slower (around 25 iterations).

5.3.3 Questionnaire

Fig. 5.7 displays the distribution of the scores for the questionnaire about the transitions. The Friedman tests revealed a significant effect of the *condition* factor for question Q1 (*Transition between the modes was challenging*) ($\chi^2(3) = 26.6$, $p < 0.001$) and for Q2 (*Collaboration improved after the transition*)

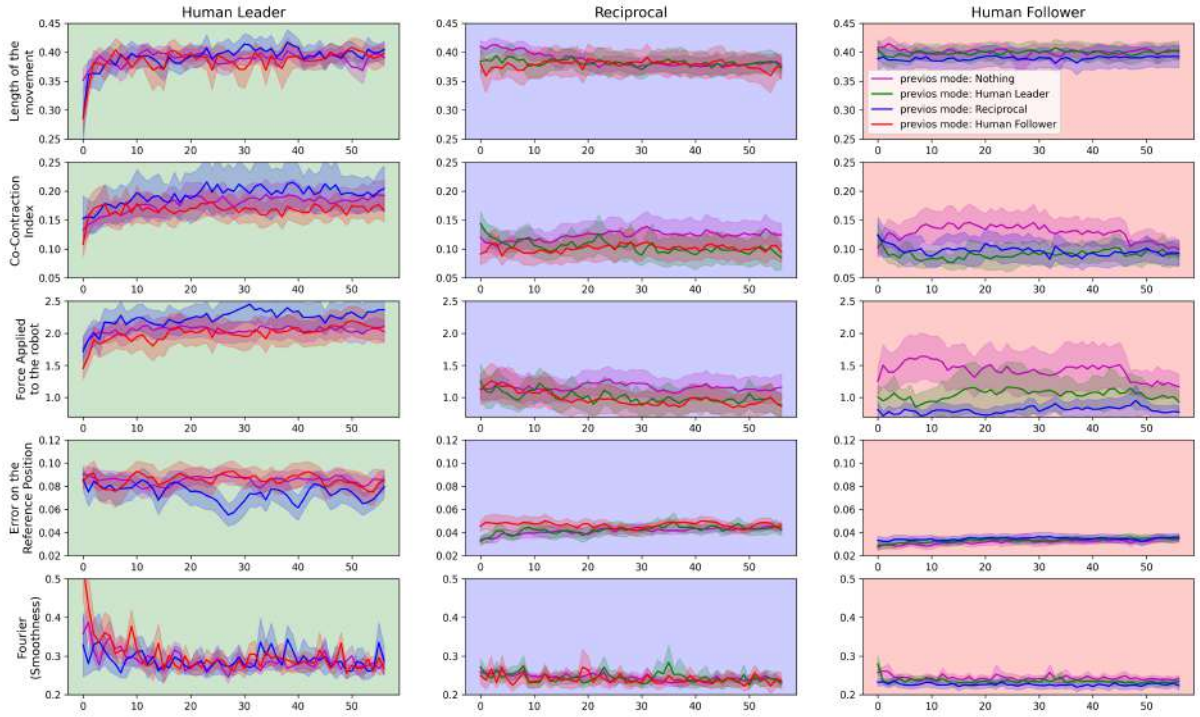

Figure 5.2: Progression of chosen scores sorted according to current mode and previous mode: in the columns are the current modes while the different colors are used to distinguish what the score was previously (purple when there is not a precedent mode namely in the first two minutes of the experiments, green for human leader in the previous mode, blue for reciprocal in the previous mode, red for human follower in the previous mode). In the rows are arranged the different scores.

Table 5.2: Linear regressions between the trial number and these dependent measures to identify when participants reached steady state performance. Regressions were calculated for each of the six experimental conditions and the modes, iteratively for the last 60, 59, 58 trials and so forth until the slopes were not significantly different from zero (i.e. the 95 % intervals did include zero, the first appearance of $p > 0.05$).

R→HL	HF→HL	HL→R	HF→R	HL→HF	R→HF	HL	R	HF
7	10	13	10	14	17	**12**	20	25

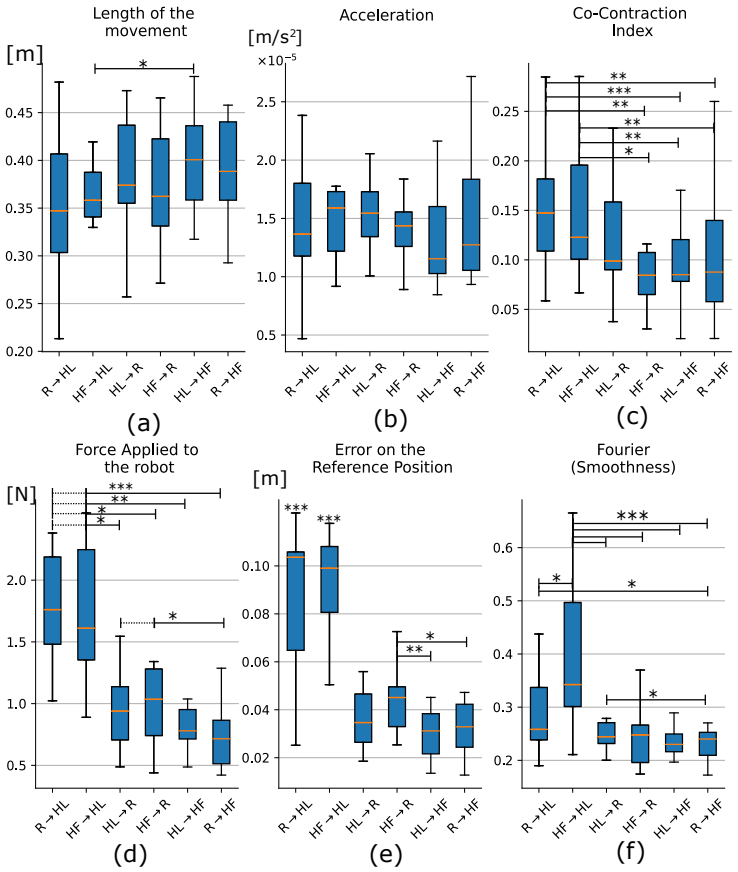

Figure 5.3: Comparison of the experimental conditions at the first 5 iterations after the switching: (M_1) Length of the movement; (M_2) Acceleration; (M_3) Co-Contraction index of the subject and measured using EMG sensors; (M_4) Force applied to the cobot; (M_5) Error on the reference position; (M_6) Fourier. The six experimental conditions are the combinations of the three control modes: Human Leader(HL), Human Follower(HF) and Reciprocal(R).

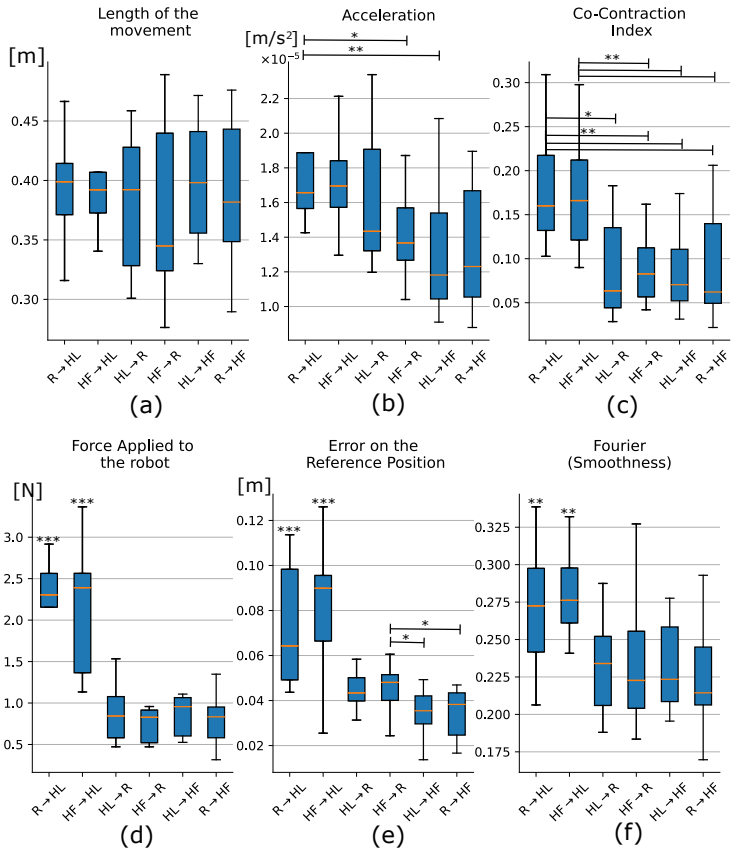

Figure 5.4: Comparison of the experimental conditions at Steady State: to identify steady state linear regressions were calculated for each of the six experimental conditions iteratively for the last 60, 59, 58 trials and so forth until the slopes were not significantly different from zero (i.e. the 95 % intervals did include zero).

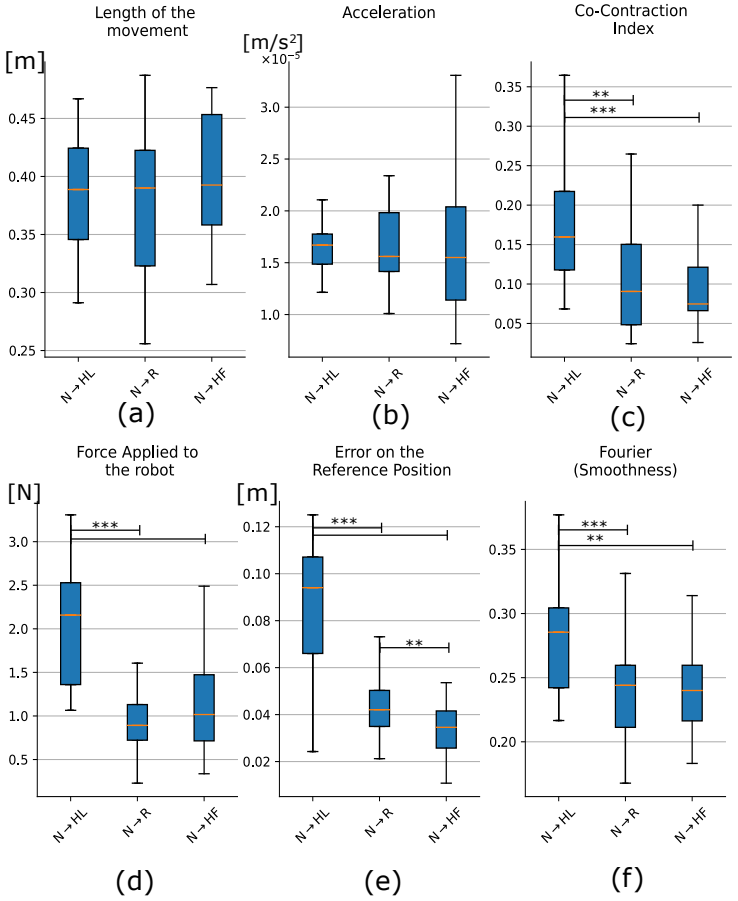

Figure 5.5: Comparison of the control modes at steady state: to compare the control modes fairly and without them being affected by the transitions, we compared the scores before the transitions occurred.

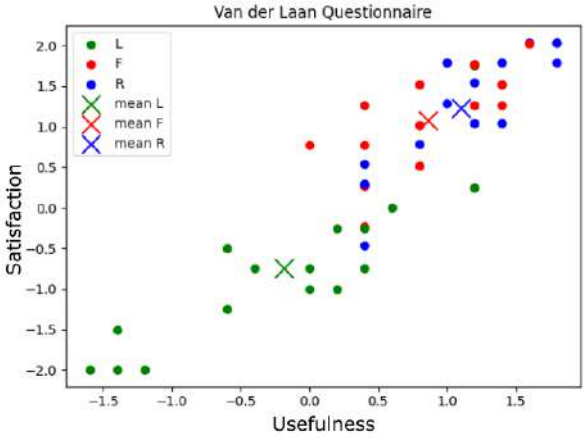

Figure 5.6: Results of the Van der Laan questionnaire. This scale assesses system acceptance on two dimensions: a Usefulness scale and a Satisfying scale.

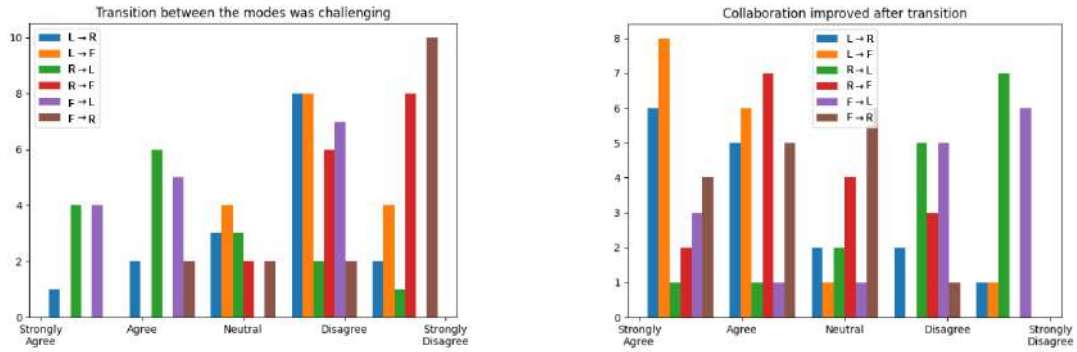

Figure 5.7: Subjective questions about the transition.

($\chi^2(3) = 25.7$, $p < 0.001$). For Q1, post-hoc tests indicated a significant difference between $F{\rightarrow}L$ and $L{\rightarrow}R$ ($p = 0.045$), $L{\rightarrow}R$ and $F{\rightarrow}R$ ($p = 0.003$), $L{\rightarrow}R$ and $R{\rightarrow}F$ ($p = 0.005$), $F{\rightarrow}R$ and $L{\rightarrow}F$ ($p = 0.03$) and a close difference between $L{\rightarrow}F$ and $R{\rightarrow}F$ ($p = 0.052$), while the other comparisons did not reach significance. For Q2, post-hoc tests indicated a significant difference between $R{\rightarrow}L$ and $L{\rightarrow}R$ ($p = 0.01$), $F{\rightarrow}L$ and $L{\rightarrow}R$ ($p = 0.001$), $F{\rightarrow}L$ and $L{\rightarrow}F$ ($p = 0.01$), $L{\rightarrow}R$ and $R{\rightarrow}F$ ($p = 0.045$), and close to be different between $R{\rightarrow}L$ and $L{\rightarrow}F$ ($p = 0.07$), while the other comparisons did not reach significance.

Fig. 5.8 displays the distribution of the scores for the questionnaire about the three modes. The Friedman tests revealed a significant effect of the *condition* factor for question Q1 (*The mode was engaging*) ($\chi^2(3) = 8.4$, $p = 0.01$), for Q2 (*The mode was demanding*) ($\chi^2(3) = 28.6$, $p < 0.001$), for Q3 (*The mode required high cognitive effort*) ($\chi^2(3) = 13.6$, $p = 0.001$), for Q4 (*The mode required high physical effort*) ($\chi^2(3) = 29.1$, $p < 0.001$) and for Q5 (*The mode was boring*) ($\chi^2(3) = 12.16$, $p = 0.002$). For Q1, post-hoc tests indicated a significant difference between R and F ($p = 0.02$). For Q2, post-hoc tests indicated a significant difference between L and R ($p = 0.003$) and L and F ($p = 0.001$). For Q3, post-hoc tests indicated a significant difference between R and F ($p = 0.04$) and L and F ($p = 0.02$). For Q4, post-hoc tests indicated a significant difference between L and the other two conditions($p = 0.004, p = 0.001$ respectively). For Q5, post-hoc tests indicated a significant difference between R and L ($p = 0.007$). All the other comparisons did not reach significance.

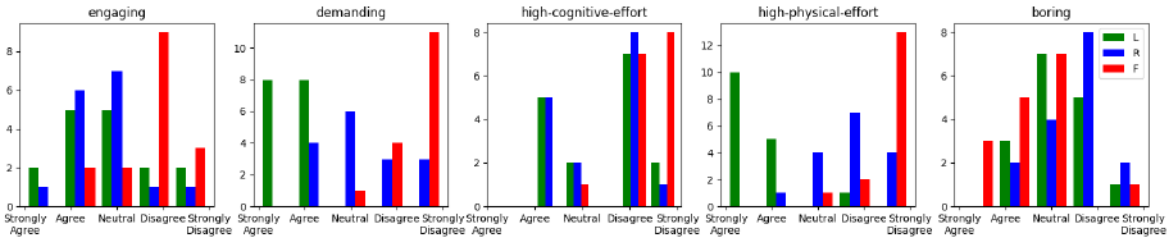

Figure 5.8: Subjective questions about the three modes: Human Leader (L), Human Follower (F) and Reciprocal (R).

5.4 Discussion

This section discussed the main results in terms of transitions between modes and modes individually, both in terms of objective metrics and questionnaires. Finally, we discuss some of the possible limitations of the existing study.

5.4.1 Transitions

Fig. 5.3 reports on the performances we chose to evaluate (length of the movement, acceleration, co-contraction index, force, error, and smoothness) at the first iterations after the switching between one mode to another. We observe statistical differences in movement length only between the second ($F \rightarrow L$) and fifth experimental condition ($L \rightarrow F$). Although there are no statistical differences, we observe a lower median for both the first ($R \rightarrow L$) and fourth transitions ($F \rightarrow R$). Similar considerations apply to the error on the reference position (statistical differences for $R \rightarrow L$, $F \rightarrow L$ and $F \rightarrow R$). These results suggest that for these three experimental modes, the quality of motion is affected by the transition losing the ability to follow the reference. We think this is because the participants are accustomed to greater robot autonomy, and when this fails, they do not take over quickly enough to take the leadership.

We also observed an interesting effect regarding co-contraction and applied force. The co-contraction index of the third experimental condition ($L \rightarrow R$) is similar to that of the first two conditions ($R \rightarrow L$ and $F \rightarrow L$), despite not showing statistical differences from the last three (as the first two do). The applied force, on the other hand, shows how both the third and fourth conditions ($L \rightarrow R$ and $F \rightarrow R$ respectively) show differences from the last two, and the fourth has a higher median. These results suggest that the operator applies a different force profile dependent on what the transition was. This type of behavior may be due to a stiffening of the operator (and thus an increase in ICC without a consequent increase in the force applied on the cobot) in the transition phase. We think this may be due to either a desire to maintain stability in the movement or an attempt to better understand the type of interaction being performed with the cobot.

Fig. 5.7 showed how the subjects perceived the transitions. Subjective questionnaires showed that the subjects found challenging to pass to F modes (Fig. 5.7a) and, on the contrary, they showed that the simplest transition is $L \rightarrow R$. Collaboration perception is improved in the cases where previously the human is leader (Fig. 5.7b) while it remains more or less constant in the switching from human leader to reciprocal, conversely, it is worsened when the human is leader after the transition. Similar behavior has been observed previously in movement length. This indicator reinforces our hypothesis that subjects have difficulty taking over abruptly when the cobot's cooperation fails. Similar unwanted behavior can also be imagined in the case of two human subjects in which one of the two participants stops making a contribution to the collaboration. Undoubtedly, such conduct would be misinterpreted by the second participant. Indeed, it is well known that, in general, people tend to appreciate more those who evolve

their behavior from negative to positive while they appreciate less those who change from a perceived positive behavior to a negative one. In the literature, this effect is called the "gain-loss effect" [13], and it has been shown that it can also be applied to interaction with robots [158].

So, to answer (**Th1:***How the switching between modes is perceived by the human? Is the performance influenced in the first iterations of the task after the switching?*), we can state that indeed the transition influences movement performance in the early stages and that the quality of the movement depends on how it was previously performed. As for (**Th3:** *Do humans prefer some transitions with respect to others?*), however, we can say that subjects prefer to abandon the human leader mode and prefer to either follow the robot or to collaborate (reciprocal).

Fig. 5.4 reports on the performance metrics after the steady state is reached. We expected that at steady state, the impact of switching had now been nullified, and instead, some results suggest that operator performance is still affected. Indeed, although we observed no statistical differences in movement length, there is a lower median for both the fourth transitions. Similar considerations apply to the error on the reference position (statistical differences for the first two and the fourth). Interestingly, the movement length for the human leader cases is about the same as for the other cases while, the error is very different. We think this is due to the fact that the human imposes a different trajectory than the cobot but still functional for task execution. These results refer to (**Th2:** *Does a past transition influence the collaboration after the steady state is reached?*), suggesting that the performance of the collaboration is also influenced after the steady state is reached.

5.4.2 Modes

Fig. 5.5 reports on the performance metrics for the three control modes observed separately after the steady state is reached. We can observe that there were no statistical differences in movement length, so movement performance was therefore not affected by mode choice. On the other hand, if we look at the distance to the reference trajectory, we notice statistically significant differences that allow us to say that in the three cases the human-robot pair performed three different trajectories. Looking at the other graphs (ICC, force, and smoothness), we observe statistical differences only between L and the other two modes. These results suggest that the R mode does not significantly affect the operator's effort and smoothness of the motion while allowing the operator to impose his own trajectory, as observed in the error from the reference. This happens because of the way R was constructed, in fact, whenever the subject decides to change the trajectory from that imposed by the cobot the subject increases its stiffness inducing the cobot to become compliant.

In Fig. 5.8 we could make the following observations: the subjects perceive the R and the F modes as engaging, the F is not demanding while the L is highly demanding also from a cognitive point of view and from a physical point of view, the R mode is arranged in the middle of these two extremes, subjects perceive the R mode as less boring with respect to the other modes. In a similar way, Fig. 5.6 displays the three modes on the Van der Laan scale assigning both a score of satisfaction and of use-fullness. We could observe that the mean value of the R and of the F mode are very close to each other, and at the same time, they are distant from the mean of the L modes. In accordance with this scale, there is small benefit in the R with respect to using F mode. Thus, answering question **Th5** (*For this specific task, does human prefer one mode with respect to another?*), we could state that subjects much prefer to collaborate with a cobot in R and L modes than a cobot in F mode. At the same time, we note a slight preference toward the R mode. Talking with participants, we got the idea that subjects preferred approaches in which the cobot was active because they were less strenuous. At the same time, we think R mode was better perceived by subjects because they felt they had more control over the task. Moreover, we think R is more convenient because it is less boring, more engaging (with respect to F mode), and require less effort (with respect to L mode). For this reason, we think it is better suited for tasks in which it is

important to be engaging (for instance, when human and robot executes dangerous movements).

The statistical analyses performed (Sec. 5.2.5), show how the general human subject finds equilibrium in its behavior (and thus scores settle) faster in the human leader case. In contrast, human follower is, in general, slower to converge to an equilibrium solution. The reciprocal mode condition generally requires intermediate times. Thus, answering question **Th4** (*Does human adapt faster to some modes with respect to others?*), we could state that human subjects adapt to the cobot's control modes at different times and that the greater the participant's autonomy, the shorter the time. This result is probably due to the fact that subjects search harder for solutions that limit the amount of fatigue in performing the movement. Furthermore, it has been shown that humans, in general, has a greater ability to adapt to tasks than the robot [75], we think that in the L case, the subject has full decision-making power and thus is not somehow slowed down by the cobot's reduced capabilities as is the case in the R and F cases.

5.4.3 Limitations

Our results should be considered carefully. First, the study was conducted with participants from the university environment, and while few participants were familiar with robots, the results cannot be generalized to a generic population, especially with industry workers that may have different attitudes when interacting with a cobot [144]. Second, the planar sawing task was simple and common. In this sense, we do not know if our results can be generalized to other tasks involving large and heavy loads with movements on the three dimensions, a situation that is often found in manufacturing where robots physically assist workers (e.g., manipulating car parts, such as wheels [145]). In any case, the results we obtained allow us to demonstrate how important the type of training the operator must undergo is and how important it is to manage the robot controller transitions in a consonant manner.

5.5 Conclusion

In this chapter, we studied how humans adapt in a collaborative sawing task when cobot suddenly changes the control strategy. The results suggest that in this kind of task, not only the type the current role of the cobot, but also the past ones influence the behavior of the human operator. In our specific task, the results seem to indicate that: transition influences movement performance in the early stages (**Th1**) and at steady state (**Th2**), subjects prefer to abandon the human leader mode and prefer to adopt modes in which there is either R or F modes (**Th3**), they adapts faster to L mode (**Th4**), subjects prefer R mode (**Th5**). In future works, we would like to use the collected data to build a model of how a human adapts to a robot. We think that such a model can be used to optimize the robot's impedance profile, especially when transitioning from one profile to another.

6

Conclusions

In this closing chapter, we elaborate on the main results presented in the thesis and the perspectives and possible future research directions on the topics of human-robot collaboration and adaptation.

The work in this thesis stems from a multi-disciplinary approach that results in a set of tools for improving human-robot collaboration. When human and robot physically interact several aspects must be considered: **the robot's control, the interaction with the enviromnent, the human kinematic and dynamic behaviour, the ergonomic of this latter, and how he/she will react to the robot movements.** This human-centered approach is justified to propose methods in which a robot can collaborate with a human partner in an ergonomic fashion while being able to physically interact effectively with him/her. To guarantee proficient and adequate cooperative behaviors, robots need to advance their cognitive, social and physical interaction skills. In Chapter 1 we review the current work in these areas of research, acknowledging the main limitations due to the complexity of modeling and identifying the human state. We formalize the concept of human-robot cooperation and collaboration, and we overview the main interaction control approaches that enable low-level physical interaction between the robot and the human. The knowledge of the human "state" is required by both the high and the low level control to build human-aware control plans: hence we present the main methods used to model and perceive the humans. Finally, we report on the current main application of robots interacting and cooperating with humans.

Human-aware robot collaborators capable of long-term interactions in real situations are the next grand challenge. Many papers attempt to model human behavior from both dynamic and kinematic perspectives. Nevertheless, we think that his behavior is very complex because it includes aspects that are variable between subjects. For example, an injured subject will tend to perform a movement differently than a healthy subject. Similarly subjects with greater confidence and knowledge of the robot will have a different approach than inexperienced individuals. Moreover, this behavior changes as the subject adapts to the robot. We think that if human behavior could be modeled (probabilistically), the interaction with the robot would be improved. A key aspect of this modeling is to find an effective representation of the person in terms of personalized models.

In Chapter 2 we presented two ways to represent the movements of the human: a **digital human model** of 66 joints, and a **latent space** of two dimensions in which movements are mapped. We used them for providing **online ergonomics feedback to human workers** during their activities, also when they physically interact with robots. A Digital Human Model is used to visualize, with color-coded spheres, the body areas and joints that are subject to efforts and non-ergonomic postures. We used as score some state of the art methods like the RULA and the RULA continous score. Moreover we proposed an estimation of the human internal torques using the dynamic model of the dhm and the force

measured by the robot. All these scores can be visualize on the DHM while the subject it is performing a movement. Our second contribution is Latent Ergonomics Maps (LEMs). They are synthetic representations of the overall ergonomics scores projected onto a bidimensional latent space that maps human postures. The result is an intuitive color-coded map where the human posture is a point, a movement is a line, and their associated color is an estimation of the ergonomics score of choice. LEMs can be used for bio-feedback or self-correction, as a visual tool for teaching, or simply to inform the human. Their potential goes beyond the online feedback for the human, as they can be used to inform the robot as well, which can find applications in planning ergonomically optimal collaborative motions. Advantages of LEMs include their ease of interpretation also for non-experts, and the computational efficiency, enabling online feedback. A limitation of projecting the map on a 2D latent space, which is necessary for visualization purposes, is the information loss that may result from such a strong dimensionality reduction. However, the error is tolerable for ergonomics scores based on postural information, and otherwise acceptable if coupled with the visualization of efforts on the Digital Human Model.

In future works, we want to combine the prediction of intended movement [56] with LEMs, therefore predicting future ergonomics scores for the intended movement. This, we think, will enable us to alert the human of possible risks associated with ergonomics in particular during human-robot collaboration. The idea is to inform the robot about the ergonomics risk associated with planned collaborative robot trajectories as in [240], and then to optimize these trajectories using ergonomics optimization as in [85, 86]. More generally, we think that an algorithm that predicts human movement can be used proactive strategies of the robot.

For this reason, in Chapter 3 we reviewed methods for human posture prediction and we presented a novel approach. Our framework allows us **to predict human posture** in a Human-Robot Collaboration scenario where the human hand motion is constrained by the robot's end-effector. We propose a two-phase method: in the first phase, we leverage a dataset of human demonstrations to learn a distribution over the null-space of the human Jacobian using a Gaussian Process; in the second phase, we optimize the weights of the weighted pseudo-inverse of the Jacobian. Our method computes a probabilistic estimation of the future postures that satisfy the kinematic constraints imposed by the physical link between the human and the robot and, at the same time, it is coherent with the human preferences of movement. In fact, humans are not entirely "controllable": humans are highly redundant systems that are over-actuated for many manipulation tasks. In other words, humans can execute the same task in many different ways. For instance, lifting a box from the floor might be performed by bending the back, but also by bending the knees. Individual preferences of movement and musculo-skeletal problems might add to the intrinsic variability of the human movement, thus increasing the variance of all possible postures in response to a robot action. For these reasons, when the human is physically coupled with the robot to accomplish a task, it is not possible to know with certainty how a human will move when the robot imposes a trajectory, which makes it challenging to select the best trajectories for the robot in collaborative tasks. In this context, data-driven probabilistic models of human movements, learned from demonstrations, can provide interesting insights into human preferences while capturing the variance of demonstrated movements. A limit of this kind of solutions is that a small error in the joint estimation can cause a large error in the estimation of the end-effector position (i.e., the human hand), which makes the prediction kinematically inconsistent. This error poses a nontrivial problem, especially when the human is physically coupled to the robot because it can compromise the quality of the collaboration. For these reasons human posture prediction in HRC should be: probabilistic, based on the kinematic model of the subject and constricted in the pose of the end-effector.

In the future, we want to extend our human model and integrate the algorithm into our framework for ergonomics control, which aims to optimize a collaborative robot's motions to maximize the comfort and

the ergonomics of the human collaborator. A byproduct of our method is the probabilistic computation of ergonomics scores for a given robot's EE trajectory, which is a critical element for planning and optimizing the robot's trajectories. One simplification we have made in our work is to place the robot as the leader and the human as the follower. We would like, in the future to carry out more experiments and see if we get different kinematic patterns by considering different roles. This fact made us think about how the subject's behavior changes depending on what role it plays toward the robot and led us to further investigation in this direction.

In Chapter 4 we perform a human study in which we compare different paradigms of interaction: the **robot behaves as a cooperator (leader or follower) or collaborator (variable impedance)** during a co-manipulation task with a human. The goal in this experiment is twofold: investigate the human motor behavior in a task we already evaluated in a human-human dyad; and try to emulate the such behavior on the robot control side. Given the results from the human-human experiment, whenever the robot is assigned a leadership, the robot is considered to have full autonomy over the task, while the robot and the human share that same autonomy during a collaboration. Both behaviors are expressed by changing the desired Cartesian stiffness of the robot's end-effector: robot leader at high stiffness, robot follower at low stiffness. Moreover, in this experiment the autonomy of the task is arbitrated by the human arm co-contraction, using two different variable impedance control profiles: reciprocal and mirrored.

The reciprocal profile turns the robot behavior from a leader to a follower while the human co-contracts his/her arm, and consequently, turns from a follower to a leader. Therefore, in this case, the autonomy is taken from the robot into the hands of the human so to speak. This profile is similar to the one implemented in Peternel *et al.* [178] that was arbitrated by the sum of the muscle activation signals from a pair of antagonist muscles. The mirrored profile considers that the robot and the human should always share the task in equal parts, there is never a total leader nor a total follower. In this profile, the robot's desired Cartesian stiffness is directly proportional to the human arm co-contraction. This is a similar behavior to the one observed for human-human collaboration behaviors where both agents had high values of arm co-contraction. Both variable impedance control profiles are tested.

Our study shows that with a robot leader informed of the task trajectory, the human makes less effort, but in terms of task accuracy and effort, a reciprocal collaborative strategy seems preferable for a human. Our results are relevant for the design of human-robot collaborative workstations. They also evoke new questions to further understand human behavior, precisely the human arm impedance, during joint work with humans and robots. We noticed that giving some degree of autonomy to human is overall positive: human benefits from the robot's assistance while the robot compliance can leave the necessary degree of maneuver to the human to correct the task when needed. Moreover Collaboration helps maintaining the task engagement and so attentive to the task thus reducing the risk of accidents. In our study, the robot reference trajectory and its duration were fixed: they were arbitrarily set to have a reasonable speed that would not challenge the participants. In future would be interesting to investigate whether time-varying trajectories are more suitable for collaboration. In this study, 15 trials were done for each experimental condition, and we observed a certain trend of subjects converging to one strategy over another. We wondered, though, if these strategies would be different after hours of interaction. A key aspect of collaboration in fact is adaptation.

Adaptation is the process in which an agent changes slightly over time to be able to improve his performance. In Chapter 5 we did a survey of how adaptation affects human-robot interaction. Moreover, we studied how humans adapt to cobot's changes in the control strategy. We propose a human study in which 18 participants executed a collaborative human-robot sawing task where the robot altered between three different control strategies. We examined human adaptation when robot suddenly changed the

control strategy from one to another, resulting in six experimental conditions. The experiments were performed on a setup involving Kuka LBR iiwa robotic arm. The results suggest that in this kind of task, not only the type the current role of the cobot, but also the past ones influence the behavior of the human operator. In our specific task, the results seem to indicate that: transition influences movement performance in the early stages and at steady state, subjects adapts faster to leader mode.

We think this work is an example of how important it is to consider the adaptive process in many environments where humans and robots interact: industry, home automation, rehabilitation exoskeletons. In future works, we would like to use the collected data to build a model of how a human adapts to a robot. We think this model could provide us with an indispensable tool for collaboration. Indeed, if the robot could predict how a subject adapts to a given policy it could vary its policy with the intent of accelerating the adaptation (in case the equilibrium condition was good) or on the contrary guide it to another equilibrium condition. These kinds of strategies are called mutual adaptation [162], and are already found in the literature, but to the best of our knowledge, there are few cases where they are used in pHRI. Whereas we think that, for example, a variable impedance control algorithm, lends itself well to this kind of formulation.

Overall, during the course of this PhD thesis it was possible to develop tools that can serve as a basis for a physical human-robot interaction considering human ergonomics and adaptation to robot's Collaboration strategies. In our approach, the next step beyond this thesis is to put those pieces together in a single application, where human motion prediction (kinematics and motor behaviour during adaptation) is used to optimize the reference trajectory for the variable impedance profiles. We think that a type framework that seeks to optimize at the same time of cost functions on the robot and the human can be a great step forward in realizing the industra of the future. To do so, we think, the tools provided in this thesis can be necessary building blocks to a complete and reliable human model. In fact, we have proposed a visualization tool, a prediction tool, and two studies on what are human behaviors.

Moreover, it will be interesting to study how much knowledge and results from cobots could be re-used or transfered in a human-exoskeleton interaction. In fact, exoskeletons can be regarded as collaborative robots with the difference that, in most cases, they share more touch points with humans than robots. For this reason, some considerations about the redundancy of the human are lost but nonetheless what has been observed for the kinematics and motor behavior of the human may remain true. Particularly for exoskeletons and robotic prostheses, adaptation plays a key role since the human must wear these tools throughout the day and in many cases the human needs their support to perform the simplest activities (walking for example). For these reasons, subjects find solutions after a long period of interaction that need to be considered.

Bibliography

[1] Gitai partners with JAXA to send telepresence robots to space [online]. https://spectrum.ieee.org/automaton/robotics/space-robots/gitai-partners-with-jaxa-to-send-telepresence-robots-to-space.

[2] Fares J Abu-Dakka and Matteo Saveriano. Variable impedance control and learning–a review. *arXiv preprint arXiv:2010.06246*, 2020.

[3] Don Joven Agravante, Andrea Cherubini, Alexander Sherikov, Pierre-Brice Wieber, and Abderrahmane Kheddar. Human-humanoid collaborative carrying. *IEEE Transactions on Robotics*, 35(4):833–846, 2019.

[4] Arash Ajoudani, Cheng Fang, Nikos Tsagarakis, and Antonio Bicchi. Reduced-complexity representation of the human arm active endpoint stiffness for supervisory control of remote manipulation. *The International Journal of Robotics Research*, 37(1):155–167, 2018.

[5] Arash Ajoudani, Nikos Tsagarakis, and Antonio Bicchi. Tele-impedance: Teleoperation with impedance regulation using a body–machine interface. *The International Journal of Robotics Research*, 31(13):1642–1656, 2012.

[6] Arash Ajoudani, Andrea Maria Zanchettin, Serena Ivaldi, Alin Albu-Schäffer, Kazuhiro Kosuge, and Oussama Khatib. Progress and prospects of the human–robot collaboration. *Autonomous Robots*, 42(5):957–975, Jun 2018.

[7] Omar Mounir Alaoui, Fabien Expert, Guillaume Morel, and Nathanaël Jarrassé. Using arm swing movements to maintain the walking state in a self-balanced lower-limb exoskeleton. In *2022 International Conference on Robotics and Automation (ICRA)*, pages 6444–6450. IEEE, 2022.

[8] Alin Albu-Schaffer, Christian Ott, Udo Frese, and Gerd Hirzinger. Cartesian impedance control of redundant robots: Recent results with the dlr-light-weight-arms. In *2003 IEEE International conference on robotics and automation (Cat. No. 03CH37422)*, volume 3, pages 3704–3709. IEEE, 2003.

[9] Arsha Ali, Hebert Azevedo-Sa, Dawn M Tilbury, and Lionel P Robert Jr. Using trust for heterogeneous human-robot team task allocation. *arXiv preprint arXiv:2110.04332*, 2021.

[10] Dario Amodei, Chris Olah, J. Steinhardt, Paul F. Christiano, John Schulman, and Dan Mané. Concrete problems in ai safety. *ArXiv*, abs/1606.06565, 2016.

[11] Salvatore M. Anzalone, Sofiane Boucenna, Serena Ivaldi, and Mohamed Chetouani. Evaluating the engagement with social robots. *International Journal of Social Robotics*, 7(4):465–478, Aug 2015.

[12] Salvatore M Anzalone, Sofiane Boucenna, Serena Ivaldi, and Mohamed Chetouani. Evaluating the engagement with social robots. *International Journal of Social Robotics*, 7(4):465–478, 2015.

[13] Elliot Aronson and Darwyn Linder. Gain and loss of esteem as determinants of interpersonal attractiveness. *Journal of experimental social psychology*, 1(2):156–171, 1965.

[14] Tamim Asfour, Mirko Waechter, Lukas Kaul, Samuel Rader, Pascal Weiner, Simon Ottenhaus, Raphael Grimm, You Zhou, Markus Grotz, and Fabian Paus. Armar-6: A high-performance humanoid for human-robot collaboration in real-world scenarios. *IEEE Robotics & Automation Magazine*, 26(4):108–121, 2019.

[15] Keyhan Kouhkiloui Babarahmati, Carlo Tiseo, Joshua Smith, Hsiu Chin Lin, Mustafa Suphi Erden, and Michael Mistry. Fractal impedance for passive controllers. *arXiv preprint arXiv:1911.04788*, 2019.

[16] Jimmy Baraglia, Maya Cakmak, Yukie Nagai, Rajesh Rao, and Minoru Asada. Efficient human-robot collaboration: when should a robot take initiative? *The International Journal of Robotics Research*, page 027836491668825, 02 2017.

[17] Christoph Bartneck, Dana Kulić, Elizabeth Croft, and Susana Zoghbi. Measurement instruments for the anthropomorphism, animacy, likeability, perceived intelligence, and perceived safety of robots. *International Journal of Social Robotics*, 1(1):71–81, Jan 2009.

[18] Tito Bassani, Elena Stucovitz, Zhihui Qian, Matteo Briguglio, and Fabio Galbusera. Validation of the anybody full body musculoskeletal model in computing lumbar spine loads at l4l5 level. *Journal of Biomechanics*, 58:89 – 96, 2017.

[19] Marco Baumgartner, Tobias Kopp, and Steffen Kinkel. Analysing factory workers acceptance of collaborative robots: A web-based tool for company representatives. *Electronics*, 11(1), 2022.

[20] Maciej Bednarczyk, Hassan Omran, and Bernard Bayle. Emg-based variable impedance control with passivity guarantees for collaborative robotics. *IEEE Robotics and Automation Letters*, 2022.

[21] Maciej Bednarczyk, Hassan Omran, and Bernard Bayle. Emg-based variable impedance control with passivity guarantees for collaborative robotics. *IEEE Robotics and Automation Letters*, pages 1–1, 2022.

[22] Christian J Bell, Pradeep Shenoy, Rawichote Chalodhorn, and Rajesh PN Rao. Control of a humanoid robot by a noninvasive brain–computer interface in humans. *Journal of neural engineering*, 5(2):214, 2008.

[23] Lefteris Benos, Avital Bechar, and Dionysis Bochtis. Safety and ergonomics in human-robot interactive agricultural operations. *Biosystems Engineering*, 200:55–72, 2020.

[24] Lefteris Benos, Dimitrios Tsaopoulos, and Dionysis Bochtis. A review on ergonomics in agriculture. part i: Manual operations. *Applied Sciences*, 10(6):1905, 2020.

[25] Lefteris Benos, Dimitrios Tsaopoulos, and Dionysis Bochtis. A review on ergonomics in agriculture. part ii: Mechanized operations. *Applied Sciences*, 10(10):3484, 2020.

[26] Aaron Bestick, Ruzena Bajcsy, and Anca D. Dragan. Implicitly Assisting Humans to Choose Good Grasps in Robot to Human Handovers. In *2016 International Symposium on Experimental Robotics*, volume 1, pages 341–354. Springer International Publishing, (2017). Series Title: Springer Proceedings in Advanced Robotics.

[27] A. Bolotnikova, S. Courtois, and A. Kheddar. Autonomous initiation of human physical assistance by a humanoid. In *2020 29th IEEE International Conference on Robot and Human Interactive Communication (RO-MAN)*, pages 857–862, 2020.

[28] Anastasia Bolotnikova, Sébastien Courtois, and Abderrahmane Kheddar. Autonomous initiation of human physical assistance by a humanoid. In *2020 29th IEEE International Conference on Robot and Human Interactive Communication (RO-MAN)*, pages 857–862. IEEE.

[29] Michael Bombile and Aude Billard. Capture-point based balance and reactive omnidirectional walking controller. In *2017 IEEE-RAS 17th International Conference on Humanoid Robotics (Humanoids)*, pages 17–24. IEEE, 2017.

[30] Francesco Bossi, Cesco Willemse, Jacopo Cavazza, Serena Marchesi, Vittorio Murino, and Agnieszka Wykowska. The human brain reveals resting state activity patterns that are predictive of biases in attitudes toward robots. *Science Robotics*, 5(46), 2020.

[31] Ronald Newbold Bracewell and Ronald N Bracewell. *The Fourier transform and its applications*, volume 31999. McGraw-Hill New York, 1986.

[32] Cynthia Breazeal. *Designing Sociable Robots*. MIT Press, Cambridge, MA, USA, 2002.

[33] Gwendolyn M Bryan, Patrick W Franks, Stefan C Klein, Robert J Peuchen, and Steven H Collins. A hip–knee–ankle exoskeleton emulator for studying gait assistance. *The International Journal of Robotics Research*, 40(4-5):722–746, 2021.

[34] Anais Brygo, Ioannis Sarakoglou, Nikos Tsagarakis, and Darwin Caldwell. Tele-manipulation with a humanoid robot under autonomous joint impedance regulation and vibrotactile balancing feedback. 11 2014.

[35] Jonas Buchli, Freek Stulp, Evangelos Theodorou, and Stefan Schaal. Learning variable impedance control. *The International Journal of Robotics Research*, 30(7):820–833, 2011.

[36] Gabriele Buondonno, Federico Patota, Hongbo Wang, Alessandro De Luca, and Kazuhiro Kosuge. A model predictive control approach for the partner ballroom dance robot. In *2015 IEEE International Conference on Robotics and Automation (ICRA)*, pages 774–780. IEEE, 2015.

[37] Etienne Burdet, Gowrishankar Ganesh, Chenguang Yang, and Alin Albu-Schäffer. Interaction force, impedance and trajectory adaptation: by humans, for robots. In *Experimental Robotics*, pages 331–345. Springer, 2014.

[38] Etienne Burdet, Rieko Osu, David W Franklin, Theodore E Milner, and Mitsuo Kawato. The central nervous system stabilizes unstable dynamics by learning optimal impedance. *Nature*, 414(6862):446–449, 2001.

[39] Joel W Burdick. On the inverse kinematics of redundant manipulators: Characterization of the self-motion manifolds. In *Advanced Robotics: 1989*, pages 25–34. Springer, 1989.

[40] Baptiste Busch, Guilherme Maeda, Yoan Mollard, Marie Demangeat, and Manuel Lopes. Postural optimization for an ergonomic human-robot interaction. In *2017 IEEE/RSJ International Conference on Intelligent Robots and Systems (IROS)*, pages 2778–2785. IEEE, 2017.

[41] Antoine Bussy, Pierre Gergondet, Abderrahmane Kheddar, François Keith, and André Crosnier. Proactive behavior of a humanoid robot in a haptic transportation task with a human partner. In *2012 IEEE RO-MAN: The 21st IEEE International Symposium on Robot and Human Interactive Communication*, pages 962–967. IEEE, 2012.

[42] Sylvain Calinon, Florent Guenter, and Aude Billard. On learning, representing, and generalizing a task in a humanoid robot. *IEEE Transactions on Systems, Man, and Cybernetics, Part B (Cybernetics)*, 37(2):286–298, 2007.

[43] Angelo Cangelosi and Tetsuya Ogata. *Speech and Language in Humanoid Robots*. Springer Netherlands, Dordrecht, 2016.

[44] Marc G Carmichael, Stefano Aldini, Richardo Khonasty, Antony Tran, Christian Reeks, Dikai Liu, Kenneth J Waldron, and Gamini Dissanayake. The anbot: An intelligent robotic co-worker for industrial abrasive blasting. In *2019 IEEE/RSJ International Conference on Intelligent Robots and Systems (IROS)*, pages 8026–8033. IEEE, 2019.

[45] Justin Carpentier, Florian Valenza, Nicolas Mansard, et al. Pinocchio: fast forward and inverse dynamics for poly-articulated systems. https://stack-of-tasks.github.io/pinocchio, 2015–2019.

[46] Konstantinos Chatzilygeroudis and Jean-Baptiste Mouret. Using parameterized black-box priors to scale up model-based policy search for robotics. In *2018 IEEE International Conference on Robotics and Automation (ICRA)*, pages 1–9. IEEE, 2018.

[47] Konstantinos Chatzilygeroudis, Roberto Rama, Rituraj Kaushik, Dorian Goepp, Vassilis Vassiliades, and Jean-Baptiste Mouret. Black-box data-efficient policy search for robotics, 2017.

[48] Maxime Chaveroche, Adrien Malaisé, Francis Colas, François Charpillet, and Serena Ivaldi. A variational time series feature extractor for action prediction. *arXiv preprint arXiv:1807.02350*, 2018.

[49] Kaiqi Chen, Jeffrey Fong, and Harold Soh. Mirror: Differentiable deep social projection for assistive human-robot communication. *arXiv preprint arXiv:2203.02877*, 2022.

[50] Min Chen, Stefanos Nikolaidis, Harold Soh, David Hsu, and Siddhartha Srinivasa. Trust-aware decision making for human-robot collaboration: Model learning and planning. *ACM Transactions on Human-Robot Interaction (THRI)*, 9(2):1–23, 2020.

[51] Yujiao Cheng, Weiye Zhao, Changliu Liu, and Masayoshi Tomizuka. Human motion prediction using semi-adaptable neural networks. In *2019 American Control Conference (ACC)*, pages 4884–4890. IEEE, 2019.

[52] Andrea Cherubini, Robin Passama, André Crosnier, Antoine Lasnier, and Philippe Fraisse. Collaborative manufacturing with physical human–robot interaction. *Robotics and Computer-Integrated Manufacturing*, 40:1–13, 2016.

[53] Francesco Chiacchio, Georgios Petropoulos, and David Pichler. The impact of industrial robots on eu employment and wages: A local labour market approach. Technical report, Bruegel working paper, 2018.

[54] Andrea S Ciullo, Manuel G Catalano, Antonio Bicchi, and Arash Ajoudani. A supernumerary soft robotic hand-arm system for improving worker ergonomics. In *International Symposium on Wearable Robotics*, pages 520–524. Springer, 2018.

[55] Arturo Cruz-Maya, Roxana Agrigoroaie, and Adriana Tapus. Improving user's performance by motivation: Matching robot interaction strategy with user's regulatory state. In *International Conference on Social Robotics*, pages 464–473. Springer, 2017.

[56] Oriane Dermy, Maxime Chaveroche, Francis Colas, François Charpillet, and Serena Ivaldi. Prediction of human whole-body movements with ae-promps. In *2018 IEEE-RAS 18th International Conference on Humanoid Robots (Humanoids)*, pages 572–579. IEEE, 2018.

[57] Oriane Dermy, Alexandros Paraschos, Marco Ewerton, François Charpillet, Jan Peters, and Serena Ivaldi. Prediction of intention during interaction with iCub with probabilistic movement primitives. *Frontiers in Robotics and AI*, 4:45, 2017.

[58] Louise Devigne, Marco Aggravi, Morgane Bivaud, Nathan Balix, Catalin Stefan Teodorescu, Tom Carlson, Tom Spreters, Claudio Pacchierotti, and Marie Babel. Power wheelchair navigation assistance using wearable vibrotactile haptics. *IEEE transactions on haptics*, 13(1):52–58, 2020.

[59] Alexander Dietrich, Christian Ott, and Alin Albu-Schäffer. An overview of null space projections for redundant, torque-controlled robots. *The International Journal of Robotics Research*, 34(11):1385–1400, 2015.

[60] Pierre Dillenbourg et al. The evolution of research on computer-supported collaborative learning. In *Technology-enhanced learning*. 2009.

[61] Nat Dilokthanakul, Pedro AM Mediano, Marta Garnelo, Matthew CH Lee, Hugh Salimbeni, Kai Arulkumaran, and Murray Shanahan. Deep unsupervised clustering with gaussian mixture variational autoencoders. *arXiv preprint arXiv:1611.02648*, 2016.

[62] Jay Dixon, Bryan Hong, and Lynn Wu. *The employment consequences of robots: Firm-level evidence*. Statistics Canada Ontario, 2020.

[63] Jianwei Dong, Jianming Xu, Qiaoqian Zhou, and Songda Hu. Physical human–robot interaction force control method based on adaptive variable impedance. *Journal of the Franklin Institute*, 357(12):7864–7878, 2020.

[64] Davide Dottori. Robots and employment: evidence from italy. *Economia Politica*, 38(2):739–795, 2021.

[65] Keith L Doty, Claudio Melchiorri, Eric M Schwartz, and Claudio Bonivento. Robot manipulability. *IEEE Transactions on Robotics and Automation*, 11(3):462–468, 1995.

[66] Ilias El Makrini, Greet Van De Perre, Glenn Mathijssen, Victor Van Wymeersch, Maxim Vochten, Wilm Decré, and Bram Vanderborght. Improving user ergonomics through adaptable cobot behaviour - part 1 - a generic algorithm for the computation of optimal ergonomic postures. In *IROS 2019*, pages 1–4, 10 2019.

[67] Mustafa Suphi Erden and Aude Billard. Hand impedance measurements during interactive manual welding with a robot. *IEEE transactions on robotics*, 31(1):168–179, 2015.

[68] Paul Evrard, Elena Gribovskaya, Sylvain Calinon, Aude Billard, and Abderrahmane Kheddar. Teaching physical collaborative tasks: object-lifting case study with a humanoid. In *2009 9th IEEE-RAS International Conference on Humanoid Robots*, pages 399–404. IEEE, 2009.

[69] Paul Evrard and Abderrahmane Kheddar. Homotopy switching model for dyad haptic interaction in physical collaborative tasks. In *World Haptics 2009-Third Joint EuroHaptics conference and Symposium on Haptic Interfaces for Virtual Environment and Teleoperator Systems*, pages 45–50. IEEE, 2009.

[70] Maurizio Faccio, Irene Granata, Alberto Menini, Mattia Milanese, Chiara Rossato, Matteo Bottin, Riccardo Minto, Patrik Pluchino, Luciano Gamberini, Giovanni Boschetti, et al. Human factors in cobot era: a review of modern production systems features. *Journal of Intelligent Manufacturing*, pages 1–22, 2022.

[71] Simone Fani, Simone Ciotti, Manuel G. Catalano, Giorgio Grioli, Alessandro Tognetti, Gaetano Valenza, Arash Ajoudani, and Matteo Bianchi. Simplifying Telerobotics: Wearability and Teleimpedance Improves Human-Robot Interactions in Teleoperation. *IEEE Robotics Automation Magazine*, 25(1):77–88, March 2018.

[72] Federica Ferraguti, Cristian Secchi, and Cesare Fantuzzi. A tank-based approach to impedance control with variable stiffness. In *2013 IEEE international conference on robotics and automation*, pages 4948–4953. IEEE, 2013.

[73] Fanny Ficuciello, Amedeo Romano, Luigi Villani, and Bruno Siciliano. Cartesian impedance control of redundant manipulators for human-robot co-manipulation. In *2014 IEEE/RSJ International Conference on Intelligent Robots and Systems*, pages 2120–2125, 2014.

[74] Naomi T Fitter, Mayumi Mohan, Katherine J Kuchenbecker, and Michelle J Johnson. Exercising with baxter: preliminary support for assistive social-physical human-robot interaction. *Journal of neuroengineering and rehabilitation*, 17(1):1–22, 2020.

[75] Paul M Fitts. Human engineering for an effective air-navigation and traffic-control system. 1951.

[76] David W Franklin, Etienne Burdet, Keng Peng Tee, Rieko Osu, Chee-Meng Chew, Theodore E Milner, and Mitsuo Kawato. Cns learns stable, accurate, and efficient movements using a simple algorithm. *Journal of neuroscience*, 28(44):11165–11173, 2008.

[77] Giovanni Franzese, Anna Mészáros, Luka Peternel, and Jens Kober. Ilosa: Interactive learning of stiffness and attractors. *arXiv preprint arXiv:2103.03099*, 2021.

[78] Paolo Gallina, Nicola Bellotto, and Massimiliano Di Luca. Progressive co-adaptation in human-machine interaction. In *2015 12th International Conference on Informatics in Control, Automation and Robotics (ICINCO)*, volume 2, pages 362–368. IEEE, 2015.

[79] Alessandro Gasparetto and Lorenzo Scalera. A brief history of industrial robotics in the 20th century. *Advances in Historical Studies*, 8(1):24–35, 2019.

[80] Ahmad Gazar, Gabriele Nava, Francisco Javier Andrade Chavez, and Daniele Pucci. Jerk control of floating base systems with contact-stable parameterized force feedback. *IEEE Transactions on Robotics*, 2020.

[81] E Amir M Ghalamzan, Firas Abi-Farraj, Paolo Robuffo Giordano, and Rustam Stolkin. Human-in-the-loop optimisation: mixed initiative grasping for optimally facilitating post-grasp manipulative actions. In *2017 IEEE/RSJ International Conference on Intelligent Robots and Systems (IROS)*, pages 3386–3393. IEEE, 2017.

[82] Benyamin Ghojogh, Ali Ghodsi, Fakhri Karray, and Mark Crowley. Factor analysis, probabilistic principal component analysis, variational inference, and variational autoencoder: Tutorial and survey. *arXiv preprint arXiv:2101.00734*, 2021.

[83] Alberto Giammarino, Juan M Gandarias, Pietro Balatti, Mattia Leonori, Marta Lorenzini, and Arash Ajoudani. Super-man: Supernumerary robotic bodies for physical assistance in human-robot conjoined actions. *arXiv preprint arXiv:2201.06365*, 2022.

[84] Waldez Gomes, Pauline Maurice, Jan Babič, Jean-Baptiste Mouret, and Serena Ivaldi. In a Collaborative Co-manipulation, Humans Have a Motor Behaviour Similar to a Leader. working paper or preprint, February 2022.

[85] Waldez Gomes, Pauline Maurice, Eloïse Dalin, Jean-Baptiste Mouret, and Serena Ivaldi. Improving ergonomics at work with personalized multi-objective optimization of human movements. In *12th International Conference on Applied Human Factors and Ergonomics*, 2021.

[86] Waldez Gomes, Pauline Maurice, Eloïse Dalin, Jean-Baptiste Mouret, and Serena Ivaldi. Multi-objective trajectory optimization to improve ergonomics in human motion. *IEEE Robotics and Automation Letters*, 7(1):342–349, 2022.

[87] S. Grafakos, F. Dimeas, and N. Aspragathos. Variable admittance control in phri using emg-based arm muscles co-activation. In *2016 IEEE International Conference on Systems, Man, and Cybernetics (SMC)*, pages 001900–001905, Oct 2016.

[88] Stavros Grafakos, Fotios Dimeas, and Nikos Aspragathos. Variable admittance control in phri using emg-based arm muscles co-activation. In *2016 IEEE International Conference on Systems, Man, and Cybernetics (SMC)*, pages 001900–001905. IEEE, 2016.

[89] Diego Felipe Paez Granados, Breno A Yamamoto, Hiroko Kamide, Jun Kinugawa, and Kazuhiro Kosuge. Dance teaching by a robot: Combining cognitive and physical human–robot interaction for supporting the skill learning process. *IEEE Robotics and Automation Letters*, 2(3):1452–1459, 2017.

[90] Paul L. Gribble et al. Role of cocontraction in arm movement accuracy. *Journal of Neurophysiology*, 2003.

[91] Nikolaus Hansen. Benchmarking a bi-population CMA-ES on the BBOB-2009 function testbed. In *11th Annual Conference Companion on Genetic and Evolutionary Computation Conference (GECCO): Late Breaking Papers*, pages 2389–2396, 2009.

[92] Sue Hignett and Lynn Mcatamney. Rapid entire body assessment (reba). *Applied ergonomics*, 31:201–5, 05 2000.

[93] Neville Hogan. Adaptive control of mechanical impedance by coactivation of antagonist muscles. *IEEE Transactions on automatic control*, 29(8):681–690, 1984.

[94] Neville Hogan. Impedance control of industrial robots. *Robotics and Computer-Integrated Manufacturing*, 1(1):97–113, 1984.

[95] Yongjun Hong, Uiwon Hwang, Jaeyoon Yoo, and Sungroh Yoon. How generative adversarial networks and their variants work: An overview. *ACM Computing Surveys (CSUR)*, 52(1):1–43, 2019.

[96] Y. Hu, M. Benallegue, G. Venture, and E. Yoshida. Interact with me: An exploratory study on interaction factors for active physical human-robot interaction. *IEEE Robotics and Automation Letters*, 5(4):6764–6771, 2020.

[97] Shuhei Ikemoto, Heni Ben Amor, Takashi Minato, Hiroshi Ishiguro, and Bernhard Jung. Physical interaction learning: Behavior adaptation in cooperative human-robot tasks involving physical contact. In *RO-MAN 2009-The 18th IEEE International Symposium on Robot and Human Interactive Communication*, pages 504–509. IEEE, 2009.

[98] M. Ison, I. Vujaklija, B. Whitsell, D. Farina, and P. Artemiadis. Simultaneous myoelectric control of a robot arm using muscle synergy-inspired inputs from high-density electrode grids. In *2015 IEEE International Conference on Robotics and Automation (ICRA)*, pages 6469–6474, 2015.

[99] Nathanaël Jarrassé, Themistoklis Charalambous, and Etienne Burdet. A framework to describe, analyze and generate interactive motor behaviors. *PloS one*, 7(11):e49945, 2012.

[100] Nathanael Jarrasse, Vittorio Sanguineti, and Etienne Burdet. Slaves no longer: review on role assignment for human–robot joint motor action. *Adaptive Behavior*, 22(1):70–82, 2014.

[101] Matthew Johnson, Brandon Shrewsbury, Sylvain Bertrand, Tingfan Wu, Daniel Duran, Marshall Floyd, Peter Abeles, Douglas Stephen, Nathan Mertins, Alex Lesman, John Carff, William Rifenburgh, Pushyami Kaveti, Wessel Straatman, Jesper Smith, Maarten Griffioen, Brooke Layton, Tomas De Boer, Twan Koolen, and Jerry Pratt. Team IHMC's lessons learned from the DARPA robotics challenge trials. *Journal of Field Robotics*, 32, 03 2015.

[102] Steven Jens Jorgensen, Michael W. Lanighan, Sylvain S. Bertrand, Andrew Watson, Joseph S. Altemus, R. Scott Askew, Lyndon Bridgwater, Beau Domingue, Charlie Kendrick, Jason Lee, and et al. Deploying the nasa valkyrie humanoid for ied response: An initial approach and evaluation summary. *2019 IEEE-RAS 19th International Conference on Humanoid Robots (Humanoids)*, Oct 2019.

[103] Leslie Pack Kaelbling, Michael L. Littman, and Anthony R. Cassandra. Planning and acting in partially observable stochastic domains. *Artificial Intelligence*, 101(1):99 – 134, 1998.

[104] H. Kamide, Y. Mae, K. Kawabe, S. Shigemi, M. Hirose, and T. Arai. New measurement of psychological safety for humanoid. In *2012 7th ACM/IEEE International Conference on Human-Robot Interaction (HRI)*, pages 49–56, 2012.

[105] Yasuhiro Kato, Pietro Balatti, Juan M Gandarias, Mattia Leonori, Toshiaki Tsuji, and Arash Ajoudani. A self-tuning impedance-based interaction planner for robotic haptic exploration. *arXiv preprint arXiv:2203.05413*, 2022.

[106] Abderrahmane Kheddar. Human-robot haptic joint actions is an equal control-sharing approach possible? In *2011 4th International Conference on Human System Interactions, HSI 2011*, pages 268–273. IEEE, 2011.

[107] Mahdi Khoramshahi and Aude Billard. A dynamical system approach for detection and reaction to human guidance in physical human–robot interaction. *Autonomous Robots*, 44(8):1411–1429, 2020.

[108] Mahdi Khoramshahi, Guillaume Morel, and Nathanael Jarrasse. Intent-aware control in kinematically redundant systems: Towards collaborative wearable robots. In *2021 IEEE International Conference on Robotics and Automation (ICRA)*, 2021.

[109] Byungchan Kim, Jooyoung Park, Shinsuk Park, and Sungchul Kang. Impedance learning for robotic contact tasks using natural actor-critic algorithm. *IEEE Transactions on Systems, Man, and Cybernetics, Part B (Cybernetics)*, 40(2):433–443, 2009.

[110] W. Kim, M. Lorenzini, P. Balatti, Y. Wu, and A. Ajoudani. Towards ergonomic control of collaborative effort in multi-human mobile-robot teams. In *2019 IEEE/RSJ International Conference on Intelligent Robots and Systems (IROS)*, pages 3005–3011, 2019.

[111] Wansoo Kim, Pietro Balatti, Edoardo Lamon, and Arash Ajoudani. Moca-man: A mobile and reconfigurable collaborative robot assistant for conjoined human-robot actions. In *2020 IEEE International Conference on Robotics and Automation (ICRA)*, pages 10191–10197, 2020.

[112] Wansoo Kim, Marta Lorenzini, Pietro Balatti, Phuong DH Nguyen, Ugo Pattacini, Vadim Tikhanoff, Luka Peternel, Claudio Fantacci, Lorenzo Natale, Giorgio Metta, et al. Adaptable workstations for human-robot collaboration: A reconfigurable framework for improving worker ergonomics and productivity. *IEEE Robotics & Automation Magazine*, 26(3):14–26, 2019.

[113] Taisuke Kobayashi, Emmanuel Dean-Leon, Julio Rogelio Guadarrama-Olvera, Florian Bergner, and Gordon Cheng. Multi-contacts force-reactive walking control during physical human-humanoid interaction. In *2019 IEEE-RAS 19th International Conference on Humanoid Robots (Humanoids)*, pages 33–39. IEEE, 2019.

[114] Yong-Ku Kong, Sung-yong Lee, Kyung-Suk Lee, and Dae-Min Kim. Comparisons of ergonomic evaluation tools (alla, rula, reba and owas) for farm work. *International journal of occupational safety and ergonomics*, 24(2):218–223, 2018.

[115] Petar Kormushev, Dragomir N Nenchev, Sylvain Calinon, and Darwin G Caldwell. Upper-body kinesthetic teaching of a free-standing humanoid robot. In *2011 IEEE International Conference on Robotics and Automation*, pages 3970–3975. IEEE, 2011.

[116] Kazuhiro Kosuge and Yasuhisa Hirata. Human-robot interaction. In *2004 IEEE International Conference on Robotics and Biomimetics*, pages 8–11. IEEE, 2004.

[117] Kazuhiro Kosuge, Hiromu Kakuya, and Yasuhisa Hirata. Control algorithm of dual arms mobile robot for cooperative works with human. In *2001 IEEE International Conference on Systems, Man and Cybernetics. e-Systems and e-Man for Cybernetics in Cyberspace (Cat. No. 01CH37236)*, volume 5, pages 3223–3228. IEEE, 2001.

[118] Philipp Kratzer, Marc Toussaint, and Jim Mainprice. Prediction of human full-body movements with motion optimization and recurrent neural networks. In *2020 IEEE International Conference on Robotics and Automation (ICRA)*, pages 1792–1798. IEEE, 2020.

[119] Shitij Kumar, Celal Savur, and Ferat Sahin. Survey of human–robot collaboration in industrial settings: Awareness, intelligence, and compliance. *IEEE Transactions on Systems, Man, and Cybernetics: Systems*, 51(1):280–297, 2020.

[120] Jessica Lanini, Hamed Razavi, Julen Urain, and Auke Ijspeert. Human intention detection as a multiclass classification problem: Application in physical human–robot interaction while walking. *IEEE Robotics and Automation Letters*, 3(4):4171–4178, 2018.

[121] Claudia Latella, Naveen Kuppuswamy, Francesco Romano, Silvio Traversaro, and Francesco Nori. Whole-body human inverse dynamics with distributed micro-accelerometers, gyros and force sensing. *Sensors*, 16(5):727, 2016.

[122] Claudia Latella, Marta Lorenzini, Maria Lazzaroni, Francesco Romano, Silvio Traversaro, M Ali Akhras, Daniele Pucci, and Francesco Nori. Towards real-time whole-body human dynamics estimation through probabilistic sensor fusion algorithms. *Autonomous Robots*, 43(6):1591–1603, 2019.

[123] Martin Lawitzky, Alexander Mörtl, and Sandra Hirche. Load sharing in human-robot cooperative manipulation. In *19th International Symposium in Robot and Human Interactive Communication*, pages 185–191. IEEE, 2010.

[124] Dongheui Lee, Christian Ott, Yoshihiko Nakamura, and Gerd Hirzinger. Physical human robot interaction in imitation learning. In *2011 IEEE International Conference on Robotics and Automation*, pages 3439–3440. IEEE, 2011.

[125] Jangwon Lee. A survey of robot learning from demonstrations for human-robot collaboration. *arXiv preprint arXiv:1710.08789*, 2017.

[126] Jeongseok Lee, Michael X Grey, Sehoon Ha, Tobias Kunz, Sumit Jain, Yuting Ye, Siddhartha S Srinivasa, Mike Stilman, and C Karen Liu. Dart: Dynamic animation and robotics toolkit. *Journal of Open Source Software*, 3(22):500, 2018.

[127] Timothée Lesort, Vincenzo Lomonaco, Andrei Stoian, Davide Maltoni, David Filliat, and Natalia Díaz-Rodríguez. Continual learning for robotics: Definition, framework, learning strategies, opportunities and challenges. *Information Fusion*, 58:52 – 68, 2020.

[128] Jiaman Li, Ruben Villegas, Duygu Ceylan, Jimei Yang, Zhengfei Kuang, Hao Li, and Yajie Zhao. Task-generic hierarchical human motion prior using vaes. In *2021 International Conference on 3D Vision (3DV)*, pages 771–781. IEEE, 2021.

[129] W. Li, C. Jaramillo, and Y. Li. Development of mind control system for humanoid robot through a brain computer interface. In *2012 Second International Conference on Intelligent System Design and Engineering Application*, pages 679–682, 2012.

[130] Yanan Li, Gerolamo Carboni, Franck Gonzalez, Domenico Campolo, and Etienne Burdet. Differential game theory for versatile physical human–robot interaction. *Nature Machine Intelligence*, 1(1):36–43, 2019.

[131] Yanan Li and Shuzhi Sam Ge. Human–robot collaboration based on motion intention estimation. *IEEE/ASME Transactions on Mechatronics*, 19(3):1007–1014, 2013.

[132] Yanan Li, Keng Peng Tee, Wei Liang Chan, Rui Yan, Yuanwei Chua, and Dilip Kumar Limbu. Continuous role adaptation for human–robot shared control. *IEEE Transactions on Robotics*, 31(3):672–681, 2015.

[133] Hung Yu Ling, Fabio Zinno, George Cheng, and Michiel Van De Panne. Character controllers using motion vaes. *ACM Transactions on Graphics (TOG)*, 39(4):40–1, 2020.

[134] Yiming Liu, Raz Leib, William Dudley, Ali Shafti, A Aldo Faisal, and David W Franklin. The role of haptic communication in dyadic collaborative object manipulation tasks. *arXiv preprint arXiv:2203.01287*, 2022.

[135] Zhenguang Liu, Shuang Wu, Shuyuan Jin, Qi Liu, Shouling Ji, Shijian Lu, and Li Cheng. Investigating pose representations and motion contexts modeling for 3d motion prediction. *IEEE Transactions on Pattern Analysis and Machine Intelligence*, 2022.

[136] Alfonso Montellano López, Joris Vaillant, François Keith, Philippe Fraisse, and Abderrahmane Kheddar. Compliant control of a humanoid robot helping a person stand up from a seated position. In *2014 IEEE-RAS International Conference on Humanoid Robots*, pages 817–822. IEEE, 2014.

[137] Marta Lorenzini, Wansoo Kim, Elena De Momi, and Arash Ajoudani. A synergistic approach to the real-time estimation of the feet ground reaction forces and centers of pressure in humans with application to human–robot collaboration. *IEEE Robotics and Automation Letters*, 3(4):3654–3661, 2018.

[138] Dylan P Losey, Craig G McDonald, Edoardo Battaglia, and Marcia K O'Malley. A review of intent detection, arbitration, and communication aspects of shared control for physical human–robot interaction. *Applied Mechanics Reviews*, 70(1), 2018.

[139] Jim Mainprice, E Akin Sisbot, Léonard Jaillet, Juan Cortés, Rachid Alami, and Thierry Siméon. Planning human-aware motions using a sampling-based costmap planner. In *2011 IEEE International Conference on Robotics and Automation*, pages 5012–5017. IEEE, 2011.

[140] Adrien Malaisé, Pauline Maurice, Francis Colas, François Charpillet, and Serena Ivaldi. Activity recognition with multiple wearable sensors for industrial applications. In *ACHI 2018-Eleventh International Conference on Advances in Computer-Human Interactions*, 2018.

[141] A. Malaisé, P. Maurice, F. Colas, and S. Ivaldi. Activity recognition for ergonomics assessment of industrial tasks with automatic feature selection. *IEEE Robotics and Automation Letters*, 4(2):1132–1139, 2019.

[142] Christian Mandery, Matthias Plappert, Júlia Borras, and Tamim Asfour. Dimensionality reduction for whole-body human motion recognition. In *2016 19th International Conference on Information Fusion (FUSION)*, pages 355–362. IEEE, 2016.

[143] Antonio Gonzales Marin, Mohammad S Shourijeh, Pavel E Galibarov, Michael Damsgaard, Lars Fritzsch, and Freek Stulp. Optimizing contextual ergonomics models in human-robot interaction. In *2018 IEEE/RSJ International Conference on Intelligent Robots and Systems (IROS)*, pages 1–9. IEEE, 2018.

[144] Pauline Maurice, Ludivine Allienne, Adrien Malaisé, and Serena Ivaldi. Ethical and social considerations for the introduction of human-centered technologies at work. In *2018 IEEE Workshop on Advanced Robotics and its Social Impacts (ARSO)*, pages 131–138, 2018.

[145] Pauline Maurice, Adrien Malaisé, Clélie Amiot, Nicolas Paris, Guy-Junior Richard, Olivier Rochel, and Serena Ivaldi. Human movement and ergonomics: An industry-oriented dataset for collaborative robotics. *The International Journal of Robotics Research*, 38(14):1529–1537, 2019.

[146] Pauline Maurice, Vincent Padois, Yvan Measson, and Philippe Bidaud. Human-oriented design of collaborative robots. *International Journal of Industrial Ergonomics*, 57:88–102, 2017.

[147] Pauline Maurice, Vincent Padois, Yvan Measson, and Philippe Bidaud. Assessing and improving human movements using sensitivity analysis and digital human simulation. *International Journal of Computer Integrated Manufacturing*, 32(6):546–558, 2019.

[148] Pauline Maurice, Vincent Padois, Yvan Measson, and Philippe Bidaud. Digital human modeling for collaborative robotics. In *DHM and Posturography*, pages 771–779. Elsevier, 2019.

[149] Pauline Maurice, Jernej Čamernik, Daša Gorjan, Benjamin Schirrmeister, Jonas Bornmann, Luca Tagliapietra, Claudia Latella, Daniele Pucci, Lars Fritzsche, Serena Ivaldi, and Jan Babič. Objective and subjective effects of a passive exoskeleton on overhead work. *IEEE Transactions on Neural Systems and Rehabilitation Engineering*, 28(1):152–164, 2020.

[150] Lynn McAtamney and E Nigel Corlett. Rula: a survey method for the investigation of work-related upper limb disorders. *Applied ergonomics*, 24(2):91–99, 1993.

[151] Qinxue Meng, Daniel Catchpoole, David Skillicom, and Paul J Kennedy. Relational autoencoder for feature extraction. In *2017 International Joint Conference on Neural Networks (IJCNN)*, pages 364–371. IEEE, 2017.

[152] Xuming Meng and Roman Weitschat. Dynamic projection of human motion for safe and efficient human-robot collaboration. In *2021 IEEE International Conference on Robotics and Automation (ICRA)*, pages 3765–3771, October 2021.

[153] Riccardo Mengacci, Franco Angelini, Manuel G Catalano, Giorgio Grioli, Antonio Bicchi, and Manolo Garabini. Stiffness bounds for resilient and stable physical interaction of articulated soft robots. *IEEE Robotics and Automation Letters*, 4(4):4131–4138, 2019.

[154] Giselle Merino, Lincoln da Silva, Diego Mattos, Bruno Guimarães, and Eugenio Merino. Ergonomic evaluation of the musculoskeletal risks in a banana harvesting activity through qualitative and quantitative measures, with emphasis on motion capture (xsens) and emg. *International Journal of Industrial Ergonomics*, 69:80–89, 2019.

[155] Fabio Morbidi, Louise Devigne, Catalin Teodorescu, Bastien Fraudet, Émilie Leblong, Tom Carlson, Marie Babel, Guillaume Caron, Sarah Delmas, François Pasteau, et al. Assistive robotic technologies for next-generation smart wheelchairs. *IEEE Robotics and Automation magazine*, 2023.

[156] Alexander Mörtl, Martin Lawitzky, Ayse Kucukyilmaz, Metin Sezgin, Cagatay Basdogan, and Sandra Hirche. The role of roles: Physical cooperation between humans and robots. *The International Journal of Robotics Research*, 31(13):1656–1674, 2012.

[157] Toshiharu Mukai, Shinya Hirano, Morio Yoshida, Hiromichi Nakashima, Shijie Guo, and Yoshikazu Hayakawa. Tactile-based motion adjustment for the nursing-care assistant robot riba. In *2011 IEEE International Conference on Robotics and Automation*, pages 5435–5441. IEEE, 2011.

[158] Yoshiki Nakamura and Hiroyuki Umemuro. The effect of robots listening attitude change on the self-disclosure of the elderly: A preliminary study. In *Proceedings of the 2022 ACM/IEEE International Conference on Human-Robot Interaction*, pages 932–936, 2022.

[159] M Nardo, D Forino, and T Murino. The evolution of man–machine interaction: The role of human in industry 4.0 paradigm. *Production & Manufacturing Research*, 8(1):20–34, 2020.

[160] A.Y.C. Nee, S.K. Ong, G. Chryssolouris, and D. Mourtzis. Augmented reality applications in design and manufacturing. *CIRP Annals*, 61(2):657–679, 2012.

[161] Heramb Nemlekar, Jignesh Modi, Satyandra K Gupta, and Stefanos Nikolaidis. Two-stage clustering of human preferences for action prediction in assembly tasks. *arXiv preprint arXiv:2103.14994*, 2021.

[162] Stefanos Nikolaidis, David Hsu, and Siddhartha Srinivasa. Human-robot mutual adaptation in collaborative tasks: Models and experiments. *The International Journal of Robotics Research*, 36(5-7):618–634, 2017.

[163] Stefanos Nikolaidis, David Hsu, and Siddhartha Srinivasa. Human-robot mutual adaptation in collaborative tasks: Models and experiments. *The International Journal of Robotics Research*, 36(5-7):618–634, 2017.

[164] Stefanos Nikolaidis and Julie Shah. Human-robot cross-training: computational formulation, modeling and evaluation of a human team training strategy. In *2013 8th ACM/IEEE International Conference on Human-Robot Interaction (HRI)*, pages 33–40. IEEE, 2013.

[165] Shengli Niu. Ergonomics and occupational safety and health: An ilo perspective. *Applied Ergonomics*, 41(6):744–753, 2010. Special Section: Selection of papers from IEA 2009.

[166] T. Ortmaier, M. Groger, D.H. Boehm, V. Falk, and G. Hirzinger. Motion estimation in beating heart surgery. *IEEE Transactions on Biomedical Engineering*, 52(10):1729–1740, 2005.

[167] Kazuya Otani, Karim Bouyarmane, and Serena Ivaldi. Generating assistive humanoid motions for co-manipulation tasks with a multi-robot quadratic program controller. In *2018 IEEE International Conference on Robotics and Automation (ICRA)*, pages 3107–3113. IEEE, 2018.

[168] Ivana Palunko, Philine Donner, Martin Buss, and Sandra Hirche. Cooperative suspended object manipulation using reinforcement learning and energy-based control. In *2014 IEEE/RSJ International Conference on Intelligent Robots and Systems*, pages 885–891. IEEE, 2014.

[169] Alexandros Paraschos, Christian Daniel, Jan Peters, and Gerhard Neumann. Using probabilistic movement primitives in robotics. *Autonomous Robots*, 2018.

[170] Alexandros Paraschos, Rudolf Lioutikov, Jan Peters, and Gerhard Neumann. Probabilistic prioritization of movement primitives. *IEEE Robotics and Automation Letters*, 2017.

[171] Peter Pastor, Mrinal Kalakrishnan, Sachin Chitta, Evangelos Theodorou, and Stefan Schaal. Skill learning and task outcome prediction for manipulation. In *2011 IEEE International Conference on Robotics and Automation*, pages 3828–3834. IEEE, 2011.

[172] Patrice Pavis. *Dictionary of the theatre: Terms, concepts, and analysis*. University of Toronto Press, 1998.

[173] L. Penco, N. Scianca, V. Modugno, L. Lanari, G. Oriolo, and S. Ivaldi. A multimode teleoperation framework for humanoid loco-manipulation: An application for the icub robot. *IEEE Robotics Automation Magazine*, 26(4):73–82, 2019.

[174] Aldo O Perotto. *Anatomical guide for the electromyographer: the limbs and trunk*. Charles C Thomas Publisher, 2011.

[175] Michael Peshkin and J Edward Colgate. Cobots. *Industrial Robot: An International Journal*, 1999.

[176] Luka Peternel, Cheng Fang, Nikos Tsagarakis, and Arash Ajoudani. A selective muscle fatigue management approach to ergonomic human-robot co-manipulation. *Robotics and Computer-Integrated Manufacturing*, 58:69–79, 2019.

[177] Luka Peternel, Wansoo Kim, Jan Babič, and Arash Ajoudani. Towards ergonomic control of human-robot co-manipulation and handover. In *2017 IEEE-RAS 17th International Conference on Humanoid Robotics (Humanoids)*, pages 55–60. IEEE, 2017.

[178] Luka Peternel, Nikos Tsagarakis, and Arash Ajoudani. A human–robot co-manipulation approach based on human sensorimotor information. *IEEE Transactions on Neural Systems and Rehabilitation Engineering*, 25(7):811–822, 2017.

[179] Luka Peternel, Nikos Tsagarakis, Darwin Caldwell, and Arash Ajoudani. Adaptation of robot physical behaviour to human fatigue in human-robot co-manipulation. In *2016 IEEE-RAS 16th International Conference on Humanoid Robots (Humanoids)*, pages 489–494, 2016.

[180] Luka Peternel, Nikos Tsagarakis, Darwin Caldwell, and Arash Ajoudani. Robot adaptation to human physical fatigue in human–robot co-manipulation. *Autonomous Robots*, 42(5):1011–1021, 2018.

[181] Katherine L Poggensee and Steven H Collins. How adaptation, training, and customization contribute to benefits from exoskeleton assistance. *Science Robotics*, 6(58):eabf1078, 2021.

[182] Laura Punnett and David H Wegman. Work-related musculoskeletal disorders: the epidemiologic evidence and the debate. *Journal of electromyography and kinesiology*, 14(1):13–23, 2004.

[183] Rahaf Rahal, Giulia Matarese, Marco Gabiccini, Alessio Artoni, Domenico Prattichizzo, Paolo Robuffo Giordano, and Claudio Pacchierotti. Haptic shared control for enhanced user comfort in robotic telemanipulation.

[184] Rahaf Rahal, Giulia Matarese, Marco Gabiccini, Alessio Artoni, Domenico Prattichizzo, Paolo Robuffo Giordano, and Claudio Pacchierotti. Caring about the human operator: haptic shared control for enhanced user comfort in robotic telemanipulation. *IEEE Transactions on Haptics*, 13(1):197–203, 2020.

[185] Miquel Ramirez and Hector Geffner. Goal recognition over pomdps: Inferring the intention of a pomdp agent. In *IJCAI International Joint Conference on Artificial Intelligence*, pages 2009–2014, 01 2011.

[186] O. E. Ramos, N. Mansard, O. Stasse, C. Benazeth, S. Hak, and L. Saab. Dancing humanoid robots: Systematic use of osid to compute dynamically consistent movements following a motion capture pattern. *IEEE Robotics Automation Magazine*, 22(4):16–26, Dec 2015.

[187] Isura Ranatunga, Frank L Lewis, Dan O Popa, and Shaikh M Tousif. Adaptive admittance control for human–robot interaction using model reference design and adaptive inverse filtering. *IEEE transactions on control systems technology*, 25(1):278–285, 2016.

[188] Carl Edward Rasmussen. Gaussian processes in machine learning. In *Summer School on Machine Learning*, pages 63–71. Springer, 2003.

[189] Andreas Risskov Sørensen, Oskar Palinko, and Norbert Krüger. Classification of visual interest based on gaze and facial features for human-robot interaction. In *Proceedings of the 16th International Joint Conference on Computer Vision, Imaging and Computer Graphics Theory and Applications*, (2020), November. SCITEPRESS Digital Library.

[190] Lionel Robert. Personality in the human robot interaction literature: A review and brief critique. In *Robert, LP (2018). Personality in the Human Robot Interaction Literature: A Review and Brief Critique, Proceedings of the 24th Americas Conference on Information Systems, Aug*, pages 16–18, 2018.

[191] Francesco Romano, Gabriele Nava, Morteza Azad, Jernej Čamernik, Stefano Dafarra, Oriane Dermy, Claudia Latella, Maria Lazzaroni, Ryan Lober, Marta Lorenzini, et al. The codyco project achievements and beyond: Toward human aware whole-body controllers for physical human robot interaction. *IEEE Robotics and Automation Letters*, 3(1):516–523, 2017.

[192] Jeremy Roschelle and Stephanie D Teasley. The construction of shared knowledge in collaborative problem solving. In *Computer supported collaborative learning*. Springer.

[193] Francisco J Ruiz-Ruiz, Alberto Giammarino, Marta Lorenzini, Juan M Gandarias, Jesus M Gomez-de Gabriel, and Arash Ajoudani. Improving standing balance performance through the assistance of a mobile collaborative robot. *arXiv preprint arXiv:2109.12038*, 2021.

[194] MW Rysz and Siddhartha S Mehta. A risk-averse optimization approach to human-robot collaboration in robotic fruit harvesting. *Computers and Electronics in Agriculture*, 182:106018, 2021.

[195] Alessio Sampieri, Guido D'Amely, Andrea Avogaro, Federico Cunico, Geri Skenderi, Francesco Setti, Marco Cristani, and Fabio Galasso. Pose forecasting in industrial human-robot collaboration. *arXiv preprint arXiv:2208.07308*, 2022.

[196] Shane Saunderson and Goldie Nejat. Hybrid hierarchical learning for adaptive persuasion in human-robot interaction. *IEEE Robotics and Automation Letters*, 2022.

[197] Allison Sauppé and Bilge Mutlu. Robot deictics: How gesture and context shape referential communication. In *2014 9th ACM/IEEE International Conference on Human-Robot Interaction (HRI)*, pages 342–349, 2014.

[198] Andrew Sawers and Lena H. Ting. Perspectives on human-human sensorimotor interactions for the design of rehabilitation robots. *Journal of NeuroEngineering and Rehabilitation*, 11(1):142, Oct 2014.

[199] Brian Scassellati. Theory of mind for a humanoid robot. *Autonomous Robots*, 12(1):13–24, Jan 2002.

[200] Sofia Scataglini and Gunther Paul. *DHM and Posturography*. Academic Press, (2019).

[201] Elke Schneider, Sarah Copsey, and Xabier Irastorza. *Occupational Safety and Health in Figures: Work-related Musculoskeletal Disorders in the EU-Facts and Figures*. Office for Official Publications of the European Communities, 2010.

[202] Felix Schoeller, Mark Miller, Roy Salomon, and Karl J. Friston. Trust as extended control: Human-machine interactions as active inference. *Frontiers in Systems Neuroscience*, 15, 2021.

[203] Mario Selvaggio, Marco Cognetti, Stefanos Nikolaidis, Serena Ivaldi, and Bruno Siciliano. Autonomy in physical human-robot interaction: A brief survey. *IEEE Robotics and Automation Letters*, 2021.

[204] Reza Shadmehr and Ferdinando A Mussa-Ivaldi. Adaptive representation of dynamics during learning of a motor task. *Journal of neuroscience*, 14(5):3208–3224, 1994.

[205] A. Shafti, A. Ataka, B. Lazpita, A. Shiva, H. Wurdemann, and K. Althoefer. Real-time robot-assisted ergonomics*. *2019 International Conference on Robotics and Automation (ICRA)*, 2019.

[206] Ali Shafti, Ahmad Ataka, B Urbistondo Lazpita, Ali Shiva, Helge A Wurdemann, and Kaspar Althoefer. Real-time robot-assisted ergonomics. In *2019 International Conference on Robotics and Automation (ICRA)*, pages 1975–1981. IEEE, 2019.

[207] Ali Shafti, Jonas Tjomsland, William Dudley, and A Aldo Faisal. Real-world human-robot collaborative reinforcement learning. *arXiv preprint arXiv:2003.01156*, 2020.

[208] Bruno Siciliano. Kinematic control of redundant robot manipulators: A tutorial. *Journal of intelligent and robotic systems*, 3(3):201–212, 1990.

[209] David Silver and Joel Veness. Monte-carlo planning in large POMDPs. In J. D. Lafferty, C. K. I. Williams, J. Shawe-Taylor, R. S. Zemel, and A. Culotta, editors, *Advances in Neural Information Processing Systems 23*, pages 2164–2172. Curran Associates, Inc., (2010).

[210] J Ernesto Solanes, Luis Gracia, Pau Munoz-Benavent, Jaime Valls Miro, Marc G Carmichael, and Josep Tornero. Human–robot collaboration for safe object transportation using force feedback. *Robotics and Autonomous Systems*, 107:196–208, 2018.

[211] Seungmoon Song and Steven H Collins. Optimizing exoskeleton assistance for faster self-selected walking. *IEEE Transactions on Neural Systems and Rehabilitation Engineering*, 29:786–795, 2021.

[212] Ines Sorrentino, Francisco Javier Andrade Chavez, Claudia Latella, Luca Fiorio, Silvio Traversaro, Lorenzo Rapetti, Yeshasvi Tirupachuri, Nuno Guedelha, Marco Maggiali, Simeone Dussoni, et al. A novel sensorised insole for sensing feet pressure distributions. *Sensors*, 20(3):747, 2020.

[213] Neville Anthony Stanton, Alan Hedge, Karel Brookhuis, Eduardo Salas, and Hal W Hendrick. *Handbook of human factors and ergonomics methods*. CRC press, 2004.

[214] Olivier Stasse, Paul Evrard, Nicolas Perrin, Nicolas Mansard, and Abderrahmane Kheddar. Fast foot prints re-planning and motion generation during walking in physical human-humanoid interaction. In *2009 9th IEEE-RAS International Conference on Humanoid Robots*, pages 284–289. IEEE, 2009.

[215] N. Stefanov, A. Peer, and M. Buss. Role determination in human-human interaction. In *World Haptics*, pages 51–56, March 2009.

[216] D Stegeman and H Hermens. Standards for surface electromyography: The european project surface emg for non-invasive assessment of muscles (seniam). 2007.

[217] Jörg Stückler and Sven Behnke. Following human guidance to cooperatively carry a large object. In *2011 11th IEEE-RAS International Conference on Humanoid Robots*, pages 218–223. IEEE, 2011.

[218] Dag Sverre Syrdal, Kerstin Dautenhahn, Kheng Lee Koay, and Michael L Walters. The negative attitudes towards robots scale and reactions to robot behaviour in a live human-robot interaction study. In *Adaptive and Emergent Behaviour and Complex Systems*, pages 109–115, (2009). SSAISB.

[219] Aaquib Tabrez, Matthew B Luebbers, and Bradley Hayes. A survey of mental modeling techniques in human–robot teaming. *Current Robotics Reports*, pages 1–9, 2020.

[220] Susumu Tachi. *Telexistence*. World Scientific 2nd edition, (2015).

[221] Jukka Takala and S Niu. Responses to the equity challenge in safety and health at work: improvement of working conditions in equitable bases. In *27th international congress on occupational health*, pages 23–28, 2003.

[222] Leila Takayama, Doug Dooley, and Wendy Ju. Expressing thought: Improving robot readability with animation principles. In *Proceedings of the 6th International Conference on Human-Robot Interaction*, HRI '11, page 69–76, New York, NY, USA, 2011. Association for Computing Machinery.

[223] Yoshiyuki Tanaka, Kazuo Nishikawa, Naoki Yamada, and Toshio Tsuji. Analysis of operational comfort in manual tasks using human force manipulability measure. *IEEE transactions on haptics*, 8(1):8–19, 2014.

[224] Gaurav Tevatia and Stefan Schaal. Inverse kinematics for humanoid robots. In *Proceedings 2000 ICRA. Millennium Conference. IEEE International Conference on Robotics and Automation. Symposia Proceedings (Cat. No. 00CH37065)*, volume 1, pages 294–299. IEEE, 2000.

[225] Yeshasvi Tirupachuri, Gabriele Nava, Diego Ferigo, Luca Tagliapietra, Claudia Latella, Francesco Nori, and Daniele Pucci. Towards partner-aware humanoid robot control under physical interactions. In *IntelliSys*, 2019.

[226] Yeshasvi Tirupachuri, Gabriele Nava, Lorenzo Rapetti, Claudia Latella, and Daniele Pucci. Trajectory advancement during human-robot collaboration. In *2019 28th IEEE International Conference on Robot and Human Interactive Communication (RO-MAN)*, pages 1–8. IEEE, 2019.

[227] Antony Tran, Dikai Liu, Ravindra Ranasinghe, and Marc Carmichael. A method for quantifying a robot's confidence in its human co-worker in human-robot cooperative grit-blasting. In *ISR 2018; 50th International Symposium on Robotics*, pages 1–8. VDE, 2018.

[228] US Bureau of Labor Statistics. *Nonfatal Occupational Injuries and Illnesses Requiring Days Away from Work, 2015*, 2016.

[229] L. v. der Spaa, M. Gienger, T. Bates, and J. Kober. Predicting and optimizing ergonomics in physical human-robot cooperation tasks. In *2020 IEEE International Conference on Robotics and Automation (ICRA)*, pages 1799–1805, 2020.

[230] Jinke D Van Der Laan, Adriaan Heino, and Dick De Waard. A simple procedure for the assessment of acceptance of advanced transport telematics. *Transportation Research Part C: Emerging Technologies*, 5(1):1–10, 1997.

[231] Linda F. van der Spaa, Tamas Bates, Michael Gienger, and Jens Kober. Predicting and optimizing ergonomics in physical human-robot cooperation tasks. In *IEEE International Conference on Robotics and Automation (ICRA)*, 2020.

[232] Ming Z Huang Hareendra Varma. Optimal rate allocation in kinematically redundant manipulators–the dual projection method.

[233] Ashesh Vasalya. *Human and Humanoid robot co-workers: motor contagions and whole-body handover*. PhD thesis, Université de Montpellier, December 2019.

[234] Ashesh Vasalya, Gowrishankar Ganesh, and Abderrahmane Kheddar. More than just co-workers: Presence of humanoid robot co-worker influences human performance. *PLOS ONE*, 13(11):1–19, 11 2018.

[235] Juan P Vasconez, George A Kantor, and Fernando A Auat Cheein. Human–robot interaction in agriculture: A survey and current challenges. *Biosystems engineering*, 179:35–48, 2019.

[236] Ben Vermeulen, Andreas Pyka, and Pier Paolo Saviotti. Robots, structural change, and employment: Future scenarios. *Handbook of Labor, Human Resources and Population Economics*, pages 1–37, 2020.

[237] Lorenzo Vianello, Waldez Gomes, Pauline Maurice, Alexis Aubry, and Serena Ivaldi. Cooperation or collaboration? on a human-inspired impedance strategy in a human-robot co-manipulation task. 2022.

[238] Lorenzo Vianello, Waldez Gomes, Freek Stulp, Alexis Aubry, Pauline Maurice, and Serena Ivaldi. Latent ergonomics maps: Real-time visualization of estimated ergonomics of human movements. *Sensors*, 22(11):3981, 2022.

[239] Lorenzo Vianello, Jean-Baptiste Mouret, Eloïse Dalin, Alexis Aubry, and Serena Ivaldi. Human posture prediction during physical human-robot interaction. *IEEE Robotics and Automation Letters*, 6(3):6046–6053, 2021.

[240] Lorenzo Vianello, Jean-Baptiste Mouret, Eloise Dalin, Alexis Aubry, and Serena Ivaldi. Human posture prediction during physical human-robot interaction. *IEEE Robotics and Automation Letters*, 2021.

[241] Lorenzo Vianello, Luigi Penco, Waldez Gomes, Yang You, Salvatore Anzalone, Pauline Maurice, Vincent Thomas, and Serena Ivaldi. Human-humanoid interaction and cooperation: a review. *Current Robotics Reports*, 2021.

[242] Alessandro Vinciarelli, Maja Pantic, and Hervé Bourlard. Social signal processing: Survey of an emerging domain. *Image and Vision Computing*, 27(12):1743 – 1759, 2009.

[243] Theo Vos, Ryan M Barber, Brad Bell, Amelia Bertozzi-Villa, Stan Biryukov, Ian Bolliger, Fiona Charlson, Adrian Davis, Louisa Degenhardt, Daniel Dicker, et al. Global, regional, and national incidence, prevalence, and years lived with disability for 301 acute and chronic diseases and injuries in 188 countries, 1990–2013: a systematic analysis for the global burden of disease study 2013. *The Lancet*, 386(9995):743–800, 2015.

[244] Johanna Wallén. *The history of the industrial robot*. Linköping University Electronic Press, 2008.

[245] Michael L. Walters, Dag S. Syrdal, Kerstin Dautenhahn, René te Boekhorst, and Kheng Lee Koay. Avoiding the uncanny valley: robot appearance, personality and consistency of behavior in an attention-seeking home scenario for a robot companion. *Autonomous Robots*, 24(2):159–178, Feb 2008.

[246] Hongbo Wang and Kazuhiro Kosuge. Control of a robot dancer for enhancing haptic human-robot interaction in waltz. *IEEE transactions on haptics*, 5(3):264–273, 2012.

[247] Jingguo Wang and Yangmin Li. Hybrid impedance control of a 3-dof robotic arm used for rehabilitation treatment. In *2010 IEEE International Conference on Automation Science and Engineering*, pages 768–773, 2010.

[248] Darrell M West. What happens if robots take the jobs? the impact of emerging technologies on employment and public policy. *Centre for Technology Innovation at Brookings, Washington DC*, 2015.

[249] Ronald Wilcox, Stefanos Nikolaidis, and Julie Shah. Optimization of temporal dynamics for adaptive human-robot interaction in assembly manufacturing. *Robotics*, 8:441, 2013.

[250] Rachel Wood, Paul Baxter, and Tony Belpaeme. A review of long-term memory in natural and synthetic systems. *Adaptive Behavior*, 20(2):81–103, 2012.

[251] D. Woods, John M. Wyma, E. Yund, T. Herron, and B. Reed. Factors influencing the latency of simple reaction time. *Frontiers in Human Neuroscience*, 9, 2015.

[252] Robert H Wortham and Andreas Theodorou. Robot transparency, trust and utility. *Connection Science*, 29(3):242–248, 2017.

[253] Chenguang Yang, Gowrishankar Ganesh, Sami Haddadin, Sven Parusel, Alin Albu-Schaeffer, and Etienne Burdet. Human-like adaptation of force and impedance in stable and unstable interactions. *IEEE transactions on robotics*, 27(5):918–930, 2011.

[254] Amir Yazdani, Roya Sabbagh Novin, Andrew Merryweather, and Tucker Hermans. Estimating human teleoperator posture using only a haptic-input device. *arXiv preprint arXiv:2002.10586*, 2020.

[255] Kazuhiko Yokoyama, Hiroyuki Handa, Takakatsu Isozumi, Yutaro Fukase, Kenji Kaneko, Fumio Kanehiro, Yoshihiro Kawai, Fumiaki Tomita, and Hirohisa Hirukawa. Cooperative works by a human and a humanoid robot. In *2003 IEEE International Conference on Robotics and Automation (Cat. No. 03CH37422)*, volume 3, pages 2985–2991. IEEE, 2003.

[256] Irati Zamalloa, Risto Kojcev, Alejandro Hernández, Inigo Muguruza, Lander Usategui, Asier Bilbao, and Victor Mayoral. Dissecting robotics-historical overview and future perspectives. *arXiv preprint arXiv:1704.08617*, 2017.

[257] Heng Zhang, Qi Sheng, Jiawei Hu, Xinjun Sheng, Zhenhua Xiong, and Xiangyang Zhu. Cooperative transportation with mobile manipulator: A capability map-based framework for physical human–robot collaboration. *IEEE/ASME Transactions on Mechatronics*, 2022.

[258] Jianjing Zhang, Hongyi Liu, Qing Chang, Lihui Wang, and Robert X Gao. Recurrent neural network for motion trajectory prediction in human-robot collaborative assembly. *CIRP Annals*, 2020.

[259] Juanjuan Zhang, Pieter Fiers, Kirby A Witte, Rachel W Jackson, Katherine L Poggensee, Christopher G Atkeson, and Steven H Collins. Human-in-the-loop optimization of exoskeleton assistance during walking. *Science*, 356(6344):1280–1284, 2017.

[260] Ce Zheng, Wenhan Wu, Taojiannan Yang, Sijie Zhu, Chen Chen, Ruixu Liu, Ju Shen, Nasser Kehtarnavaz, and Mubarak Shah. Deep learning-based human pose estimation: A survey, 2020.

[261] Tian Zhou, Jackie S Cha, Glebys Gonzalez, Juan P Wachs, Chandru P Sundaram, and Denny Yu. Multimodal physiological signals for workload prediction in robot-assisted surgery. *ACM Transactions on Human-Robot Interaction (THRI)*, 9(2):1–26, 2020.

Résumé

Cette thèse présente plusieurs contributions dans le domaine de l'interaction physique homme-robot. En premier lieu, elle propose une méthode pour prédire la posture humaine pendant qu'un humain interagit physiquement avec un robot. Deuxièmement, elle décrit des algorithmes et des outils de simulation pour visualiser le score d'ergonomie humaine associé au mouvement d'un humain, en temps réel, même lorsque l'humain est physiquement couplé au robot. Troisièmement, la thèse fait progresser les connaissances sur la façon de contrôler et d'adapter le comportement du robot pendant la collaboration, grâce à des études expérimentales impliquant des humains et des robots dans des scénarios de comanipulation. La première étude examine les meilleures stratégies d'impédance pour que le robot puisse collaborer avec l'humain lors de la co-manipulation d'un tuyau dans une tâche d'insertion de précision, tandis que la deuxième étude examine comment les humains s'adaptent aux stratégies d'impédance changeantes d'un robot lors d'une tâche de sciage collaborative.

Mots-clés:

Abstract

The thesis presents several contributions in the area of human-robot physical interaction. First, it proposes a method to predict human posture while a human interacts physically with a robot. Second, it describes algorithms and simulation tools to visualize the human ergonomics score associated with the movement of a human, in real-time, even when the human is physically coupled with the robot. Third, the thesis advances the knowledge on how to control and adapt the robot behaviour during collaboration, thanks to experimental studies involving humans and robots in comanipulation scenarios. The first study investigates the best impedance strategies for the robot to collaborate with the human during a co-manipulation of a pipe in a precision insertion task, while the second study investigates how humans adapt to changing impedance strategies of a robot during a collaborative sawing task.

Keywords: